Optimal Design and Operation of Process Integrated Distillation

Andersen, Torben Ravn

Publication date:
2002

Optimal Design and Operation of Process Integrated Distillation

Torben Ravn Andersen

Lyngby 2002

Preface

This thesis has been written to partially satisfy the requirements for the Ph.D. degree. The present work has been carried out at the Computer Aided Process Engineering Center (CAPEC), Department of Chemical Engineering at the Technical University of Denmark (DTU).

I would like to take this opportunity to thank my supervisor Professor Sten Bay Jørgensen (Department of Chemical Engineering, DTU) for enabling me to do the Ph.D. project. I also appreciate very much the inspiring discussions, encouragement and comments to the manuscript.

During the completion of this work I stayed abroad twice, at the Norwegian University of Science and Technology (NTNU) and at the San Diego State University (SDSU) respectively. I would like to thank Professor Signe Ratkje and Gelein de Koijer, from the Department of Physical Chemistry (now Department of Chemistry), NTNU, Trondheim, Norway, who introduced me to the world of irreversible thermodynamics. I also thank Professor Peter Salamon and Gino Siragusa from the Department of Chemistry, SDSU, California, USA, and Associate Professor Bjarne Andresen from the Ørsted Laboratory (HCØ), University of Copenhagen, Copenhagen, Denmark, who introduced me to the other world of finite–time thermodynamics. Even though this thesis does not bear the stamp of neither worlds, the common denominator for both stays abroad is that they have been very valuable professionally as well as personally.

I also thank Associate Professor Morten Brøns (Department of Mathematics, DTU) for his support and always willingness to help with the treatment of the more exotic theoretical mathematics issues of bifurcation analysis.
The project has received financial support from the following sources: Nordic Energy Research Programme, the Danish Energy Agency, Danisco Distillers A/S (now Danish Distillers A/S), CAPEC and the Technical University of Denmark. This support is gratefully acknowledged.

During the past five years I have been working and also socializing with a lot of fine people. In the beginning in the Process Design, Dynamics and Control Group (PDDC), later on within the Computer Aided Process Engineering Center. Some of the people were Ph.D.'s, some fellow students and other again technical staff. I would like to thank all of You for a number of reasons: A few of these are: solid assistance in running the experiments both with day as well as night shifts, assistance with the subsequent GC analyses, discussions and feedback during the entire

project, pleasant times when participating in various conferences, meetings and parties. The gratitude in particular applies to: Arne Koggersbøl, Hassan Yazdi, Klavs Esbjerg, Britta Rønde Andersen, Bodil Recke, Kurt Creutzburg, Anette Havstreym, Rene Skotte, Mario Richard Eden, John Bagterp Jørgensen, Lars Gregersen, Lee Hong Wen.

Thanks to my closest relatives and friends. And finally last but not least thanks to those nearest and dearest to me: Bodil for Your love, support, encouragement, patience and understanding during the past years – it was essential to me in finishing this project. Cecilie and Elvira for being the wonderful children that You are and for making me see life in its proper perspective.

Torben Ravn Andersen

June 30th, 2002.

People believe 50 percent of what they hear,
75 percent of what they see,
and 100 percent of what the computer tells them.

Original source unknown
- quotation from Kister (1992)

1

Abstract

The present dissertation contains research results of various topics within optimal design and operation of process integrated distillation.

In spite of the relatively low energy efficiency (typically only a few percent), distillation still remains one of the most widely used separation techniques in the chemical and petrochemical industry. This may be illustrated by the fact that distillation accounts for more than 3 % of the total energy dissipation in the USA, Mix *et al.* (1978), Humphrey and Siebert (1992). Energy consumption attributed to distillation has been reported as high as 5-6 % within the industrialized countries by Pilavachi (1996).

The prevailing use of distillation combined with its low energy efficiency, increasing demands on environmentally 'neutral' technology and generally increasing economic competition, constantly calls for plants with increased degree of process integration. Within the last two decades an increasing effort has been made in attempting to clear up the "mysteries" of plant nonlinear statics and dynamics as well as operational implications of integrated processes and process designs.
Several types of steady state multiplicity are now known and generally accepted to occur within chemical engineering processes. The term *multiplicity* refers to multiple solutions for given operating conditions, and can be subdivided into input, output, and state multiplicity. These are defined as follows:

- Input multiplicity occurs when multiple input values exist for a given set of outputs.
- Output multiplicity occurs when multiple output values exist for a given set of inputs.
- State multiplicity occurs when multiple values of internal states exist for a given set of inputs **and** outputs.

The outputs considered are normally quality variables like product compositions, whereas the inputs typically are selected manipulable flow rates.

This work contains results of three main subjects within the integration of distillation processes:

- Experimental validation of an input multiplicity in heat integrated binary distillation, and its influence on control structure selection
- Analysis of nonlinear static behavior in heterogeneous azeotropic distillation sequences
- Investigation of dynamical implications from nonlinear effects in ternary heterogeneous azeotropic distillation.
- Optimal design and duty distribution in heat integrated distillation with internal heat exchangers

The results are summarized for the individual chapters below:

Chapter 4: Experimental Validation of Input Multiplicity in Binary Distillation – Influence on Control Structure Selection
In this chapter, an input multiplicity in energy integrated binary distillation is investigated using both simulation models and experiments on an industrial size pilot plant. The input multiplicity is predicted to occur within the feasible operating window. From the predictions the degree of separation is expected to go through a maximum when boil up is increased keeping all other inputs constant. The multiplicity is related to the binary distillation properties. Three experiments were carried out. The results from these experiments verify the existence of the proposed input multiplicity. Control strategy and configuration selection issues to reduce or possibly avoid performance reducing implications of these phenomena are discussed. The findings show that attention from the process design community should be drawn to this field of research, since it is driven by changes in operability and stability resulting in performance reducing behavior which is brought about by these phenomena.

Chapter 5: Steady State Multiplicities in Heterogeneous Azeotropic Distillation Sequences
Steady state multiplicity in heterogeneous azeotropic distillation sequences is studied in this chapter. Two sequences, suitable for ethanol dehydration (using cyclohexane as entrainer), are treated as sample problems and compared. As a basis the ∞/∞ analysis method which assumes infinite reflux rate and infinite number of trays, is extended to and applied on heterogeneous azeotropic distillation sequences in order to determine steady state bifurcation diagrams from thermodynamic considerations. The bifurcation diagrams are very different for the two sequences despite their similar structures. In particular, it is predicted that output multiplicity of the single azeotropic column, can induce output multiplicity of one sequence. It is further predicted that output multiplicity can be avoided by

the choice of a different sequence structure. Furthermore, ∞/∞ analysis predicts state multiplicity in both heterogeneous azeotropic distillation sequences. For the ∞/∞ case it is shown that state multiplicity in heterogeneous distillation sequences can either be induced by the corresponding single column or by closing the sequence. The predicted bifurcation diagrams and multiplicities are substantiated through rigorous simulation of column sequences operating at finite reflux and with finite number of stages.

Chapters 6–7: Dynamics of a Heterogeneous Azeotropic Distillation Sequence, Part I–II

The bifurcation analysis of static solutions performed in chapter 5 is extended to a bifurcation analysis on a rigorous dynamic distillation model of the 'direct' sequence. The dynamics of nontrivial parts of the operating window are treated through dynamic simulation.

The parameter chosen as primary bifurcation parameter in the investigations is reflux ratio for the azeotropic distillation column. The occurrence of multiple steady states, as found in chapter 5, are substantiated through the bifurcation analysis. The multiple solutions occur in a typical hysteresis scenario. That is stable solutions of high and low product purity coexists, and their basins of attraction are separated by an unstable solution of intermediate purity. In the instance of composition profile type changes, in particular where optimal ethanol product purity is obtained (state multiplicity) a real eigenvalue moves very close to the imaginary axis, thus resulting in a very slow open loop dynamic behavior. The results from the bifurcation analysis indicate that complex dynamic behavior is expected to occur in the boundary region of liquid phase splitting.

The simulations in part II extends the bifurcation analysis of the heterogeneous azeotropic distillation sequence, carried out in Part I. The dynamic simulations of this sequence are carried out using rigorous models implemented in a dynamic simulator. Reflux ratio for the azeotropic column is again chosen as the parameter of variation. The results from the simulations reveal that sustained oscillations occur in the 'direct' sequence in the region close to and beyond the boundary of liquid phase splitting within the decanter. This is the first occurrence of limit cycles reported in the literature of heterogeneous azeotropic distillation. The oscillation reported here is predicted to exist within a wide range of reflux ratio. The results indicate clearly that the stable periodic solution is bounded by a cyclic fold bifurcation and a 'blue sky' catastrophe (global bifurcation). The occurrence and implications of the limit cycle on operation is discussed. A comparison of the results obtained here with the results of the ∞/∞ analysis of the direct sequence carried out in chapter 5 is given.

Chapter 8: Optimal Heat Distribution in Distillation
In this chapter investigations regarding optimal placement and duty distribution of internal heat exchangers in distillation columns have been carried out based on simulations. In particular the effect of adding 2, 4 and 19 internal heat exchangers to a 19 tray distillation column separating 2-propanol and methanol is studied. It is concluded that the minimum entropy production placement of the heat exchangers depends strongly on the degree of separation. The optimum is however rather flat, which indicates that optimal placement for a nominal operating point may remain nearly optimal in terms of entropy production even for significant changes in feed and product compositions. When compared to a conventional column run under the same operating conditions, entropy production for an optimally operating column with four thermally active stages (4TA) is reduced by 25 % as compared to 37 % for a column with six thermally active stages (6TA) column and 49 % for a column in which all the trays are equipped with heat exchangers.

References

Humphrey, J. L. and Siebert, A. F. (1992). Separation technologies. An opportunity for energy savings. *Chem. Eng. Prog.*, **88**(3), 32–41.

Mix, T. J.; Dweck, J. S.; Weinberg, M. and Armstrong, R. (1978). Energy Conservation in Distillation. *Chem. Eng. Prog.*, **74**(4), 49–55.

Pilavachi, P. A. (1996). Systems Modelling as a Design Tool for Energy Efficiency-Research within the European Union. *Comp. Chem. Engng.*, **20**(Suppl), 467–472.

2

Dansk Resumé

Denne afhandling indeholder forskningsresultater indenfor optimal design og operation af procesintegreret destillation.

Til trods for den relativ lave energieffektivitet (typisk kun nogle få procent) er destillationsprocesser stadig den suverænt mest anvendte separationsteknik i den kemiske- og petrokemiske industri. Således er energiforbruget, som har baggrund i destillationsprocesser, rapporteret så højt som 5-6% indenfor de industrialiserede lande, Pilavachi (1996). I USA er destillation skyld i mere end 3 % af den totale energi dissipation, Mix *et al.* (1978), Humphrey and Siebert (1992).

Den udbredte anvendelse af destillation sammenholdt med destillations lave energieffektivitet, øget efterspørgsel på miljømæssig neutrale teknologier, samt en generelt skærpet økonomiske konkurrence, fordrer produktions anlæg med højere grad af proces integration. Indenfor de seneste årtier er forskningsindsatsen indenfor proces integration forstærket med henblik på at opklare 'mysterierne' indenfor den ikke lineære statiske og dynamiske opførsel, såvel som de operationelle implikationer af integrerede processer og proces design.

Adskillige typer af steady state multipliciteter er kendt og generelt accepteret forekommende i kemitekniske processer. Udtrykket *multiplicitet* henfører til multiple stationære løsninger til et givet sæt af operations betingelser. Disse løsninger kan underinddeles i input, output, og state multiplicitet. Disse defineres som følger:

- Input multiplicitet forekommer når der til et givet sæt af output værdier eksisterer multiple løsninger i form af input værdier.
- Output multiplicitet forekommer når der til et givet sæt af input værdier eksisterer multiple løsninger i form af output værdier.
- State multiplicitet forekommer når der til et givet sæt af input **og** output værdier eksisterer multiple løsninger i form af interne tilstands værdier.

Med *output* forstås normalt kvalitetsvariable såsom eksempelvis produkt sammensætninger, hvor der med *input* typisk forstås manipulerbare variable såsom eksempelvis udvalgte strømningshastigheder.

Nærværende arbejde indeholder forskningsresultater fra fire forskellige emner indenfor integration af destillationsprocesser:

- Eksperimentel validering af input multiplicitet i binær energiintegreret destillation og dennes indflydelse på valg af regulator struktur.
- Analyse af ikke-lineær statisk opførsel af heterogene azeotrope destillationssekvenser.
- Undersøgelse af dynamiske implikationer fra ikke-lineære effekter i heterogen azeotrop destillation.
- Optimal design og duty distribution i energiintegreret destillation med interne varmevekslere.

Resultaterne for de enkelte kapitler i afhandlingen opsummeres nedenfor:

Kapitel 4: Eksperimentel Validering af Input Multiplicitet i Binær Destillation – Inflydelse på regulator struktur udvælgelse
I dette kapitel undersøges en input multiplicitet i binær destillation, ved brug af både simuleringsmodel for - og eksperimenter på et energiintegreret binær destillationsanlæg af industriel størrelse. Input multipliciteten forudsiges at forekomme indenfor det mulige operations område. Fra prædiktionerne forventes at separationsgraden går gennem et maksimum når boil–up øges, hvor alle andre input holdes konstante. Multipliciteten relaterer sig til destillationsegenskaberne for de indgående komponenter. I kapitlet rapporteres resultaterne fra tre udførte eksperimenter. Disse resultater verificerer eksistensen af den forudsagte input multiplicitet. Endvidere diskuteres reguleringsstrategi og udvælgelse af regulator konfiguration, med henblik på at undgå performance reducerende implikationer fra dette fænomen. De fremførte resultater viser at opmærksomhed og bevidsthed fra proces designere bør rettes imod dette forskningsområde, idet fænomenet medfører ændringer i operabilitet og stabilitet resulterende i perfomance reduceret operation.

Kapitel 5: Steady State Multipliciteter i Heterogen Azeotropisk Destillationssekvenser
Steady state multiplicitet i heterogene azeotrope destillationssekvenser studeres i dette kapitel. To passende sekvenser til dehydrering af ethanol (vha cyclohexane som entrainer) behandles som eksempler og sammenlignes. ∞/∞ analysen, som antager uendelig refluks strømningshastighed og uendelig antal destillationsbunde, bliver benyttet som basis og udvides til – og anvendes på heterogene azeotrope destillationssekvenser. Dette gøres for at bestemme steady state bifurkationsdiagrammer udfra thermodynamiske betragtninger. Bifurkationsdiagrammerne er meget forskellige for de to sekvenser på trods af deres beslægtede strukturer. Det prædikteres at output multiplicitet i den enkelte azeotrope destillationskolonne kan inducere output multiplicitet for en sekvens. Det prædik-

teres endvidere at output multiplicitet kan undgås ved at vælge en alternativ sekvens struktur. Ydermere forudsiger ∞/∞ analysen state multiplicitet for begge heterogene azeotrope destillationssekvenser. For ∞/∞ tilfældet vises det at state multiplicitet for heterogene azeotrope destillationssekvenser kan induceres af en enkelt destillationskolonne eller ved at slutte (sammenkoble) en sekvens. De prædikterede bifurkationsdiagrammer og multipliciteter underbygges gennem simuleringer med rigoristiske modeller af destillationssekvenser opererende med endelig refluks strømningshastighed og et endeligt antal destillationsbunde.

Kapitel 6–7: Dynamik af en Heterogen Azeotrop Destillationssekvens, Afsnit I–II

Bifurkationsanalysen for statiske løsninger foretaget i kapitel 5 udvides med en bifurkationsanalyse på en rigoristisk dynamisk destillationsmodel af den 'direkte' sekvens. Den dynamiske opførsel i ikke-trivielle dele af operationsområdet behandles vha dynamisk simulering.

Den primære bifurkationsparameter i undersøgelsen er refluksforholdet for den azeotrope destillationskolonne. Tilstedeværelsen af output multipliciteten fundet i kapitel 5 underbygges af den udførte bifurkationsanalyse. De multiple løsninger forekommer i et typisk hysterese forløb, dvs. stabile stationære løsninger med høj og lav produkt renhed eksisterer samtidig, og disses tiltrækningsområder (eng: 'basins of attraction') adskilles af en ustabil stationær løsning med mellemliggende produkt renhed. Når sammensætningsprofiltypen skifter, i særdeleshed der hvor optimal renhed af ethanol produktet opnås (state multiplicitet), bevæger en reel egenværdi sig meget tæt på imaginær aksen. Et skift i sammensætningsprofiltype resulterer således i en meget langsom åben–sløjfe dynamisk opførsel. Resultaterne fra bifurkationsanalysen indikerer at kompleks dynamisk opførsel forventes at forekomme i grænseområdet hvor væskefasen splitter op.

Simuleringerne i afsnit II udvider bifurkationsanalysen for den heterogene azeotrope destillationssekvens, der blev udført i afsnit I. De dynamiske simuleringer for denne sekvens udføres ved brug af rigoristiske modeller implementeret i en dynamisk simulator. Refluks forholdet for den azeotrope kolonne vælges igen som variationsparameter. Resultaterne fra simuleringerne afslører at vedvarende oscillationer forekommer for den 'direkte sekvens' i en omegn tæt på og på den anden side af grænseområdet, hvor væskefasen splittes i dekanteren. Dette er den første grænsecyklus som rapporteres i litteraturen omhandlende heterogen azeotrop destillation. Oscillationerne rapporteret her forudsiges at eksistere i et bredt område af reflux forhold. Resultaterne indikerer tydeligt at den stabile periodiske løsning afgrænses af en cyklisk fold bifurkation og en 'blue sky' katastrofe (global bifurkation). Forekomsten og implikationerne af grænsecyklussen på operationen diskuteres. Endelig præsenteres en sammenligning af de opnåede resultater med resultaterne fra ∞/∞ analysen for den 'direkte sekvens' foretaget i kapitel 5.

Kapitel 8: Optimal Varmefordeling i Destillation
Dette kapitel omhandler undersøgelser vedrørende optimal placering og varmefordeling af interne varmevekslere i destillationskolonner. Disse undersøgelser er foretaget på basis af simuleringer. I kapitlet studeres effekten af at tilføje 2, 4 og 19 interne varmevekslere til en 19 bunds destillationskolonne som adskiller 2-propanol fra methanol. Det konkluderes at placeringen af interne varmevekslere hvor minimal entropiproduktion opnås er stærkt afhængig af separationsgraden. Optimum (minimal entropiproduktion) er dog forholdsvis fladt, hvilket indikerer at optimal placering for et nominelt operationspunkt kan forblive nær optimalt med hensyn til entropiproduktion, selv for signifikante ændringer i føde – og produktsammensætninger. Sammenlignes med en konventionel destillationskolonne under samme operationsbetingelser, kan entropiproduktionen reduceres med 25% for en optimal opererende kolonne med 2 interne varmevekslere. Til sammenligning er reduktionen på 37% for en destillationskolonne med 4 interne varmevekslere og 49% for en kolonne hvor alle 19 destillationsbunde er udstyret med interne varmevekslere.

Referencer

Humphrey, J. L. and Siebert, A. F. (1992). Separation technologies. An opportunity for energy savings. *Chem. Eng. Prog.*, **88**(3), 32–41.

Mix, T. J.; Dweck, J. S.; Weinberg, M. and Armstrong, R. (1978). Energy Conservation in Distillation. *Chem. Eng. Prog.*, **74**(4), 49–55.

Pilavachi, P. A. (1996). Systems Modelling as a Design Tool for Energy Efficiency-Research within the European Union. *Comp. Chem. Engng.*, **20**(Suppl), 467–472.

Contents

3

Introduction

3.1 Motivation

In the view of economic competition and environmental safety regulations, process industries are subject to an incessant pressure to improve the production economy and provide sustainable production methods with the application of environmentally 'neutral' technologies. In this race some companies find that their competitive capacity may be significantly improved by building a deeper understanding of the manufacturing processes and their integration.

The gained knowledge can be exploited for operating the resulting process integrated system optimally. For many productions there is a tight connection between production economy and the establishment of manufacturing processes with no or only little impact on the environment. In particular this applies for productions where energy intensive separation methods, such as eg. distillation, are used. Tight integration of processes or optimality for integrated processes however is giving rise to operational problems, since the system may be more difficult to operate and control.

The tendency to obtain complex or undesired nonlinear behavior of integrated process plants is traditionally handled by overdesign of equipment within the process design community. From a manufacturing community point of view the common practice in dealing with this type of behavior, is backing off from the optimal operating point in order to ensure good behavior (controllability), at the cost of operating the plant suboptimally.

Obviously a systematic approach with the integration of process design, operational optimization and controllability issues may prove to be very competitive, since such an approach may bring about significant reduction in the equipment- and operational cost, increase efficiency and provide environmentally sustainable solutions. Within the last two decades an increasing effort has been made in attempting to clear up the "mysteries" of plant nonlinear statics and dynamics as well as operational implications of integrated processes and process designs.

The task of developing this systematism naturally is a major challenge.

Evidently, a completely automated - 'push the button' type of - framework is hardly likely to be developed in the immediate near future, and the presented work in this thesis does not aim at getting 'the final answers' to a systematic approach of integrating process design, operational optimization and control design. The approach taken here however is systematical and it exploits methods and tools which profitably may be incorporated in such a framework. The approach reveals nonlinear dynamical behavior and operational implications, which such a process systems engineering framework needs to be able to handle.

3.2 Purpose

With the above motivation in mind, the purpose of the present work is to gain knowledge of nonlinear effects and consequential dynamic implications in distillation when process integration and optimal operation is considered. This knowledge should be incorporated and applied in the selection and design of a suitable control scheme.

In order to understand the behavior of process integrated distillation, investigations and understanding of simple binary distillation need to be carried out. The knowledge obtained for a simple case may prove to be valuable as well as extendable to a more complex case.

Moving up in dimension of the composition space as well as in complexity, an important issue in process integration of distillation processes is design and operation of heterogeneous azeotropic distillation. Heterogeneous azeotropic distillation is carried out at lower temperatures than homogeneous azeotropic distillation with a heavy entrainer. In terms of energy exploitation this is much more effective. Heterogeneous azeotropic distillation may typically be performed at approximately 100°C instead of more than 200°C for homogeneous azeotropic distillation. In reality azeotropic distillation is at least a two-step procedure most often with recycle of entrainer. Thus the subject of interactions of process integration becomes inevitably important.

Process integration can provide significant energy savings. The energy efficiency for distillation processes is typically only a few percent ($\approx$ 5 %). Another purpose of this project is to investigate optimal design and operation for the maximization of exergy efficiency. Investigations will be made on energy optimal design by process integrating distillation, by optimizing the coupling between the mass transfer and energy transfer. Also establishment of bounds for maximum achievable performance in terms of exergy efficient distillation will be touched upon.

The more specific investigations will include:

1. Study of a static input multiplicity in binary distillation caused by changes in equilibrium conditions from pressure changes. Furthermore study the implications on dynamics and control design of this input multiplicity.

2. Bifurcation analysis for different sequence designs of heterogeneous azeotropic distillation.

3. From knowledge of the bifurcation mappings of 2, investigate the nonlinear dynamics and operational implications of heterogeneous azeotropic distillation.

4. Investigation of optimal design for exergy efficient binary distillation.

3.3 Main contributions

In this work the main contributions made to the field of optimal design and operation of process integrated distillation are:

1. Experimental verification of a steady state input multiplicity in binary distillation caused by changes in equilibrium conditions from pressure changes.

2. Extension and application of the ∞/∞ analysis method to heterogeneous azeotropic distillation sequences in order to determine steady state bifurcation diagrams from thermodynamic considerations.

3. A thorough (but by no means complete) analysis of the dynamics of a heterogeneous azeotropic distillation sequence, in which physical insight is used in the explanation of the dynamic phenomena observed.

4. Demonstration of that nonlinear process dynamics and controllability issues need to be dealt with during process design and operational optimization of process integrated distillation.

5. Demonstration of optimal placement and duty distribution of internal heat exchangers in binary distillation columns.

3.4 Publications

During the project, a number of articles have been published or prepared for publication. Furthermore a number of papers have been published at conferences with reviewed proceedings. The list of publications is given below, with indication of corresponding chapters where possible.

Articles published/prepared for publication in international journals:

1. *Multiple Steady States in Heterogeneous Azeotropic Distillation Sequences.* K. Esbjerg, T.R. Andersen, S.B. Jørgensen, D. Müller and W. Marquardt, *Industrial & Engineering Chemistry Research*, 37, pp. 4434-4452 (1998). Chapter 5 in thesis.

2. *Principles of Control Thermodynamics.* P. Salamon, J. D. Nulton, G. Siragusa, T. R. Andersen, and A. Limon, *Energy*, 26, 307-319 (2001).

3. *Positioning heat exchangers in binary tray distillation using isoforce operation.* G. de Koeijer, S. Kjelstrup, H. van der Kooi, B. Gross, K.F. Knoche and T.R. Andersen, *Energy Conversion and Management*, 43, 1571–1581 (2002).

4. *Experimental Validation of an Input Multiplicity in Binary Distillation – Influence on Control Structure Selection.* T.R. Andersen, L.H. Wen, A. Koggersbøl and S.B. Jørgensen, manuscript in preparation for publication (2002). Chapter 4 in thesis.

5. *Analysis of the Dynamics of a Heterogeneous Azeotropic Distillation Sequence I-II.* T.R. Andersen, M. Brøns and S.B. Jørgensen, manuscript in preparation for publication (2002). Chapters 6 and 7 in thesis.

Reviewed Conference Proceedings:

1. *An Output Multiplicity in Binary Distillation : Experimental Verification.* A. Koggersbøl, T. R. Andersen, J. Bagterp and S. B. Jørgensen, *Computers in Chemical Engineering*, 20, S835–S840 (1996).

2. *Towards Integration of Controllability into Plant Design.* S.B. Jørgensen, R. Gani and T.R. Andersen, *Proceedings MED-99 Conference*, Israel (1999).

3. *Positioning heat exchangers in binary tray distillation using isoforce operation.* G. de Koeijer, S. Kjelstrup, H. van der Kooi, B. Gross, K.F. Knoche and T.R. Andersen, *Efficiency, Costs, Optimization, Simulation and environmental aspects of energy systems (ECOS'99)*, Tokyo, 471–476, ISBN: 4-9980762-0-5 (1999).

4. *Energy Efficient Distillation by Optimal Distribution of Heating and Cooling Requirements.* T.R Andersen, G. Siragusa, B. Andresen, P. Salamon, and S.B. Jørgensen. *Computer Aided Chemical Engineering*, 8, Elsevier, pp. 709–714, (2000). Chapter 8 in thesis.

5. *Distillation Control using Passivity.* D.P. Coffey, E.B. Ydstie, T.R. Andersen and S.B. Jørgensen, 2001, *Computer Aided Chemical Engineering*, 9, Elsevier, pp. 627-632 (2001)

3.5 Outline

The chapters of this thesis have been organized as a collection of five articles. Then follows a chapter summarizing the conclusions. Lastly appendices for the different chapters are given. Since the aim of the main body of this thesis is to provide the reader with a set of practically independent articles, the reader is warned that reiterations on the opening, introduction and background to some of the chapters may occur.

In chapter 4 one aspect of the static behavior of simple binary distillation is treated. In particular an input multiplicity caused by changes in equilibrium conditions from pressure changes is investigated and experimentally verified. The implications on operation and control structure selection is discussed.

The subject of chapter 5 is the static behavior of heterogeneous azeotropic distillation sequences.

Chapters 6 and 7 builds on the information obtained in chapter 5. An investigation of the dynamics of one of the heterogeneous azeotropic distillation sequences treated in chapter 5 is carried out in these two chapters (6 and 7). Part I (chapter 6) presents a bifurcation analysis of the sequence. In part II (chapter 7) the same sequence is simulated dynamically. The two chapters will benefit from being read in conjunction.

Chapter 8 examine the optimal design and behavior of distillation columns with exergy efficient design.

Finally chapter 9 sums up the major conclusions of this work and suggests future work.

4

Experimental Validation of Input Multiplicity in Binary Distillation

Influence on Control Structure Selection

Steady state multiplicities are known to occur within multicomponent distillation. Also in simple binary distillation output multiplicities have been reported and experimentally verified. These phenomena have received only limited interest within the process design community. In this chapter, an input multiplicity in energy integrated binary distillation is investigated using both simulation models and experiments on an industrial size pilot plant. The findings show that attention from the process design community should be drawn to the research field of nonlinear phenomena analysis, since the implications are changes in operability and stability, which result in performance reducing behavior. The input multiplicity is predicted to occur within the feasible operating window. From the predictions the degree of separation is expected to go through a maximum when boil up is increased keeping all other inputs constant. The input multiplicity is related to the binary distillation properties. Three experiments were carried out. The results from these experiments clearly verify the existence of the proposed input multiplicity. The influence of variations in tray efficiency due to entrainment on the input multiplicity is discussed. Control strategy and configuration selection issues to reduce or possibly avoid performance reducing implications of these phenomena are discussed.

4.1 Introduction

For chemical production and refinement plants process integration - in particular energy integration - represents a large potential for energy savings. However, the increase in complexity caused by energy couplings thus introduced may change plant characteristics drastically and thereby have significant impact on plant control configuration and on operability and hence on achievable plant performance.

Distillation columns are very often included in energy integration networks. The other members of such a network could be different types of process equipment, or the network could consist in a train of distillation columns alone. In the simple case energy coupling could be established just between the first and the last column in such a column train. The ultimate degree of energy integration for distillation columns is integration of condenser and reboiler of a single column through a direct or indirect heat pump. In this chapter the study of a distillation column integrated with an indirect heat pump reveals some general characteristics of energy integrated distillation plants. The characteristics of interest are those which affect the operability of distillation columns. Here two steady state aspects are pertinent for binary distillation:

- Output multiplicity: The existence of multiple steady state solutions in terms of system outputs when the inputs are specified constant.
- Input multiplicity: The existence of multiple steady state solutions in terms of system inputs when the outputs are specified constant.

The dynamic consequence of output multiplicity is the occurrence of open loop unstable poles, which must be stabilized through control. This phenomenon has been investigated theoretically by Jacobsen and Skogestad (1991). They found that output multiplicity for binary distillation may arise from singular points in the nonlinear conversion between mass or volumetric flow rates and molar flow rates. This type of output multiplicity was experimentally verified by Kienle *et al.* (1995) and Koggersbøl *et al.* (1996).

A possible dynamic consequence of input multiplicity is the occurrence of right half plane zeroes, which in case of multi–loop control may give rise to an unstable closed loop behaviour. Thus to facilitate selection of control strategy and configuration it is most relevant to investigate also this phenomenon both for conventional binary distillation and for energy integrated distillation.

The purpose of this chapter is to investigate the possible occurrence of input multiplicity for an energy integrated distillation plant. This investigation is carried out using first a simulation model in order to reveal the phenomena behind the multiplicity. Thereafter experimental verification of this multiplicity is undertaken and their practical relevance is discussed.

4.2 Background

In Koggersbøl (1995) the distillation pressure dynamics and the operational implications thereof was investigated. During this analysis, simulations revealed that the degree of separation may go through a maximum

when the heat to the reboiler, Q_B, is gradually increased, keeping all other inputs constant. The input multiplicity was simulated for constant stage efficiency and thus the multiplicity has to be related to a trade off in separation properties between higher pressure and higher boil up (Koggersbøl (1995)).

Assuming that the column pressure is allowed to float and that separation improves with decreasing pressure, an increase in the heat input to the reboiler (keeping all other inputs constant) gives rise to two opposing effects:

Effect 1: The first effect may be visualized in a McCabe–Thiele diagram as a change of the operating lines, thereby giving better separation as illustrated in Figure 4.1. Here a saturated liquid feed mixture of composition z_F is separated into 2 products of composition x_D and x_B. As the vapor flow rate is gradually increased, the slopes of the operating lines approaches the diagonal, thus resulting in fewer ideal equilibrium stages necessary to obtain the specified purities, i.e. enhanced product purity for a fixed number of stages.

Effect 2: The second effect is pressure impact on separation, i.e. increased pressure due to higher internal flow rates, for many mixtures including the one investigated here, alters (flattens) the equilibrium curve. This second effect yields a more difficult separation as the relative volatility is decreased as illustrated in Figure 4.2.

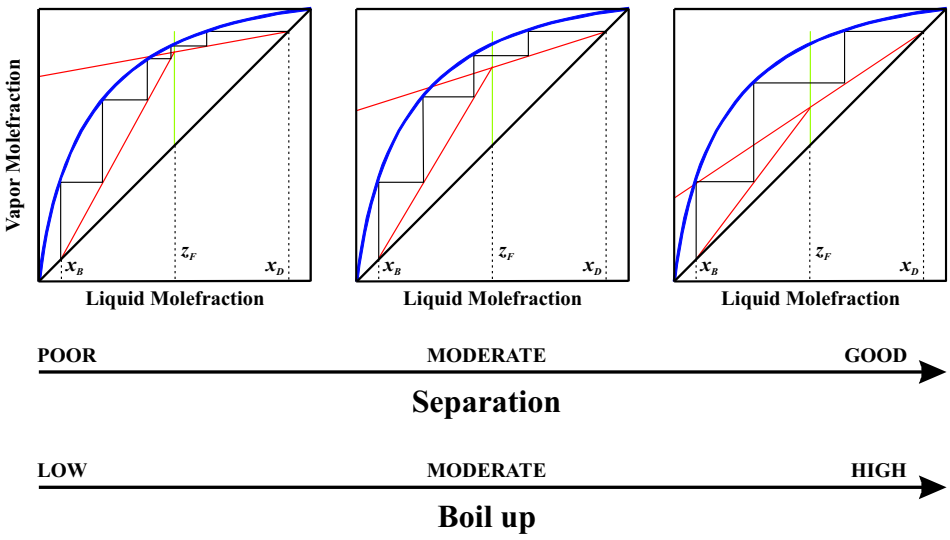

Figure 4.1. Illustration of how boil up affects the slopes of operating lines in the McCabe-Thiele diagram.

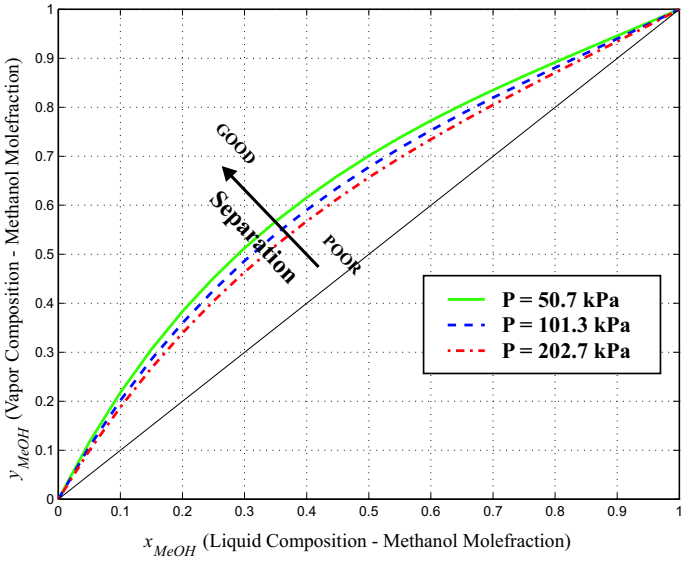

Figure 4.2. Illustration of how pressure affects the vapor-liquid equilibrium of the methanol-isopropanol system. Vapor-liquid equilibrium calculated by the original UNIFAC method. Vapor pressure evaluated by the Antoine equation.

At low to moderate vapor flow rates an increase in the heat input to the reboiler will give better separation since the first effect is dominating. However in search for still higher bottom purity, possibly trying to exploit the column beyond design specifications, one would increase the vapor flow rate further. But a point will be reached where the operating line is not improved significantly, while the column pressure is still very much a function of the boil up. Effect 2 then becomes dominant over effect 1, meaning that the steady state gain sign (x_B/Q_B) becomes negative. The process remains stable in open loop.

This trade off between the two effects is studied more closely in this chapter. First a plant description of the experimental facility used in the validation experiments is given. Second the main results of a simulation study carried out by Koggersbøl (1995) are given. Then follows a section where experimental design and necessary plant modifications made in order to perform the validation experiments are described. The experimental results are presented and discussed in the preceding section. Subsequently a discussion of the practical implications of the input multiplicity on plant operation and control structure selection is given, and finally the main conclusions of this work are presented.

4.3 Distillation Plant Description

Figure 4.3 shows a schematic of an energy integrated distillation plant suitable for separating a mixture of methanol and isopropanol. The plant consist of a distillation column, a thermosiphon reboiler, a total condenser and a reflux drum. The column has 19 sieve trays. In order to reduce energy consumption, the reboiler and condenser are energy integrated through a heat pump. The heat pump transfers the energy released from the condenser to the reboiler. The experimental facility is located at the Department of Chemical Engineering at the Technical University of Denmark.

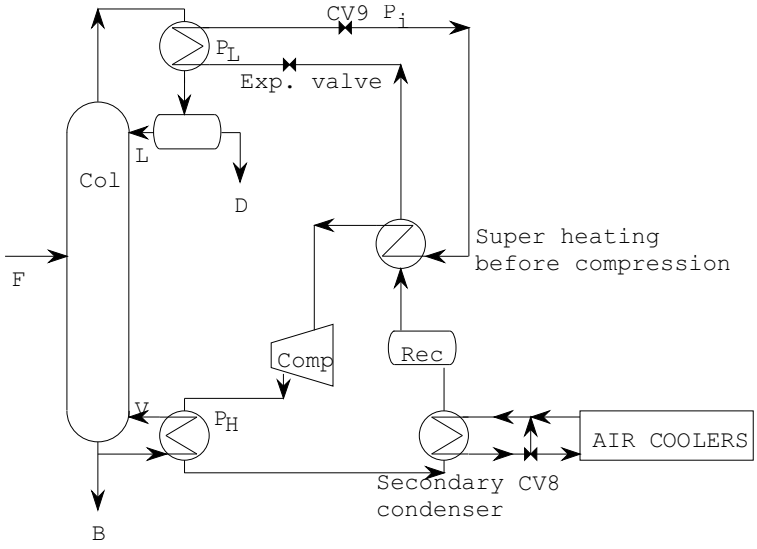

Figure 4.3. Schematic flow sheet of the plant.

On trays 1, 5, 10, 15 , and 19 PT100 temperature sensors are located in the liquid hold-up. In combination with pressure measurements (located in column bottom, on tray 10 and in column top) the temperature measurements are used for concentration estimates. All flows in and out of the system and the reflux flow rate are measured on a mass basis. Feed, bottom product, and distillate are sampled manually (at steady state) for later gas chromatography analysis.

The heat pump has an expansion valve (Exp.valve) which throttles high pressure liquid freon to a lower pressure (P_L) suitable for evaporation in the condenser. After the condenser there is a control valve (CV9) by which the freon vapor flowrate can be manipulated. After superheating the vapor the compressor elevates the pressure to a high pressure (P_H) suitable for condensation in the reboiler. A small part of the condensation takes place in a secondary condenser which by a cooling water circuit is connected to a set of air-fan coolers. The cooling rate can be manipulated

by the control valve CV8, thus controlling P_H. Through a storage tank (Rec) and the super heater heat exchanger the freon circuit is closed at the expansion valve.

The basic control configuration for the plant is as follows: The high pressure P_H is controlled by CV8, the low pressure P_L is controlled by CV9, accumulator level is controlled by L, and reboiler level is controlled by B. Q_B and Q_C are then manipulated through the setpoints to P_H and P_L since these indirectly affect the temperature gradients of the reboiler and the condenser. The concentration profile is manipulated in the high gain direction by D, and in the low gain direction by a combination of P_H and P_L by which column pressure is also controlled. Thus, this configuration resembles the standard (D, V)-configuration which is open loop stable.

4.4 Simulation Study

Koggersbøl (1995) developed a detailed rigorous model suitable for simulating the distillation plant sketched in figure 4.3. The main assumptions for the model were:

- Quasi stationary ideal vapor phase
- Vapor-liquid equilibrium calculated by original UNIFAC
- Constant stage efficiency of 60% on all trays (estimated from experimental data)
- Constant heat of vaporization throughout the column
- Pressure drop across trays calculated by the correlations of Zuiderweg (1982)

A possible dynamic consequence of input multiplicity is the occurrence of right half plane zeroes, which in case of multi–loop control may give rise to an unstable closed loop behaviour. Thus to facilitate selection of control strategy and configuration it is most relevant to investigate also this phenomenon both for conventional binary distillation and for energy integrated distillation.

Koggersbøl (1995) showed by simulations, the development of the real part of the right most eigenvalue when varying boil up under two point product composition control for different pressure control schemes. The three pressure control schemes simulated were:

- No control of column pressure
- Pressure control of top tray pressure

- Pressure control of bottom tray pressure

The simulations showed for increasing boil up rate, that when both product compositions were controlled (after having changed the boil up in open loop), eigenvalues with positive real part eventually occurred in the case of column pressure floating and for top pressure controlled.

The real parts of the eigenvalues, in the case of bottom pressure controlled, however remained negative. This is seen in figure 4.4.

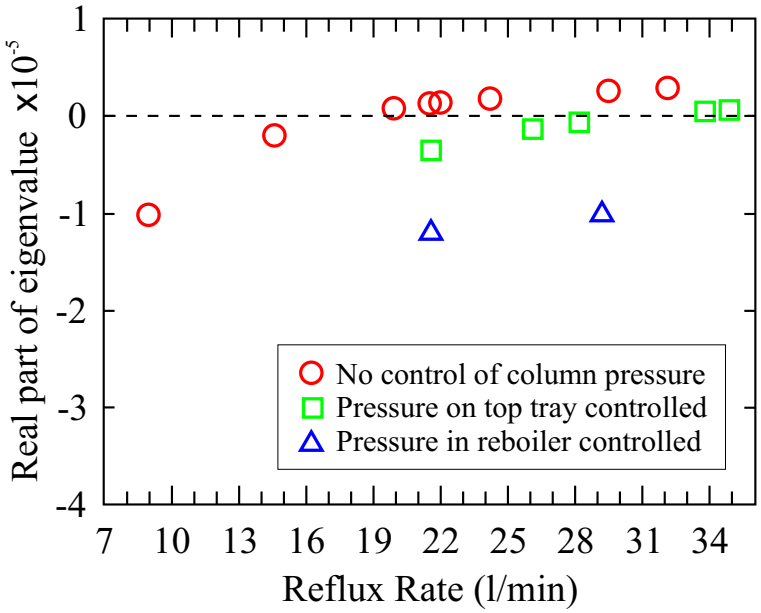

Figure 4.4. Real part of the "right most" eigenvalue of the plant model plotted as a function of the reflux rate. x_D controlled by D, x_B controlled by P_H (corresponding to Q_B). (Data from Koggersbøl (1995))

Koggersbøl (1995) also showed the input multiplicity for a simpler example. The plant modelled here was the same as displayed in figure 4.3, except with no heat pump connected.

The aim of this work is to experimentally investigate this input multiplicity.

4.5 Experimental Design

The optimum for the separation is expected to be relatively flat. Thus the experiments have the risk of being 'clouded' by or at best very sensitive to inaccuracies in flow measurements and feed composition disturbances. Early attempts to verify the input multiplicity failed due to such circumstances. Therefore two significant improvements of the plant had to be undertaken before the experimental validation could be carried out:

- Consistent and highly accurate flow measurements
- Possibility of maintaining constant feed composition throughout the experiment

The first improvement was accomplished by implementing mass flow measurements based on the Coriolis effect on all external flows and on the reflux flow, replacing the original turbine volumetric flow measurements. This is expected to reduce the experienced flow rate deviations of 10-30% relative to about 0.2 % relative (according to the manufacturer of the Coriolis flow meters). The second improvement was obtained implementing a 8 m^3 large feed tank with an electrical agitator and purchasing additional amounts of feed constituents. Even though a total feed mixture of 8000 liters does not last an entire experiment, the amount of feed is roughly 15 times larger than the total holdup of the distillation plant under the given operating conditions (reboiler: 300 liters + 19 trays: 150 liters + reflux drum: 50 liters), thus allowing to record several steady states with the same feed mixture. Mixing of new feed during experiments of this character is therefore still necessary, but the process of mixing is improved by the agitator on the facility.

4.5.1 One-point Composition Control

As previously mentioned, the optimum for the degree of separation is expected to be flat. It may therefore be desirable that an increase/decrease in the degree of separation reflects in both the top product and the bottom product purity, thus eliminating 'noise' from shift in the location of the composition profile. It was therefore decided to fix the composition profile at an interior point within the column. Therefore the estimated methanol mole fraction at tray 15, X_{PTT15}, is controlled by manipulating the distillate flow rate, D. The effect of changing the degree of separation should thus best be seen in the composition of the bottom product, since the concentration profile is "fixed" at tray 15 (setpoint 0.75), thus leaving the change in the degree separation over the sum of 15 trays to be reflected mostly in the bottom product composition.

4.5.2 Pressure Control

Two pressure control configurations are used. In order to investigate the findings of Koggersbøl (1995) top pressure is controlled through most of the experiments, but also a switch in the configuration to bottom pressure controlled is carried out.

4.6 Experimental Results

3 experiments were carried out (February 14th–18th 2000, October 27th–31st 2000 and November 14th–19th 2000). During these experiment, lasting a total of more than 318 hours, 23 steady states were obtained. For 22 of these the distillate, the bottom product and the feed flow where sampled for later analysis on a gas chromatograph. In table 4.1 the list of experiments is given together with the duration, number of steady states obtained and the feed flow rate during the experiments.

Name	Time	Duration [hrs]	Feed flow rate [kg/hr]	Steady states obtained
I	14–18 Feb. 2000	89	66	7
II	27–31 Oct. 2000	114	70	7
III	14–19 Nov. 2000	115	110	9

Table 4.1. Input multiplicity experiments carried out in 2000.

A collection of dynamic experimental data, steady state measurement means and standard deviations, time ranges specification of the individual steady states obtained during these experiments and GC results are given in appendix A.

All measurements are subject to errors. Measurements with inaccuracies may lead to inconsistent data. In order to obtain consistent data sets, where overall mass and component balances are respected, the experimental data and the results from the GC analyses were reconciled.

4.6.1 Data Reconciliation

It is important to note that measurement errors are divided into two categories: random errors and gross errors. Random errors are independently and normally distributed with zero mean. All other errors than random errors are termed gross errors. Gross errors can for example be instrument bias.

The difficult part in data reconciliation is to choose the right objective function to minimize. Several objective functions have been proposed earlier when reconciling experimental data. It can be shown that minimization of the following objective function provides the most reasonable data reconciliation if there are no gross errors present , Bossen (1995):

$$G = \sum_i \left(\frac{y_i^m - y_i^f}{\sigma_i}\right)^2 \tag{4.1}$$

where y_i^m is the measured value, y_i^f is the calculated fitted value and σ_i is the standard deviation of measurement i. One way to compensate for the effect of gross errors is to perform the data reconciliation twice, using the first reconciliation to identify gross errors and subsequently correct for them, Bossen (1995).

The objective function used for reconciliation of the data from the multiplicity experiments is

$$G = \sum_i \left(w_i(y_i^m - y_i^f)\right)^2 \tag{4.2}$$

where w_i is the weight for measurement i. Only the overall mass and component balances are reconciled. The measured variables are:

$$\begin{aligned} \mathbf{y}^m &= \begin{bmatrix} y_1^m & y_2^m & \dots & y_8^m & y_9^m \end{bmatrix}^T \\ &= \begin{bmatrix} x_{MeOH,F} & x_{MeOH,D} & x_{MeOH,B} \\ \dots & x_{PrOH,F} & x_{PrOH,D} & x_{PrOH,B} \\ \dots & F & D & B \end{bmatrix}^T \end{aligned} \tag{4.3}$$

The minimization of the objective function 4.2 is performed subject to the following overall mass and individual component constraints:

$$\begin{aligned} 0 &= F - D - B \\ 0 &= Fx_{MeOH,F} - Dx_{MeOH,D} - Bx_{MeOH,B} \\ 0 &= Fx_{PrOH,F} - Dx_{PrOH,D} - Bx_{PrOH,B} \end{aligned} \tag{4.4}$$

The true standard deviation reflects the scaling of the variables, such that it is possible to compare flow rates and compositions. The true standard deviation however is not known for the measured variables. The standard deviation calculated from the measurements at steady state is used for this purpose. The quality of this approximation is questionable, since the standard deviations for the mass flows have been calculated from typically the last 60 minutes (sampling every 30 or 60 seconds) before the steady state has been established, whereas the standard deviations for the compositions of the three flows are calculated from 3 determinations (the minimum number of determinations in order to do statistics) on each of the flow samples taken at steady state. This means the calculation of the standard deviation of the composition measurement depends on one sample only.

Since only 3 GC-measurements have been carried out on each of the 3 sampled streams from every steady state, the measured standard deviation might differ significantly from the true standard deviation. It is therefore proposed to use the reciprocal means of the standard deviations for each of the composition variables as weights for the compositions. The means

of standard deviations for each composition variable are found from the measured GC standards:

$$\begin{aligned}\bar{\sigma}_{\mathbf{x}} &= \begin{bmatrix}\bar{\sigma}_{x_{MeOH,F}} & \bar{\sigma}_{x_{MeOH,D}} & \bar{\sigma}_{x_{MeOH,B}} \\ \bar{\sigma}_{x_{PrOH,F}} & \bar{\sigma}_{x_{PrOH,D}} & \bar{\sigma}_{x_{PrOH,B}}\end{bmatrix} \\ &= \begin{bmatrix}0.0037 & 0.0031 & 0.0013 & 0.0040 & 0.0031 & 0.0020\end{bmatrix}\end{aligned} \tag{4.5}$$

Similarly the reciprocal means of the standard deviations for each of the external mass flow rates are used as weights in the reconciliation. The means of the standard deviations for the external mass flow rates for all obtained steady states are:

$$\begin{aligned}\bar{\sigma}_{\mathbf{mass}} &= \begin{bmatrix}\bar{\sigma}_F & \bar{\sigma}_D & \bar{\sigma}_B\end{bmatrix} \\ &= \begin{bmatrix}0.0022 & 0.0012 & 0.0020\end{bmatrix}\end{aligned} \tag{4.6}$$

4.6.2 Comments to GC Analyses

The believed high uncertainty with respect to the results from the GC analyses are thought to originate from the facts that:

- The samples where not refrigerated during storage after the experiments and the samples from all 3 experiments where stored for a long time (12-21 months) before they where analyzed at the same time on gas chromatograph. The reason for the long lasting storage was lack of appropriate gas chromatograph equipment as well as human resources for carrying out the analyses. The lack of refrigeration during the long-term storage combined with lids on sample glasses not being 100 % tight (i.e. rubber packing within lids dried out on some of the older glasses), may have caused the samples to become somewhat "flat". Especially the top product samples may have suffered from this, due to the high contents of the highly volatile methanol. This is supported by the fact, that the analyzed composition deviates considerably from the on-line estimated mole fraction on tray 19 (from experience this is normally not the case – since the mixture is of high purity and very close to binary, thus Rault's law being used in the on-line estimation is a fairly good approximation).

- The equipment for the GC analyses did not include an autosampler. Thus the analyses had to be carried out with the manual injection of the samples with syringe. This method is known to be very sensitive towards small changes in the execution of the injection, and may introduce significant deviations. The variation in the calculated standard deviations for the GC results for the different samples also point in this direction.

- The reliability of the gas chromatograph equipment left somewhat to be desired. Variations in carrier gas flow rate, defect injection

membranes and other discrepancies where detected during the analyses. These unfortunate circumstances where of course attempted rectified when discovered.

- Traditional gas chromatography is known to be moderately accurate for quantitative analysis purposes. Skoog *et al.* (1988) reports precisions of 0.5 to 1% relative when using the internal standard method. The advantage of course on the other side, is that gas chromatography is "fast and easy" to carry out, as well as relatively inexpensive.

4.6.3 Quality Evaluation of Data Sets

The dominant time constant, τ_{1c} (see Skogestad and Morari (1987) and Skogestad and Morari (1988)), for the distillation column has been estimated from the obtained experimental plant data (see appendix A, section A.6). The results from the first two experiments (I and II) have to be considered with some caution. The dominant time constant for the operating conditions used in the two first experiments vary from 10.7 to 16.3 hours. The period of time for obtaining some of the "steady states" in experiment I is unfortunately questionable. The supposedly steady states 3, 4 and 6 from experiment I were achieved after 6.5 hrs, 5.7 hrs and 6.7 hrs respectively (dominant time constant being 14.0, 13.8 and 16.0 respectively) – even assuming 'perfect' control of all loops, obtaining complete steady state for the mentioned periods of time is not likely. In comparison the dominant time constant for experiment III vary from 6.8 to 7.8 hours where the fastest obtained steady states were steady states 6 and 9 achieved after a time span of 7.7 hrs and 7.8 hrs respectively.

Of the 22 reconciled 'steady state' data sets, 5 sets were sorted out as outliers for different reasons:

- The first data set of experiment I has been disqualified, since the net flow rate ($F - D - B$) was 8.5 % of F, thus giving a solid indication that steady state had not been reached for these operating conditions (in comparison, the net flow rate for the remaining 'steady states' obtained varies from 0.5 to 3.9 % of F).

- The data sets of steady state 7 of experiment I and steady state 6 of experiment II were obtained with a very low vapor flow rate (V (condensed) < 0.5 m^3/hr). These data sets were sorted out due to the fact that they go below the vapor flow rate were weeping is known to occur, and these sets are thus treated as outliers.

- The first data set of the experiment II has presumably not been taken at true steady state. Indications of this is that the net flow rate was 3.4 % of F before the data reconciliation, and also the

differential pressure over the column differ significantly from the remaining points obtained during this experiment. The differential pressure is known from experience to be one of the last variables settling at a steady state value.

- The data set of steady state 4 of experiment III had to have the product flow rates corrected by 10.6 % and -6.7 % (B and D) during the data reconciliation. Thus this data set was sorted out as being an outlier. Possible reasons for the bad data set are the operating point not being steady or compositions of samples being erroneous or noisy determined through GC analysis.

4.6.4 Top pressure controlled

In figure 4.5 the pressure difference over the distillation column for all 3 experiments have been plotted against the reflux flow rate.

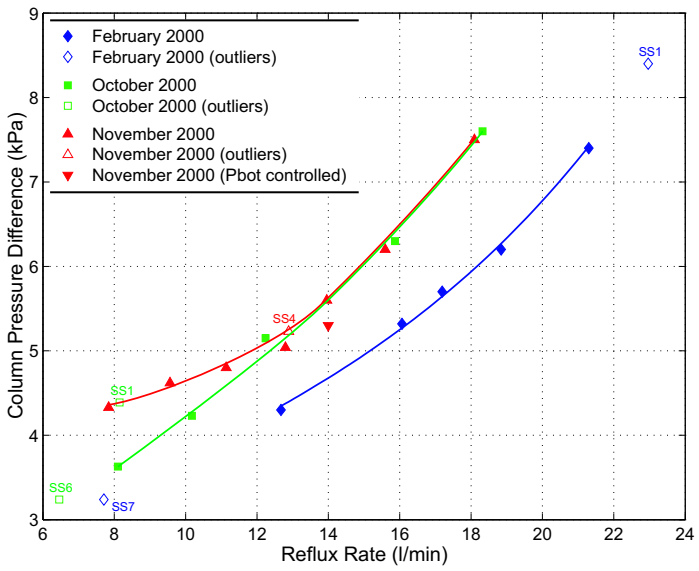

Figure 4.5. Column pressure drop vs. reflux flow rate for the 3 input multiplicity experiments.

It is seen that the first experiment (I) gives rise to a somewhat different correlation between column pressure difference and reflux flow rate. The reason for that is that for the first experiment merely a turbine flow meter was available for measuring the reflux flow. It is not only seen that this flow measurement is somewhat biased compared to the more accurate Coriolis flow meter measurements of the latter experiments, but it is also obvious that the bias is not constant over the measured range.
After having replaced the flow meter of the reflux it is evident that the pressure drop at higher reflux rates is reproducible judging from the results of experiments II and III. The reason for the higher pressure drop at lower reflux rates for experiment III is that this experiment had a higher feed

flow rate (110 kg/hr) than experiment II (70 kg/hr). At lower reflux rates the difference in feed flow rate becomes more pronounced in the pressure drop than for higher reflux rates.

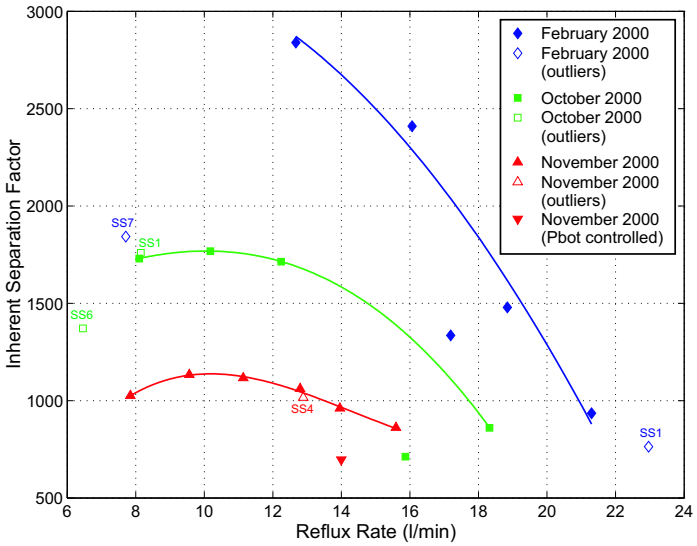

Figure 4.6. Inherent separation factor vs. reflux flow rate for the 3 input multiplicity experiments.

Figure 4.6 displays the inherent separation factor versus the reflux flow rate. The inherent separation factor has for the particular purpose been defined as:

$$\alpha^{S}_{MeOH,PrOH} = \frac{x_{MeOH,D}/x_{PrOH,D}}{x_{MeOH,B}/x_{PrOH,B}} \tag{4.7}$$

It is seen from figure 4.6 that the slope of separation for high reflux rates increases as the feed flow rate is decreased (Nov. exp. (III) $\rightarrow$ Oct. exp. (II) $\rightarrow$ Feb. exp. (I)), which is physically plausible, since the reflux ratio increases with decreasing feed flow rate.

It is obvious from the figure, that the results from experiments I and II leaves some to be desired compared to experiment III. The uncertainty of the obtained steady states and the number of outliers for the two first experiments (I and II) are much higher than for experiment III.

As seen from the plot the input multiplicity is verified. It is seen, as expected, that the optimum separation is quite flat. From the experimental data of experiment III it is seen that the optimum separation lies in the range between a reflux flow rate of 9.5 to 11 l/min. This is a bit lower than predicted by the simulations of Koggersbøl (1995). The reason is that the feed flow rate for the experiment was 23 % less than in the simulations. Also the effect of decreasing tray efficiency (entrainment) may have shifted the optimum somewhat.

4.6.5 Bottom pressure controlled

After steady state 8 in experiment III, the control configuration was changed from controlling the column top pressure to controlling the bottom pressure. Unfortunately samples were not taken out for steady state 8, thus a comparison of steady state 8 and 9 is not possible based on reconciled data from GC analysis. Therefore only estimated compositions can be used for evaluating the change in separation from steady state 8 to 9. The dynamic transients of the estimated boil up and the pressure difference between the bottom and top pressure is plotted together with the estimated product compositions in figure 4.7 during this phase of the experiment. It is seen that for this high level of boil up rate, that the sep-

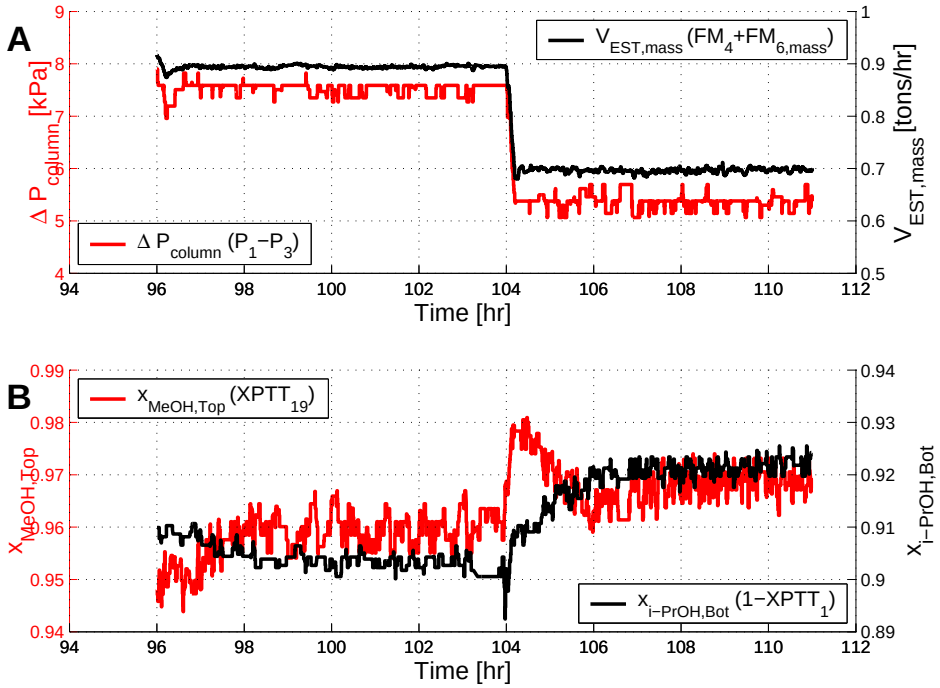

Figure 4.7. Dynamic data from input multiplicity experiment, Nov. 14th 2000 - Nov. 19th 2000. Bottom pressure controlled. **A:** Column pressure drop (ΔP_{column}) and estimated boil up ($V_{EST,mass}$). **B:** Estimated product purities ($x_{MeOH,Top}$ and ($x_{PrOH,Bot}$)).

aration decreases with increasing boil up. This indicates that the negative effect of entrainment on the separation may supersede the positive effect of a decrease in the pressure within the column (from the bottom and up through the column) as the boil up is increased.

4.6.6 Effect of tray efficiency

A number of factors influence the tray efficiency. Besides the more "design" specific factors such as weir height, hole diameters, liquid flow patterns,

vapor maldistribution, some of these are vapor-liquid loads, viscosity, liquid and vapor entrainment as well as weeping.

Increasing the vapor load normally decreases the tray efficiency (due to the reduced vapor contact time), whereas increasing the liquid load increases the tray efficiency (due to the increased liquid holdup and thus increased vapor contact time). For the performed experiments an increase in the vapor load is also accompanied by an increase in the liquid load, since the ratios of feed to product flows are basically unchanged throughout the experiment. Assuming no excessive entrainment or weeping Kister (1992) report that the two effects "normally" cancel each other, and that efficiency is practically independent of load changes.

The degree of entrainment, which is liquid transported by the gas to a tray above, is highly dependent on liquid and vapor rates. Entrainment increases with vapor velocity. At low liquid rates, entrainment is reduced with higher liquid loads, whereas at high liquid rates entrainment increases with liquid loads.

It is clear from the above, that the effect of decreasing tray efficiency, in particular from increased degree of entrainment, may shift the input multiplicity somewhat towards lower vapor flow rates.

4.7 Practical Implications

The findings are of significant relevance for facilities with atmospheric distillation or top pressure controlled and were the reflux ratio is relatively high.

The multiplicity may furthermore be relevant during optimizing control of a plant. To avoid the destabilizing effect of this multiplicity one should investigate a multivariate control design for controlling top and bottom composition. The input multiplicity may be avoided by controlling the column pressure at the column bottom rather than at the top as shown by Koggersbøl (1995).

4.8 Conclusions and Future Work

Steady state multiplicities are known to occur within multicomponent distillation. Also in simple binary distillation output multiplicities have been reported and experimentally verified. The phenomena of steady state multiplicity in distillation have received only limited interest within the process design community.

In this chapter, the occurrence of the input multiplicity predicted and simulated by Koggersbøl (1995), was experimentally verified. The demonstration was carried out on an experimental semi-industrial sized energy integrated distillation facility separating methanol from isopropanol. The multiplicity is related to the binary mixture thermodynamics properties and distillation properties, and implies that separation goes through a maximum when the boil up is increased keeping all other inputs constant. The input multiplicity was verified well within the feasible operating window.

Three experiments were carried out. The results from these experiments clearly verify the existence of the proposed input multiplicity. The influence of variations in tray efficiency due to entrainment on the input multiplicity was discussed. It is concluded that entrainment effects on the tray efficiencies is likely to shift the optimum separation somewhat towards lower vapor flow rates.

The practical relevance of these findings is that suitable control configurations and strategies can be selected to reduce the possibility of performance degradation due to these phenomena. The findings also show that attention from the process design community should be drawn to the research field of nonlinear phenomena analysis, since the implications are changes in operability and stability, which result in performance reducing behavior.

It is suggested to carry out the entire experiment (operating conditions of experiment III) with bottom pressure controlled. In this way the effect of entrainment on the input multiplicity may be quantified experimentally.

It is furthermore suggested to perform two dynamic experiments with top pressure controlled: 1) At low vapor flow rate switch to two point control and verify stability, and 2) at high vapor flow rates switch to two point control and verify instability.

Notation

Variable	Description
B	Bottom product flow rate
D	Distillate flow rate
F	Feed flow rate
G	Objective function according to equations 4.1 and 4.2
i	Index of measurement
L	Reflux flow rate
P_L	Heat pump low pressure (pressure of evaporating freon in the column condenser)

Variable	Description
P_H	Heat pump high pressure (pressure of condensing freon in the column reboiler)
Q_B	Reboiler heat transfer rate
Q_C	Condenser heat transfer rate
V	Vapor flow rate
$V_{EST,mass}$	Estimated boil up rate (mass)
w_i	Weight for measurement i
x_B	Bottom product composition (liquid mole fraction of light component)
x_D	Distillate product composition (liquid mole fraction of light component)
$x_{MeOH,B}$	Measured methanol mole fraction of bottom product
$x_{MeOH,D}$	Measured methanol mole fraction of distillate product (measured distillate purity)
$x_{MeOH,F}$	Measured methanol mole fraction of feed
$x_{PrOH,B}$	Measured isopropanol mole fraction of bottom product (measured bottom product purity)
$x_{PrOH,D}$	Measured isopropanol mole fraction of bottom product
$x_{PrOH,F}$	Measured isopropanol mole fraction of feed
$x_{MeOH,Top}$	Estimated top product purity
$x_{PrOH,Bot}$	Estimated bottom product purity
X_{PTT15}	Estimated methanol mole fraction at tray 15
y_i^f	Fitted value of measurement i
y_i^m	Measured value of measurement i
$\mathbf{y}^m$	Vector of measurements according to equation 4.3
z_F	Feed mixture composition (mole fraction of light component)
$\alpha^S_{MeOH,PrOH}$	Inherent separation factor (as defined by equation 4.7)
ΔP_{column}	Column pressure drop
σ_i	Standard deviation of measurement i
$\bar{\sigma}_i$	Standard deviation mean of measurement i
$\bar{\sigma}_{\mathbf{mass}}$	Vector of standard deviation means of external mass flow rate measurements
$\bar{\sigma}_{\mathbf{x}}$	Vector of standard deviation means of composition variables
τ_{1c}	Dominant time constant

References

Bossen, B. S. (1995). *Simulation and Optimization of Ammonia Plants*. Ph.D. thesis, Technical University of Denmark, Lyngby Denmark.

Jacobsen, E. W. and Skogestad, S. (1991). Multiple Steady States in Ideal Two–Product Distillation. *AIChE Journal*, **37**, 499–511.

Kienle, A.; Groebel, M. and Gilles, E. D. (1995). Multiplicities and instabilities in binary distillation - Theoretical and experimental results. *Chem. Eng. Sci.*, **50**, S2691–S2703.

Kister, H. Z. (1992). *Distillation Design*. McGraw-Hill,inc., New York. ISBN 0-07-034909-6.

Koggersbøl, A. (1995). *Distillation Column Dynamics, Operability and Control*. Ph.D. thesis, Technical University of Denmark, Lyngby Denmark.

Koggersbøl, A.; Andersen, T. R.; Bagterp, J. and Jørgensen, S. B. (1996). An Output Multiplicity in Binary Distillation : Experimental Verification. *Comput. Chem. Eng.*, **20**, S835–S840.

Skogestad, S. and Morari, M. (1987). The Dominant Time Constant for Distillation Columns. *Comp. Chem. Engng.*, **11**(6), 607–617.

Skogestad, S. and Morari, M. (1988). Understanding the Dynamic Behavior of Distillation Columns. *Ind. Eng. Chem. Res.*, **27**(10), 1848–1862.

Skoog, D. A.; West, D. M. and Holler, F. J. (1988). *Fundamentals of Analytical Chemistry*. Saunders College Publishing, New York. ISBN 0-03-14828-6.

Zuiderweg, F. J. (1982). Sieve trays: A view on the state of the art. *Chem. Eng. Sci.*, **37**(10), 1441–1464.

5

Steady State Multiplicities in Heterogeneous Azeotropic Distillation Sequences

In this chapter[1] *multiplicity in heterogeneous azeotropic distillation sequences is studied. Two sequences, suitable for ethanol dehydration, are treated as sample problems and compared. As a basis the* ∞/∞ *analysis method (Petlyuk and Avet'yan (1971), Bekiaris* et al. *(1993)) which assumes infinite reflux rate and infinite number of trays, is extended to and applied on heterogeneous azeotropic distillation sequences in order to determine steady state bifurcation diagrams from thermodynamic considerations. The bifurcation diagrams are very different for the two sequences despite their similar structures. In particular, it is predicted that output multiplicity of the single azeotropic column, as recently experimentally verified by Müller and Marquardt (1997a), can induce output multiplicity of one sequence. It is further predicted that output multiplicity can be avoided by the choice of a different sequence structure. Furthermore,* ∞/∞ *analysis predicts state multiplicity in both heterogeneous azeotropic distillation sequences. For the* ∞/∞ *case it is shown that state multiplicity in heterogeneous distillation sequences can either be induced by the corresponding single column behavior as reported by Gani and Jørgensen (1994) or by closing the sequence. The predicted bifurcation diagrams and multiplicities are substantiated through rigorous simulation of column sequences operating at finite reflux and with finite number of stages. Finally the implications of the thermodynamics including the liquid-liquid plait point position are demonstrated to be important for obtaining reliable predictions.*

[1] Major parts of this chapter have been published in Industrial an Engineering Chemistry Research, Vol. 37, No. 11, 1998. Some sections and calculations have been corrected and expanded in the present chapter.

5.1 Introduction

A commonly encountered task in the chemical process industry is the separation of azeotropic mixtures into pure components. Often, azeotropic distillation is used, where an entrainer is introduced to the azeotropic mixture. This type of process can be divided into *homogeneous* and *heterogeneous* azeotropic distillation. The term *homogeneous* azeotropic distillation is used when the mixture is homogeneous, whereas *heterogeneous* azeotropic distillation is involved with liquid-liquid phase splitting mixtures.
Due to the great industrial importance, homogeneous and heterogeneous azeotropic distillation have been studied intensively. Widagdo and Seider (1996) presented an intensive review of this research. The peculiar behavior of azeotropic distillation has been reported by Laroche *et al.* (1992), who states that for some mixtures, separation as a function of reflux goes through a maximum. This phenomenon is not seen in simple distillation. Various authors have focused on multiplicity in azeotropic distillation. Magnussen *et al.* (1979) presented simulation results showing three steady states for the ethanol-water-benzene system. Kovach and Seider (1987), Rovaglio and Doherty (1990) and Bossen *et al.* (1993) also presented simulation results with multiple steady states. Kienle and Marquardt (1991) and Gani and Jørgensen (1994) showed simulated results indicating 'internal state' multiplicity in azeotropic distillation. A theoretical understanding of the existence of output multiplicity in homogeneous azeotropic distillation was presented by Petlyuk and Avet'yan (1971) and Bekiaris *et al.* (1993). This understanding is based on the ∞/∞ method, where infinite column lengths and infinite reflux are assumed. The understanding for homogeneous azeotropic distillation was extended to heterogeneous azeotropic distillation by Bekiaris *et al.* (1996). Common for both theoretical developments is, that only single stand-alone columns are investigated. However, in reality, azeotropic distillation is at least a two-step procedure. Güttinger and Morari (1996) extended the work of Bekiaris *et al.* (1993) to homogeneous azeotropic distillation sequences. Experimental verification of multiple steady steady states in heterogeneous azeotropic distillation has been reported by Müller and Marquardt (1997a).
The purpose of this article is to extend the works of Petlyuk and Avet'yan (1971), Bekiaris *et al.* (1996) and Güttinger and Morari (1996) to heterogeneous azeotropic distillation *sequences*. Furthermore a theoretical understanding for the occurrence of state multiplicity is provided. The resulting ∞/∞ predictions are used to compare two candidate column configurations for ethanol dehydration, using cyclohexane as the entrainer. Especially it is desired to reveal if and under what conditions multiplicity exists in the two sequences.
First, the proper tools and definitions are presented. Next, the two can-

didate process alternatives are presented along with a degree of freedom analysis. An example analysis is presented for the two sequences, illustrating the application of the ∞/∞ analysis to heterogeneous azeotropic distillation sequences. Determination of realistic operating conditions are discussed. Finally a two-parameter bifurcation analysis and the sensitivity towards the thermodynamic model is discussed.

5.2 Background

The steady state bifurcation analysis is based on the powerful ∞/∞ method (Petlyuk and Avet'yan (1971), Bekiaris *et al.* (1993), Bekiaris *et al.* (1996), Güttinger and Morari (1996)), which here is extended to heterogeneous azeotropic distillation sequences. The most important definitions and tools used in this article are presented and referenced below. Subsequently the considered column sequences are introduced.

Multiplicity Several types of steady state multiplicity have been reported in literature. The term *multiplicity* refers to multiple solutions for given operating conditions, and can be subdivided into input, output, and state multiplicity. These are defined as follows:

- Input multiplicity occurs when multiple input values exist for a given set of outputs.
- Output multiplicity occurs when multiple output values exist for a given set of inputs.
- State multiplicity occurs when multiple values of internal states exist for a given set of inputs **and** outputs.

The outputs considered in this chapter are product compositions, whereas the inputs are selected flowrates.

Residue Curves Recent studies of azeotropic distillation have involved the use of residue curve diagrams (Doherty and Perkins (1978)) and distillation lines (Stichlmair *et al.* (1989)). In this article the residue curve diagrams are used. Residue curves are approximations to the liquid column profile of a packed column at total reflux. Calculation of residue curves are described for heterogeneous mixtures by Pham and Doherty (1990b) and Bossen *et al.* (1993). The residue curve diagram for a mixture is a drawing of several residue curves within the composition simplex. In a residue curve diagram, the pure component corners and the azeotrope mixture points constitute singular points. These singular points can be stable, unstable, or saddle points. Residue curves divide the composition simplex into distillation regions. A region is defined as a subset of the composition simplex in which all residue curves originate at the same singular

point and end at another. When the residue curves are used as approximations to liquid column profiles at infinite column lengths, it is required that the column profile contains at least one singular point (Petlyuk and Avet'yan (1971) and Bekiaris *et al.* (1996)). For the considered ethanol-water-cyclohexane system a residue curve map is presented in Figure 5.1.

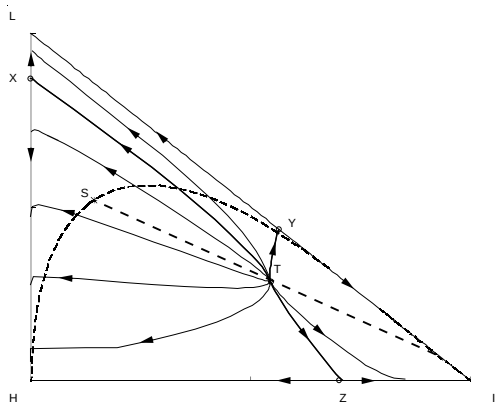

Figure 5.1. Residue curve diagram of the Ethanol(L)-Water(H)-Cyclohexane(I) system (modified UNIFAC, Larsen *et al.* (1987)).

Here, it is seen, that the composition simplex is divided into three distillation regions separated by distillation boundaries which are presented as bold curves in Figure 5.1. The ternary heterogeneous azeotrope is an unstable node, the binary azeotropes are saddle points, and the pure component corners are stable nodes. Following Bekiaris *et al.* (1996), packed distillation columns of infinite length and infinite reflux rate are referred to as ∞/∞ columns.

Heterogeneous Composition Simplex The composition simplex is a projection of the three dimensional $T - \underline{x} - \underline{y}$ space onto the base composition triangle (Figure 5.1), Pham and Doherty (1990a). This argumentation implies, that the position of the heterogeneous liquid boiling surface (the binodal curve) is dependent on temperature. The plait point is the point on the binodal curve, where a critical liquid phase exists (i.e. the point where the tie lines becomes a point). As a consequence the position of the plait point on the binodal curve depends upon temperature. In this article the implication of the plait point position on the predictions obtained from ∞/∞ analysis will be discussed in Section 5.6.

∞/∞ Analysis The ∞/∞ analysis as presented by Petlyuk and Avet'yan (1971) and Bekiaris *et al.* (1993) for single homogeneous distillation columns and by Bekiaris *et al.* (1996) for single heterogeneous distillation columns, builds on the principles described above. Under the assumption of ∞/∞ conditions all feasible column profiles are determined. These profiles contain at least one singular point. Bekiaris *et al.* (1993) defines three al-

lowable profile types to which the feasible column profiles belong. These are:

- *Type I:* The top composition of the column is that of an unstable node. The bottom composition can be situated anywhere *inside* a distillation region.
- *Type II:* The bottom composition is that of a stable node. The top composition can be situated anywhere *inside* a distillation region.
- *Type III:* The column profile runs along the boundaries and contains at least one of the saddle points.

Using these three allowable profile types, the feasible regions of the process variables are traced while varying a key process variable (the bifurcation parameter) within its definition range.

5.2.1 Process Alternatives

Two different process alternatives suitable for the heterogeneous azeotropic dehydration of ethanol, using cyclohexane as the entrainer are analyzed and compared. The two alternatives are distillation sequences consisting of an azeotropic distillation column (separating ethanol from the mixture), a dehydrating column (separating water) and a decanter. The first distillation sequence, the '*direct*' sequence, is presented in Figure 5.2a. The

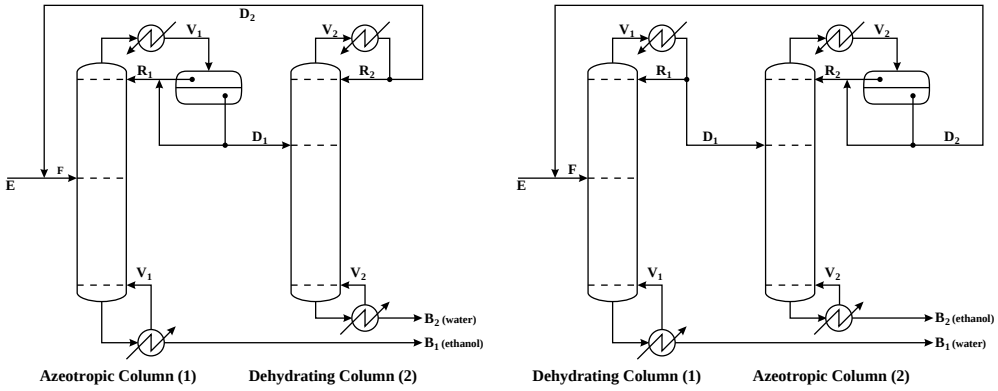

(a) Direct Sequence (b) Indirect Sequence

Figure 5.2. Flowsheet of the 'direct' and the 'indirect' sequences.

second process alternative, the '*indirect*' sequence, is presented in Figure 5.2b.

In the *direct* sequence, the feed is introduced directly into the azeotropic column. In the *indirect* sequence, on the other hand, the feed is introduced to the dehydrating column before entering the azeotropic distillation column. Both alternatives are found in the chemical industry, but are operated differently. The direct sequence is operated with a feed composition near the binary azeotrope between ethanol and water, whereas the

indirect sequence is operated with a feed composition far from the binary azeotrope, since the dehydrating column also is used as concentrator.
It is seen from Figures 5.2a and 5.2b, that the following balance equations can be written for both sequences:
Total Balance:

$$E = B_1 + B_2 \tag{5.1}$$

Column 1 balance:

$$F = D_1 + B_1 \tag{5.2}$$

Column 2 balance:

$$D_1 = D_2 + B_2 \tag{5.3}$$

Furthermore, a balance equation can be written for the feed-recycle mixing point. This balance equation is a linear combination of the above, and can be written as:

$$F = E + D_2 \tag{5.4}$$

It should be noted, that each mass balance constraint corresponds to a mass balance line within the composition simplex.

5.2.2 Degrees of Freedom in ∞/∞-Analysis

Before commencing the ∞/∞-analysis it is necessary to determine the degrees of freedom. For this purpose the equation systems and variables used for ∞/∞-analysis are considered. In the following, ternary systems are considered, as throughout the chapter.

Single Columns: If a single column is analyzed then the total mass balance, the component balances and the mole fraction summation must be satisfied:

$$F = D + B, \tag{5.5}$$

$$x_{F,i}F = x_{D,i}D + x_{B,i}B, i = 1, 2, 3, \tag{5.6}$$

$$0 = \sum_{i=1}^{3} x_{D,i} - 1. \tag{5.7}$$

Two additional constraints derive from the ∞/∞-condition:

- For type I and type II profiles as defined above either the top or the bottoms product composition is completely specified by the ∞/∞-condition. Thus, in these cases the ∞/∞-condition yields two additional composition constraints for one product composition. Note, that the remaining third mole fraction of the ternary product follows from the mole fraction summation 5.7.

- For type III profiles, the pinch point is within the column. In this case the ∞/∞-condition yields one constraint for each product composition, since both product compositions have to lie on a boundary.

Thus, the complete equation system for the ∞/∞-analysis of a single column for a ternary system consists of 7 equations with 12 variables, which are the 3 molar flow rates F, D, B and their compositions $\boldsymbol{x_F}, \boldsymbol{x_D}, \boldsymbol{x_B}$. If the feed flow rate F and the feed composition $\boldsymbol{x_F}$ are specified, then one degree of freedom remains which can be used as bifurcation parameter to track all possible steady states. Usually, one product flow rate is chosen as bifurcation parameter (Petlyuk and Avet'yan (1971); Bekiaris *et al.* (1996)).

Column Sequences: If column sequences as presented in section 5.2.1 are analyzed then the following equations must hold:

1. The mass balances for the entire sequence as well as for each column (see Eq. (5.1)–(5.3)).

2. The corresponding balance equations for each component ($i = 1, 2, 3$):

$$x_{E,i}E = x_{B1,i}B_1 + x_{B2,i}B_2, \tag{5.8}$$
$$x_{F,i}F = x_{D1,i}D_1 + x_{B1,i}B_1, \tag{5.9}$$
$$x_{D1,i}D_1 = x_{D2,i}D_2 + x_{B2,i}B_2. \tag{5.10}$$

3. The mole fraction summations

$$\sum_{i=1}^{3} x_{B1,i} = 1, \tag{5.11}$$
$$\sum_{i=1}^{3} x_{D1,i} = 1. \tag{5.12}$$

For ternary systems equations (5.1)–(5.3) and (5.8)–(5.12) comprise 14 equations.
The number of variables ($E, F, D_1, B_1, D_2, B_2, \boldsymbol{x_E}, \boldsymbol{x_F}, \boldsymbol{x_{D1}}, \boldsymbol{x_{B1}}, \boldsymbol{x_{D2}}, \boldsymbol{x_{B2}}$) is 24. The ∞/∞-condition yields two additional constraints for each column. Thus, if the flow rate E and the composition $\boldsymbol{x_E}$ of the external feed are specified, then two degrees of freedom remain. Therefore, for each of the sequences presented in section 2.1 an ∞/∞-analysis constitutes a two parameter problem.

5.2.3 Determination of Feasible Product Regions

Thus to determine feasible regions for the two sequences with fixed feed rate and mixture, requires specification of two operating parameters. In the sequel first one parameter is fixed for each sequence, while another parameter, which for both sequences is B_1, is selected as a bifurcation parameter. Thus the steady state behaviour of the product streams for each sequence are traced within the definition set $B_1 \in [0; E]$. For $E =$

100 $moles/hr$ the specified parameter for the direct sequence is $D_2 = 15\,moles/hr$ and $D_1 = 115\,moles/hr$ for the indirect sequence.
Subsequently, the fixed parameters are varied over their definition sets, described in Sections 5.4.1.1 and 5.4.1.2, in order to determine two parameter bifurcation surfaces describing the complete steady state behaviour of the sequences for fixed external feed composition. Thus providing a basis for comparing the possible steady state behaviours of the two sequences. Finally the influence of varying feed composition within a practically realistic range is investigated.

5.3 Example Analyses: ∞/∞ Predictions

In the following ∞/∞ analysis is performed for both heterogeneous distillation column sequences presented above. First, the initial ($B_1 = 0$) and final cases ($B_1 = E$) are determined. Next, the bifurcation path from the initial case to the final case is traced, as all feasible profiles are traced along the continuation path of the bifurcation parameter. For both sequence alternatives B_1 ($= E - B_2$) has been chosen as bifurcation parameter. In the subsequent predictions the modified UNIFAC group-contribution method (Larsen *et al.* (1987)) is used as thermodynamic description. For simplicity, the notations F, E, D, B correspond to flow rates, whereas F, E, D, B and V refer to positions in the composition diagrams.

5.3.1 Direct Sequence

For the direct sequence, the example ∞/∞ predictions are based on an external feed composition: $\boldsymbol{x_E} = (x_{E,cyclohexane}, x_{E,ethanol}, x_{E,water}) = (0.05, 0.7, 0.25)$, designed to illustrate the method clearly. The entrainer recycle flow rate, D_2, is specified to 15 $moles/hr$. The external feed flow rate, E, is specified to 100 $moles/hr$. The detailed description of tracing the possible column profiles can be read from appendix C.

Bifurcation Diagram Having traced all possible column profiles of the two columns (see appendix C), the bifurcation diagram can be constructed. As an example, the ethanol purity of the bottom product of column 1 and the water purity of the bottom product of column 2 are plotted, since these two purities are the quality variables of the process. The two purities are plotted against the bottom flow rate of column 2, B_2 (note that $B_2 = E - B_1$), since this plot resembles previously presented results for heterogeneous stand-alone columns (Bekiaris *et al.* (1996)). From the bifurcation diagram (Figure 5.3) it is seen, that three steady states exist for this sequence over a broad interval of B_2. Also it is seen, that optimal purity for both columns is not found for one single value of the bifurcation parameter. Obviously, there seems to be a trade-off between

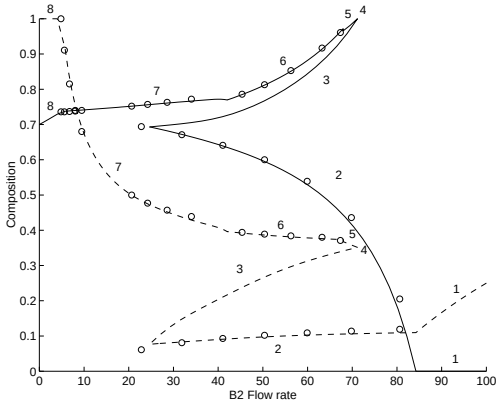

Figure 5.3. Bifurcation diagram constructed from ∞/∞ predictions of the direct sequence. Ethanol purity of the bottom product of column 1 (solid line) and water purity of the bottom product of column 2 (dashed line) are plotted against the flow rate B_2. 'o' represent simulated points. Numbers indicate the steps in ∞/∞ analysis.

obtaining pure ethanol and pure water from the direct sequence at the investigated conditions.

5.3.2 Indirect Sequence

The example analysis for the indirect sequence is based on an external feed composition: $\boldsymbol{x_E} = (0.01, 0.42517, 0.5748)$, different from that of the direct sequence. This composition is due to the different operating conditions of the two sequences. The ∞/∞ analysis is again performed with B_1 as the bifurcation parameter. This time D_1 is fixed ($D_1 = 115\,moles/hr$), hence leaving no degrees of freedom. The external feed flow rate is specified to 100 $moles/hr$. The detailed explanation of tracing all feasible column composition profiles can be found in appendix C.

Bifurcation Diagram When all possible column profiles have been traced (see appendix C) the bifurcation diagram belonging to the indirect sequence at the given operating conditions can be constructed. In Figure 5.4 the ethanol composition of the azeotropic column and the water composition of the dehydrating column are plotted against B_2 for two different values of entrainer in the feed composition. One plot (a) presents the just presented bifurcation analysis with an illustrative feed composition. The second plot (b) shows the behavior of the system when a technically relevant feed composition is used. The latter is verified by simulation. It is seen from the two bifurcation diagrams in Figure 5.4 that a tradeoff is also found for this sequence. However, the optimal purity of the two columns meet for one value of the bifurcation parameter corresponding to step 2 in the bifurcation analysis for a technically relevant feed composition. For this technically most suitable value state multiplicity exists.

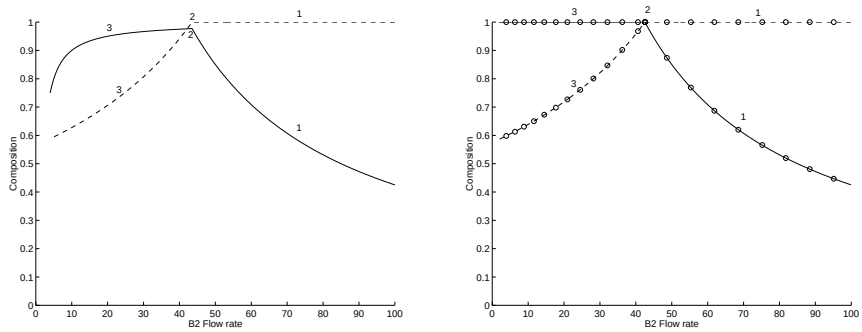

(a) $\boldsymbol{x_E} = (0.01, 0.43, 0.56)$ (b) $\boldsymbol{x_E} = (4.556 \times 10^{-6}, 0.43, 0.57)$

Figure 5.4. Bifurcation diagrams for the indirect sequence based on ∞/∞ predictions. Two different feed compositions are used, one for illustrative purposes, and one for technically relevant simulations (with simulated results). Symbols: Ethanol composition of azeotropic tower bottoms product (solid), water composition of dehydrating tower bottoms product (dashed), simulated points (circle). Numbers indicate steps in ∞/∞ analysis.

5.3.3 Preliminary Sequence Comparison

Based on the ∞/∞ predictions for the two sequences, several preliminary conclusions can be drawn. The two plants are involved with the same issue: Separation of ethanol and water using cyclohexane as the entrainer. There are, however, differences between the behavior of the two sequences for the chosen operating conditions. The column profiles and multiplicities occurring during the above continuations are summarized in Table 5.1. The direct sequence is seen to exhibit output multiplicity in steps 3–7, in analogy with the single column case (Bekiaris *et al.* (1996)). Output multiplicity does not exist for the indirect sequence. Furthermore the direct sequence exhibits a trade-off between obtaining both pure ethanol and water from the plant for the investigated operating conditions. This trade-off is smaller for the indirect sequence, and obviously dependent on the operating conditions. It is seen, that state multiplicity exists for both sequences under the chosen operating conditions. Most importantly it is seen, that the state multiplicity existing for the indirect sequence is found exactly at the desired operation point. Note that state multiplicity also occurs for the direct sequence at the maximal ethanol purity point. State multiplicities in the ∞/∞ case can lead to operational difficulties in a real column with finite number of trays and reflux rate.

5.3.4 Simulated Results

To investigate the behavior of the two sequences at finite conditions, the example analyses have been verified by rigorous simulation.

	Direct Sequence			Indirect Sequence		
Step	Type,Pinch Azeotropic Column 1	Type,Pinch Dehydrating Column 2	Note	Type,Pinch Dehydrating Column 1	Type,Pinch Azeotropic Column 2	Note
Initial	II, H	I, T		II, H	I, T	
1	II, H	I, T		II, H	I, T	
2	III, X	I, T		II, H	III, Y	SM
3	III, X	I, T	OM	III, X	III, Y	
4	II, L	I, T	OM,SM			
5	III, Y	I, T	OM			
6	I, T	I, T	OM			
7	I, T	III, X	OM			
8	I, T	II, H				
Final	I, T	II, H				infeasible

Table 5.1. Column profile types and column profile pinch points for the individual steps in the ∞/∞ predictions for both sequences. Notes: OM = step in which Output Multiplicity occurs; SM = step in which State Multiplicity occurs.

Direct Sequence The described ∞/∞ predictions were verified by dynamic simulation using DYNSIM. The details of the simulation model and the method of solution can be found in Gani *et al.* (1986) and Bossen *et al.* (1993). For the direct sequence, the finite plant simulated, consists of two 27 tray columns operated at finite internal flow rates. The azeotropic column is fed on tray 13 (counted from the top). The dehydrating column is fed on tray 5 (see Figure 5.2a). D_2 is fixed at 15 moles/hr. The simulations are performed with vapor flow rates of 400 moles/hr (yielding $V/E = 4$), which is rather low compared to the assumption of ∞ internal flow rates. That is, the deviation from the ∞/∞ assumptions in the simulations is considerable. Further it is assumed, that there is no pressure gradient in the columns and in the streams, and that the decanter is operated at a temperature of 298K (corresponding to the ∞/∞ predictions). The feed is introduced at saturation conditions. In Figure 5.3 excellent agreement between predictions and simulated results is seen, showing the applicability of the analysis. Each simulated point was found by dynamic simulation, and it turned out, that the plant was open loop unstable during step 3 (Figure 5.3), and stable along the rest of the bifurcation diagram.

Indirect Sequence For the indirect sequence the simulations were performed on the plant shown in Figure 5.2b. The dehydrating column consists of 26 trays and is fed on tray 21 (counting from the top). The azeotropic column consists of 30 trays and is fed on tray 10. D_1 is fixed at 115 moles/hr. The vapor flow rates in the columns were 416 moles/hr (column 1) and 474 moles/hr (column2). For this sequence an equilibrium

stage model including a method for quick phase determination based on necessary equilibrium conditions is used (Müller and Marquardt (1997b)) and the thermodynamics are described by a modified NRTL-model (Connemann *et al.* (1990)). Note, that the equilibrium stage model combined with this thermodynamic description has also experimentally been validated for the considered mixture ethanol/water/cyclohexane (Müller *et al.* (1997)). The simulated results demonstrated in Figure 5.4 show excellent agreement between the ∞/∞ predictions and the simulations.

The good agreement between ∞/∞ predictions and simulations for both sequences confirm that the discussed unusual steady state behaviour is not due to one single model, but rather of generic origin for the sequences.

5.4 Variation of Process Variables

The example analyses revealed possible operational inconveniences for both the direct and indirect sequence at their respective operating points. Also the example analyses showed excellent agreement between infinite and finite conditions. Thus, the ∞/∞ method may be used to predict steady state behavior when the process variables are varied. The intention is to find suitable operating points for the two sequences, and investigate/understand the steady state behavior over a broad operating region.

Direct Sequence - Reduction of Entrainer Feed Driven by the mentioned trade-off between reaching optimal purity of both ethanol and water using the direct sequence, the bifurcation analysis was repeated for a feed composition closer to the binary azeotrope between ethanol and water. The purpose was to investigate if the feed composition had any influence on this trade-off and if the multiplicity found for the illustrative feed composition would vanish. The bifurcation diagram corresponding to an external feed composition of $\boldsymbol{x_E} = (x_{E,cyclohexane}, x_{E,ethanol}, x_{E,water}) = (0.001, 0.870, 0.129)$ is presented in Figure 5.5. The bifurcation diagram in Figure 5.5 is constructed by using same ∞/∞ considerations as already presented in the previous sections. However, the steps taken are a little different from those already presented, though similar in general. Specifically the paths taken by the process variables are closer to the HL axis, due to the lower entrainer content in the plant. It is seen in Figure 5.5, that the change in feed composition does change the basic bifurcation diagram characteristics. The high purity branch of the ethanol composition in column 1 is closer to maximal purity over a larger range of the definition interval. The purity is only 1 at the usual point, but close to 1 over a much broader interval. However, a trade-off is still apparent, although this feed composition imposes better behavior on the system.

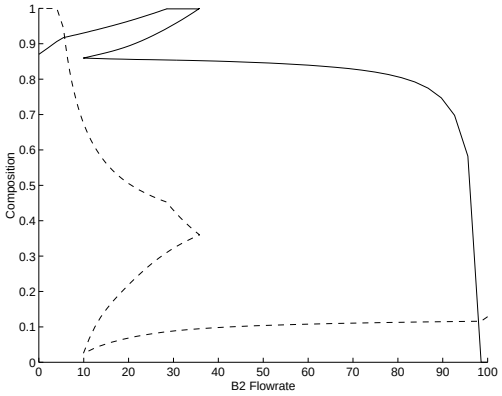

Figure 5.5. Bifurcation diagram obtained for a realistic feed composition. $\boldsymbol{x_E} = (0.001, 0.870, 0.129)$. The solid line is the ethanol composition of the azeotropic column. The dashed line is the water composition of the dehydrating column.

5.4.1 Two-Parameter Bifurcation Analyses

It was stated in the degree of freedom analysis, that two degrees of freedom exist for both sequences when the external feed composition and rate are fixed. In the presented example analyses, B_1 (or alternatively B_2) has been used as bifurcation parameter and a distillate flow rate has been specified. In order to investigate the entire range of possible steady states in detail, a two-parameter bifurcation analysis is performed for both sequences.

5.4.1.1 Direct Sequence

In the example analysis D_2 was fixed at 15 moles/hr. In order to investigate the multiplicity shown by this sequence, a two-parameter bifurcation analysis, involving both degrees of freedom, is presented. Especially it is interesting to reveal if the multiplicity vanishes for some values of B_1 and D_2 in the parameter space.

Definition Sets In order to perform the two-parameter bifurcation analysis, the full (B_1, D_2) subspace is narrowed into the *operationally feasible subspace*. This subspace is defined as the full B_1 parameter interval combined with a restricted D_2 parameter interval. The D_2 interval is chosen such that both columns show maximum purity (ethanol in column 1 and water in column 2) in the B_1 interval (not necessarily simultaneously). The restricted D_2 interval can be determined by use of geometric considerations.
Consider the case of optimal purity in the azeotropic column (column 1). In the previously described bifurcation analysis, it was shown, that optimal purity existed when step 3 was terminated. The necessary condition for obtaining optimal purity in column 1, thus, is, that step 3 should be terminated when B_1 is situated at L. However, this is not the only way

this step can be terminated. Under certain conditions, D_1 can intersect S before B_1 intersects L (remember D_1 is moving along the binodal curve in direction of S). The limit point, where B_1 intersects L, and D_1 intersects S simultaneously can be constructed geometrically in the composition simplex (see Figure 5.6) by drawing a straight line between L and S. According

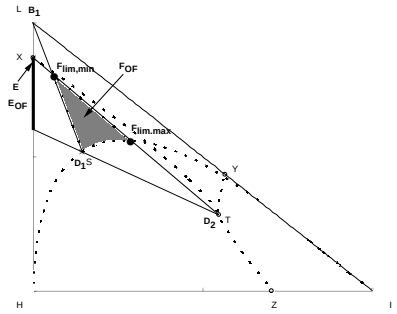

Figure 5.6. Geometric constructions for the direct sequence yielding the minimal and maximal operationally feasible values of D_2, which depends of the position of F in the composition simplex. Operationally feasible region for the external feed composition is E_{OF}. Operationally feasible region for the feed to column 1 is F_{OF}. See text for details.

to the column 1 balance equation (Eq. (5.2)) F must be positioned somewhere on the straight line between B_1 and D_1. The exact position of F on this line can be found by use of the feed-recycle balance equation (Eq. (5.4)), by drawing the line between D_2 and E. F is found as the intersection between the two balance lines. From this construction it is seen, that if F is positioned on the ED_2 line on the entrainer-rich side of the intersection, B_1 will reach the optimal purity point before D_1 reaches S. If F is positioned on the water-rich side, the converse is true. The position of F depends on the D_2 flowrate. The intersection, thus, is the minimum operationally feasible value of D_2, and can be found via the lever rule.
Also a maximal operationally feasible value of D_2 can be determined by geometric considerations. Consider again the composition simplex describing the system. In the initial case $F \equiv D_1$. As mentioned in the above, F is positioned on the balance line ED_2, also shown in Figure 5.6. The exact position of this line is governed by the flow rate D_2. The maximum *feasible* value of D_2 is found when F is positioned at the intersection between the binodal curve and the ED_2 balance line. This is due to the fact, that D_1 can not be positioned inside the heterogeneous part of the diagram due to the decanter. Note, that this value is not only the *operationally feasible* maximum value of D_2, but the maximal *feasible* value.
Thus the definition sets of the two bifurcation parameters are:

$$\begin{aligned} B_1 &\in [0; 100\, moles/hr] \\ D_2 &\in [11.5; 110.5\, moles/hr] \end{aligned}$$

It is apparent from these constructions of the *operationally feasible* parameter range, that the limits are very dependent on the positions of S and the binodal curve, and thus the analysis is very sensitive to the thermodynamic description.

Bifurcation Analysis The bifurcation parameters are varied over the operationally feasible subspace by repeating the already considered ∞/∞ method for different values of D_2. In Figure 5.7 the bifurcation diagram for the full B_2-interval is shown for two values of D_2. Both the position

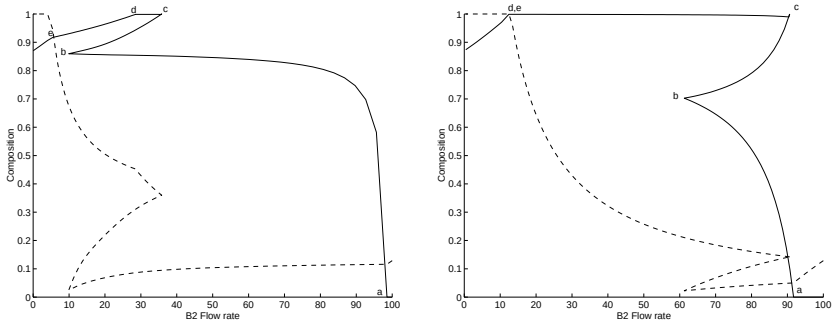

(a) $D_2 = 15\,moles/hr$ (b) $D_2 = 95\,moles/hr$

Figure 5.7. Bifurcation diagrams for the direct sequence representing a small and a large value of D_2. The points a-e denote the termination of steps 1-3 in the bifurcation analysis. The solid lines represent ethanol purity of the azeotropic column product. Dashed lines represent water composition of the dehydrating column product.

of the multiplicity region and the characteristics of the diagram are seen to change. The high purity branch is wider for large recycle flow rates, reducing the trade-off described in the example analysis. For large recycle flow rates it is seen, that the optimal purity branches of the two columns in the plant meet at a single value of B_2, where the trade-off is eliminated. In Figure 5.8 the entire ethanol purity surface spanned over the operationally feasible subspace is presented along with the projection of some important points in the parameter plane. From Figure 5.8 it is seen, that the multiplicity region $(b-c)$ is moving in the parameter plane. It is also seen, that the multiplicity region does not vanish within the operationally feasible subspace. The high purity branch of the azeotropic column $(c-d)$ broadens for increasing recycle flow rates. For the given feed composition it is seen that input multiplicity occurs for $x_{B_1,ethanol} \in [x_{E,ethanol}; max(x_{B_1,ethanol})]$.

Ethanol Content in External Feedpoint The previously performed two-parameter bifurcation analyses have shown, that manipulation of the two variables B_1 and D_2 can yield an operating point with high purity in both product streams. However, this conclusion was based on two different

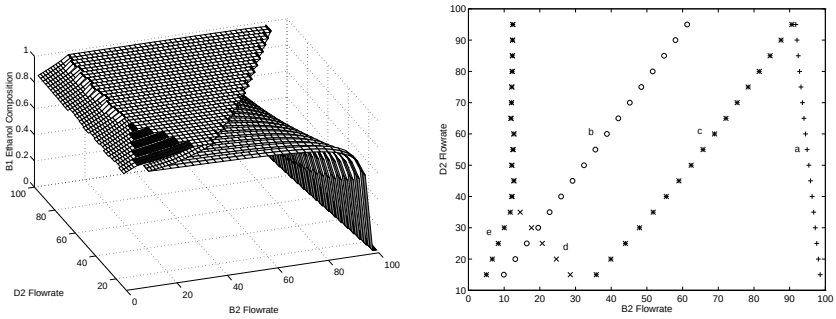

(a) Bifurcation Diagram (b) Parameter plane projection

Figure 5.8. Bifurcation diagram presenting the two-parameter bifurcation analysis for the direct sequence (a). Ethanol composition in the bottoms product of the azeotropic column is presented. Movement of points *a*-*e* (as seen in Figure 5.7) in the parameter plane are shown in b).

fixed external feed compositions. The direct sequence is operated with a feed composition near the binary ethanol-water azeotrope. The indirect sequence is operated with much lower ethanol content in the feed. In practice this means, that the direct sequence should succeed an upstream concentrator creating a feed composition near the ethanol-water azeotrope. The indirect sequence uses the dehydrating column partially as concentrator. Thus, the indirect sequence is the logical better choice for heterogeneous azeotropic ethanol dehydration, since one column is saved. However, it has not been shown how sensitive the direct sequence is towards ethanol composition in the feed. To reveal this fact, a two-parameter bifurcation analysis is performed using B_1 and $x_{E,ethanol}$ as bifurcation parameters. The cyclohexane content of the feed was fixed at 0.001. The feed point variation, thus, is on a vertical line in the composition simplex. D_2 is fixed at 13 moles/hr. This low value is selected due to the fact, that the allowable D_2 interval narrows for decreasing ethanol content, since the external feed point E approaches the binodal curve. With the chosen value for D_2, D_1 is outside the heterogeneous region in the initial case for all values of $x_{E,ethanol}$. However, this value of D_2 is not in the operationally feasible subspace for all values of $x_{E,ethanol}$. $x_{E,ethanol}$ is varied in the interval $[0.45; 0.85]$. 0.85 corresponds to a feed composition near the ethanol-water azeotrope. 0.45 corresponds to the feed composition of the indirect sequence. The effect of ethanol composition in the feed of the direct sequence is quite dramatic, as seen from Figure 5.9. For low values of the ethanol composition, the ethanol purity of the azeotropic column does not reach 1. This fact has its explanation in the operationally feasible subspace. In Figure 10 the operationally feasible regions for F (F_{OF}) and E (E_{OF}) are presented. If these variables belong to the shown regions, the bottoms ethanol composition of the azeotropic column will go through 1. If, however, E (or consequently F) is outside this region, the purity will not go through 1. This is exactly the case when the ethanol content of E

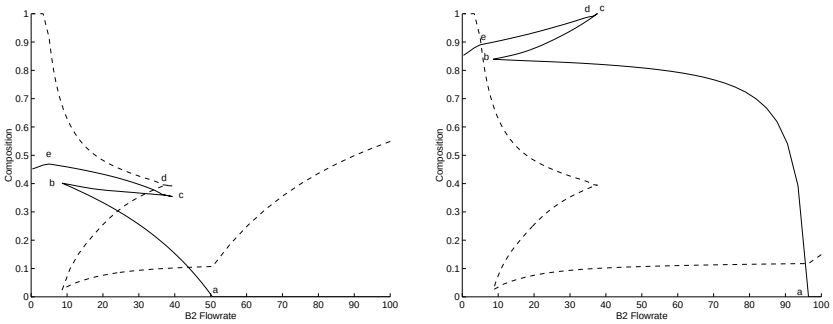

(a) $x_{E,ethanol} = 0.45$ (b) $x_{E,ethanol} = 0.85$

Figure 5.9. Bifurcation diagrams for two different values of ethanol content in the feed to the direct sequence. The solid lines represent ethanol purity of the azeotropic column. Dashed lines represent water composition of dehydrating column product.

is lowered.
Also it is seen, that the overall performance of the plant decreases, since it is not possible to obtain ethanol of a satisfactory purity. The surface spanned over the defined operating region is presented in Figure 5.10. From these considerations it can be concluded, that the upstream concentrator associated with the direct sequence can not be saved. Operation of the direct sequence is very dependent on a high ethanol content of the feed. Furthermore, the existence of output multiplicity is not influenced by varying the ethanol feed concentration.

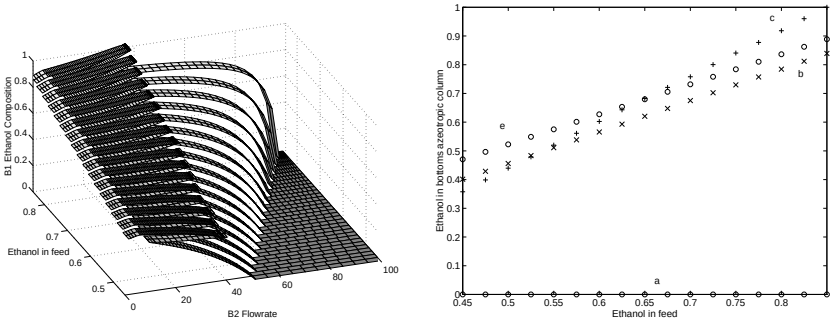

(a) Bifurcation Diagram (b) Projection

Figure 5.10. Bifurcation diagram and projection for a variation in ethanol feed composition to direct sequence. D_2=13 moles/hr. (a) the surface is shown. (b) a projection of the surface in the $x_{B_1,ethanol}, x_{E,ethanol}$ plane.

5.4.1.2 Indirect Sequence

The example analysis of the indirect sequence presented above has been carried out for $D_1 = 115\, moles/hr$. The objective of this section is to analyze the effect of variations in D_1 on the steady state behaviour of the indirekt sequence. The problem of state multiplicity might be overcome

by using another value of D_1. To investigate this, D_1 is varied in a two-parameter bifurcation analysis along with B_1 (or B_2). The issue on state multiplicity will be treated in section 5.5.

Definition Sets For the indirect sequence no maximal value of D_1 is found. However, if D_1 is less than E, it is seen from Figure 5.11 that D_1 and B_2 are positioned closer to the TX boundary.

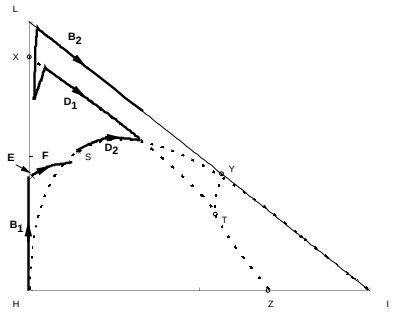

Figure 5.11. Feasible regions for the indirect sequence for $D_1 = 60 moles/hr$. For this value D_1 reaches the TX boundary before B_2 reaches the LI edge. The state multiplicity vanishes.

The smaller D_1 the closer to the boundary. There obviously is a minimal value for D_1, where maximal obtainable purity of the ethanol product is possible. For the feed composition, $\boldsymbol{x_E} = (0.01, 0.42517, 0.5748)$, the limit value is $51 moles/hr$. The definition sets for the two parameters are:

$$\begin{aligned} B_1 &\in [0; E] \ , D_1 > E \\ B_1 &\in [E - D_1; E] \ , D_1 \leq E \\ D_1 &\in [51; \infty[\end{aligned}$$

Bifurcation Analysis The bifurcation parameters are varied over the above defined subspace. D_1 has been restricted to the interval [51;150], since there is no considerable effect of increasing D_1 further. In Figure 5.12 the bifurcation diagrams are shown for two values of D_1. The effect of D_1 is significant. Obviously both the characteristics of the diagram and the B_1 interval length are effected as expected. It is seen, that if state multiplicity is non-existent, the optimal purity of both columns do not meet in a point. This means that state multiplicity can be avoided at the cost of a slightly lower purity. However, if the feed composition is changed to less entrainer, better behavior should be expected. In Figure 5.13 the entire surface spanned in the defined subspace is presented along with a projection of the limit points into the parameter plane. The ethanol composition of the bottoms product of the azeotropic column is presented. As sketched in Figure 5.13 nothing is gained by increasing D_1. However, decrease of D_1

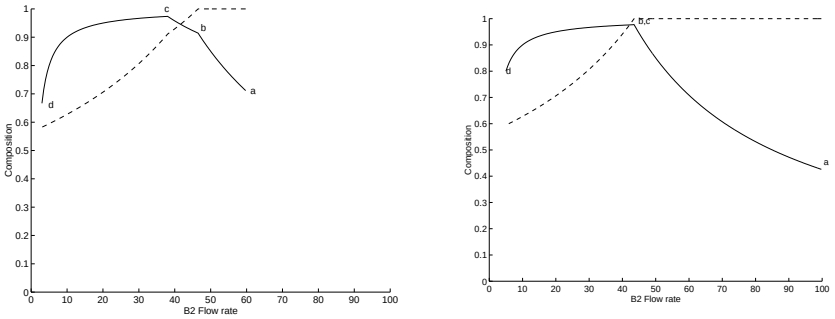

(a) $D_1 = 60\, moles/hr$ (b) $D_1 = 150\, moles/hr$

Figure 5.12. Bifurcation diagrams for the indirect sequence representing a low and a high value of D_1. The solid lines represent ethanol purity of the azeotropic column bottoms product and the dashed lines water purity of the dehydrating column bottoms product.

eliminates the observed state multiplicity. The plant therefore should be operated with lower D_1 than used in the example analysis.

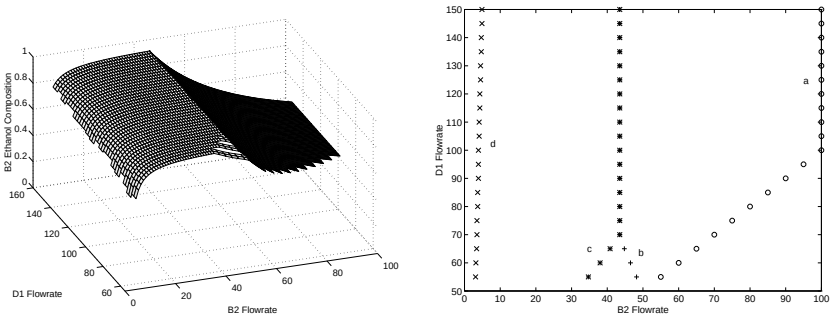

(a) Bifurcation Diagram (b) Parameter plane projection

Figure 5.13. Bifurcation diagram presenting the two-parameter bifurcation analysis for the indirect sequence along with movement of points a-d (as seen in Figure 5.12) in the parameter plane.

5.5 State Multiplicities

State multiplicity is defined as multiple internal steady states for one fixed set of values of input parameters and output variables. The example analyses presented above show that for both distillation sequences considered in this article state multiplicity exists at least for ∞/∞ conditions. The ranges of the multiple steady state profiles are illustrated in Figure 5.14. For the indirect sequence this range is seen as a composition range for distillate D_1 and distillate D_2 (Figure 5.14b) at the value of the bifurcation parameter where the state multiplicity occurs. For the direct sequence this range is seen for the composition V_1 (Figure 5.14a), since also D_1 and D_2 are fixed in this case. This section presents a more general treatment of

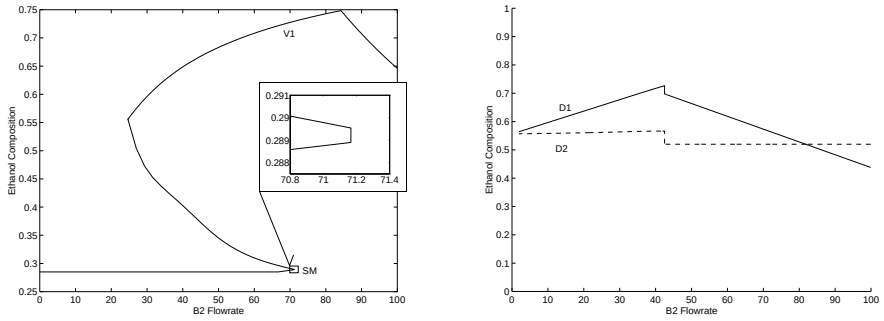

(a) Single column and direct sequence (b) Indirect sequence

Figure 5.14. State multiplicity in the two sequences. In both cases a range of compositions occur for one particular value of the bifurcation parameter.

state multiplicity in azeotropic distillation to obtain physical insight into the occurrence of this phenomenon. To analyze sources of state multiplicity the single column behavior and the effects of closing column sequences are investigated. First, state multiplicity is considered theoretically assuming infinite reflux and an infinite number of trays. Then, implications and previous simulation results on finite columns are discussed.

5.5.1 Single ∞/∞ Columns

In homogeneous columns and column sections state multiplicity arises in cases where both ends of the composition profiles each can be at a pinch point (Kienle and Marquardt (1991); Bekiaris *et al.* (1993)). However, as far as single columns are considered these cases are quite unusual. The reason is that the simultaneous occurence of a pinch at both product compositions requires that the feed point is located on a straight line between a stable and an unstable node of a distillation region. The occurrence of such a case may be illustrated by a bifurcation analysis where the column profile for one value of the bifurcation parameter change from, e.g. a type I to a type II profile. Thus for this one value of the bifurcation parameter the profile includes both pinches. Then, the same flow rates and compositions of the distillate and the bottoms product can be obtained for different steady states characterized by different composition profiles in between the two pinches.

For heterogeneous columns with decanter a different type of state multiplicity is observed (Bekiaris *et al.* (1996)). This type is a consequence of the input multiplicity of the decanter which occurs when the decanter feed, i.e. the column top composition (Figure 5.14a), is located on the same tie line, then the decanter has the same product compositions for any feed composition on this tie line. This decanter input multiplicity leads to state multiplicity of the columm with decanter if the column composition profile contains a pinch at the bottoms product. In this case, the overhead vapor

composition of the column, i.e., the feed composition of the decanter, can vary along a tie line for fixed flow rates and fixed compositions of both bottoms product and distillate drawoff.

5.5.2 ∞/∞ Column Sequences

State multiplicity in column sequences can occur as a consequence of a corresponding single column behaviour. This phenomenon is observed for the direct sequence. Here, state multiplicity occurs during step 4 in the example analysis. The pinch of the azeotropic column is located in L, so that V_1 can vary on a tie line whereas D_1 and B_1 remain constant. Thus, state multiplicity of the azeotropic column induces state multiplicity of the entire sequence. The different steady states are characterized by different composition profiles in the azeotropic column for the same product compositions and flow rates from the azeotropic column and the same state of the dehydrating column.

A quite different behavior is observed for the indirect sequence where state multiplicity occurs as a consequence of closing the sequence. As ∞/∞ column composition profiles contain at least one pinch, combining two ∞/∞ columns yields a sequence with at least two pinches. In any two pinch systems the occurence of multiplicities is quite likely as variations of concentration profiles between the pinches are feasible even for constant external stream compositions and flow rates. Thus, the presence of *two* pinches can 'decouple' the internal streams from *both* external products.

In column sequences such variations of the internal streams involve state multiplicity if they are feasible for constant inputs to the system. Otherwise, they involve input multiplicity. This condition can be visualized geometrically using the lever rule, as illustrated in Figure 5.15 for the indirect sequence.

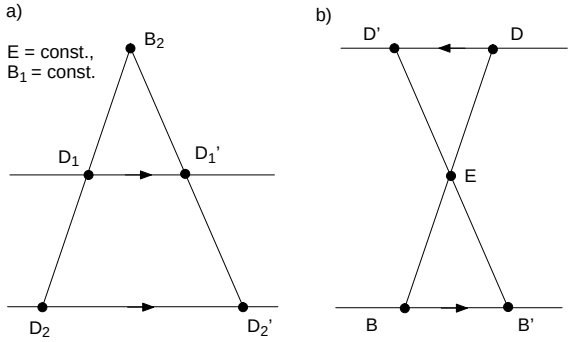

Figure 5.15. Geometric condition for multiplicity with an infinite number of different composition profiles. a) State multiplicitiy of a sequence. b) Output multiplicity of a single column.

Here, the locations of the external stream compositions E, B_1, and B_2 are fixed. Then, the application of the lever rule to the azeotropic column 2 implies, that state multiplicity corresponds to different steady states if D_1 and D_1' as well as D_2 and D_2' are positioned on parallel lines. Only in this case different steady states with the same value of the feed flow rate D_1 are possible. This reasoning leads to the following *geometrical condition for state multiplicity*: If for fixed locations of the external stream compositions (E, B_1, B_2) the locations of the internal stream compositions (D_1 and D_2) can vary on parallel not necessarily straight lines within the composition diagram, then the column sequence shows state multiplicity. If these variations can take place by continuous movements of D_1 and D_2 then state multiplicity with an infinite number of different profiles occurs.

Note that this condition is sufficient but not necessary for state multiplicity since in sequences state multiplicity can also occur due to a corresponding single azeotropic column behaviour as treated above. In the latter case, the multiple steady states differ only in the composition profiles within the azeotropic column. The internal product compositions, i.e., D_1 an D_2, are constant. Note further that contrary to the geometric analysis of output multiplicity in single columns (Petlyuk and Avet'yan (1971); Bekiaris *et al.* (1993)) the analysis of state multiplicity in sequences is carried out with regard to a fixed product composition (B_2) and a variable feed composition (D_1) of a column (Figure 5.15).

The geometrical condition defined above can be applied to explain the state multiplicity observed during step 2 of the example analysis for the indirect sequence. Figure 5.16 shows feasible variations of internal stream compositions (D_1, D_2) for fixed external stream compositions (E, B_1, B_2). Two different cases are considered. Figure 5.16 a) shows a case where

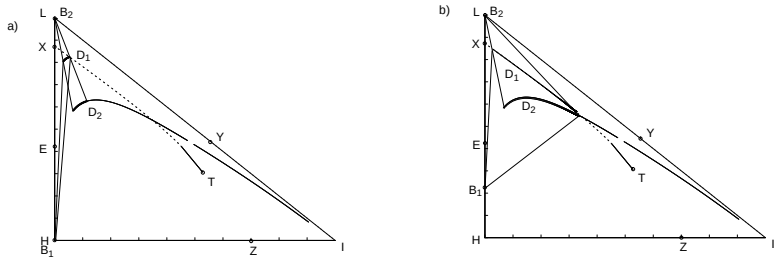

Figure 5.16. Analysis of state multiplicity for two different cases of the indirect sequence. a) State multiplicity occurs; b) no state multiplicity, but input multiplicity occurs.

the pinch of the dehydrating column 1 is located at H and the pinch of the azeotropic column 2 is located at Y. In this case, variations of D_2 are constrained to the binodal curve. As D_1 can move on a curve parallel to the binodal curve, application of the geometrical condition stated above yields state multiplicity with an infinite number of different steady states

as illustrated in Figure 5.14b.

Figure 5.16 b) illustrates a different case for the indirect sequence. Here, the pinch of the dehydrating column 1 is located in X and the pinch of the azeotropic column 2 is located in Y. Thus, for fixed external stream compositions: E, B_1, B_2, the internal stream compositions D_1, D_2 are again variable. Variations of D_1 are here constrained to the boundary residue curve XT, variations of D_2 are constrained to the binodal curve. As these curves are not parallel, state multiplicity with an infinite number of different profiles is not possible. But note that the same products can still be obtained for a range of flow rates D_1. Thus this is a case of input multiplicity.

5.5.3 Implications on Finite Columns

The predictions of state multiplicity with an infinite number of different profiles presented above are based on the assumptions that the columns contain an infinite number of trays and that they are operated at infinite reflux. Basically, ∞/∞ predictions carry over to distillation processes with some sufficiently large but finite reflux rate and finite number of trays. This basic observation is confirmed by a number of arguments. Firstly by the good agreement of ∞/∞ predictions with simulation results for finite columns as presented in the previous section. Secondly by experimental results recently reported by Güttinger *et al.* (1997) for homogeneous and by Müller and Marquardt (1997a) for heterogeneous columns. Nevertheless, due to finite conditions the behaviour of real columns also shows some deviations from ∞/∞ predictions. In particular, state multiplicity with an *inifinite* number of steady states as predicted for ∞/∞ sequences can imply state multiplicity with a *finite* number of steady states for finite sequences. A number of multiple steady states in a single heterogeneous column with decanter has been observed computationally by several authors. Two of these findings are discussed below. The simulations in Bossen *et al.* (1993) using original UNIFAC revealed three steady states with the same inlet and outlet conditions where the column profiles all are located close to the LYT boundary. In a subsequent study of the same system, Gani and Jørgensen (1994) reported ten steady states at this operating point. This number of solutions were obtained by using a pulse disturbance of different sign and duration to the reboiler heat duty from a reference steady state. Seven of these profiles had different front locations in the column, but were all close to the LYT boundary. Figure 5.17 shows all ten profiles near the ternary azeotropic point. This Figure reveals that several bottom section composition profiles follow the LY boundary until the feed tray. As the composition front approaches the feed tray, the bottom section profiles have one or more trays inside the LYTX region. From the magnification it is seen that this occurs for three of the profiles.

The magnified part of Figure 5.17 near T shows that the corresponding vapour compositions only cover a small fraction of the tie line from the XT to the TY boundary.

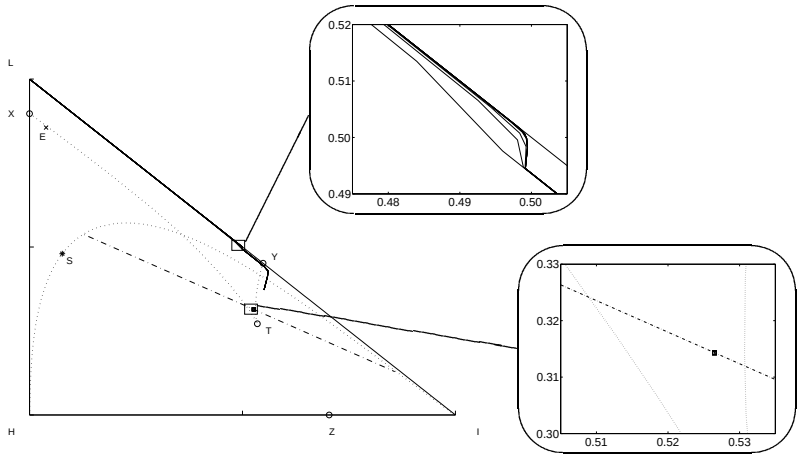

Figure 5.17. Column profiles for the steady states as reported by Gani and Jørgensen (1994).

A bifurcation analysis for ∞/∞ conditions on the single column with decanter reveals a state multiplicity at maximum ethanol purity at precisely the same distillate flow rate as found in the above simulations.

In practice a certain degree of overdesign (i.e. number of plates) is normal, in order to obtain high purity products. At some small number of trays the predicted state multiplicity may vanish. But also in these cases it is expected that finite sequences are characterized by a very high sensitivity of some state variables with respect to some inputs, i.e., operating conditions. The understanding of such sensitive behaviour is most interesting also from a practical, operational point of view. In conclusion state multiplicity is not a numerical artefact. Instead it is an operationally relevant phenomenon, which requires more detailed analysis of the implications on finite columns.

5.6 Influence of Thermodynamic Model

As ∞/∞ analysis is based on thermodynamic considerations, one could imagine, that the ∞/∞ predictions are very sensitive to the thermodynamic representation. This point was also indicated when the operationally feasible subspace was determined for the direct sequence. The different thermodynamic descriptions used in the ∞/∞ predictions and the simulation of the indirect sequence (UNIFAC and modified NRTL) yield qualitatively similar results. Therefore, good agreement has been obtained in this case. It is, however, of general interest to investigate what happens when the thermodynamic description is uncertain or when

the thermodynamics itself are different compared to the case considered above. In particular the modeling of the binodal curve is crucial for the predicted results in cases where the decanter is operated heterogeneously. For example in the previous ∞/∞ predictions it has been assumed that the decanter were operated isothermally at 298K. However, if the decanter is operated at another temperature, the results of the ∞/∞ predictions will differ considerably due to the position of the binodal curve, which is temperature dependent. One issue which is important, is the position of the plait point in the composition simplex. For 298K the plait point is situated on the entrainer rich side of both the TX and the TY boundaries. This location is the case treated by Bekiaris *et al.* (1996). The plait point can also be positioned between the TX and the TY boundaries or on the water-rich side of the TX boundary. Below, the latter case will be treated, where the position of the plait point will introduce a discontinuity in the bifurcation diagram. It is emphasized, that this discontinuity is not restricted to heterogeneous column sequences only, but also applies to single stand alone heterogeneous azeotropic distillation columns. The effect of different plait point positions is investigated using a theoretical abstraction for illustrative reasons. The binodal curve from the example analyses is used, but the plaitpoint is moved assuming horizontal tie lines (the same ethanol composition in both phases) in the composition simplex. This abstraction allows comparison of the bifurcation diagrams, thereby revealing the effects introduced by the different plaitpoint positions.

5.6.1 Direct Sequence

Consider the example analysis of the direct sequence. During step 2, D_1 moves on the TX boundary in the direction of T. B_1 moves on the HL axis, and B_2 inside the simplex, subject to balance equations. D_2 is situated at T. When step 2 terminates, D_1 (coming from a condensed homogeneous V_1) is positioned at the intersection between the TX boundary and the binodal curve. As the condensed vapor V_1 enters the heterogeneous region, the decanter splits into two liquid phases, where D_1 has the composition of the water-rich endpoint of the tie line. Thus, at the point where V_1 turns heterogeneous, D_1 will jump in the composition simplex to D_1' as seen in Figure 5.18a), introducing a discontinuity in the bifurcation diagram. In Figure 5.18b the bifurcation diagram arising from the new position of the plait point is presented. Compared to the example bifurcation diagram of the direct sequence (Figure 5.3) it is seen, that the first two steps are identical in the two cases. Between step 2 and step 3 a discontinuity occurs. The last steps are different for the new position of the plait point. This is due to the position of S, which is changed. However, this example shows the importance of using as correct thermodynamic information as possible. Not only must the thermodynamic description be adequate for the system in general - also the decanter temperature of operation must be correctly known in order to obtain reliable ∞/∞ predictions.

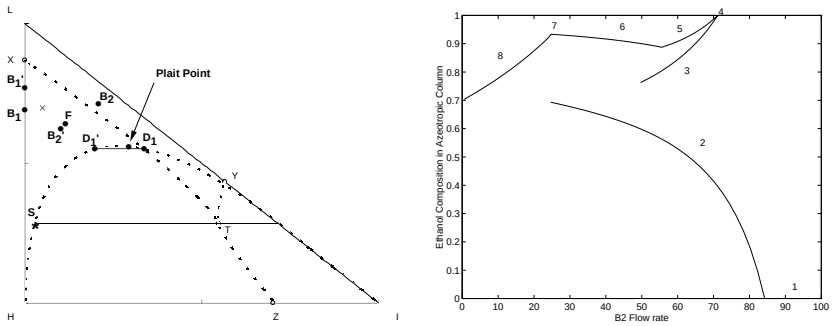

(a) Path in the simplex (b) Bifurcation Diagram

Figure 5.18. Direct sequence with an assumed plait point. (a) Path of the process variables in the discontinuity point, where D_1 jumps from D_1 to D_1'. (b) Bifurcation diagram, ethanol purity of azeotropic column bottom product, where a discontinutity is seen between step 2 and step 3.

5.6.2 Indirect Sequence

For the indirect sequence a similar argumentation applies. Using the same theoretical abstraction as thermodynamic description the following considerations can be made. In the example analysis for the indirect sequence it was seen, that the bifurcation path consisted of three steps. The second and third step were involved with movement inside the heterogeneous region. If analogously ∞/∞ analysis is carried out for the new thermodynamics, it is seen, that the first step is not changed qualitatively, since no movement occurs inside the heterogeneous region. However, the product composition path along the first step changes due to the new position of the plaitpoint and of S. The step is sketched (along with step 2) in Figure 5.19a. The second step, however, is involved with movement in

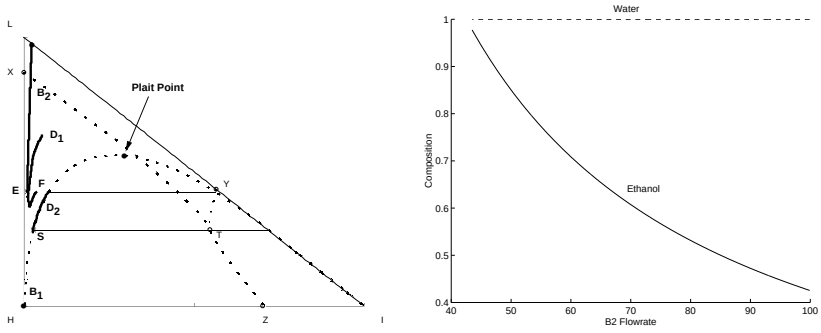

(a) Bifurcation Path (b) Bifurcation Diagram

Figure 5.19. Effect of the position of the plait point on the indirect sequence. It is seen, that the bifurcation path is restricted to two steps. D_1=115 moles/hr and $\boldsymbol{x_E} = (0.01, 0.43, 0.56)$.

the heterogeneous region. In this case, D_1 and D_2 are moving in order to continue the bifurcation path. V_2 moves inside the heterogeneous region

on the TY boundary in direction of Y. It is seen, that this step must terminate when V_2 reaches the binodal curve. This limit value terminates the continuation path. If V_2 would enter the homogeneous region, then D_2 would jump to the position of V_2, since D_2 and V_2 are identical when the decanter is homogeneous. This jump violates the balance equations, since B_2, D_2, and D_1 can no longer be situated on a mass balance line. D_1 is restricted to the TX boundary in order to yield an allowable profile type. Thus, the effect of the plait point position is, that the bifurcation parameter interval is restricted.

5.7 Discussion and Conclusions

The steady state behaviour of two heterogenous azeotropic distillation sequences designed to separate ethanol and water using cyclohexane as the entrainer has been investigated assuming infinitely long column sections and infinite reflux. Both sequences contain an azeotropic and a dehydrating column; in the direct sequence the feed is entered directly to the azeotropic column, while in the indirect sequence the feed enters first the dehydrating column, which then also is used as a concentrator. The two sequences exhibit very different steady state behavior despite the similarity of the two sequences. The direct sequence exhibits output and state multiplicity, whereas the indirect sequence, only exhibits state multiplicity. Thus, the position of the decanter within the sequence is of great importance. The conclusions of this article are not restricted to one single operating point but to all realistic operating points.

In the direct sequence the output multiplicity persists throughout the operationally feasible parameter space. Increasing recycle flow rates improves the product quality and eliminates a trade-off between the two product purities. For both of the investigated sequences state multiplicity prevails close to the optimal operating point.

The state multiplicity of the direct sequence is a consequence of the state multiplicity of the single column as found computationally by Gani and Jørgensen (1994) and analyzed by Bekiaris *et al.* (1996). The state multiplicity of the indirect sequence occurs as a consequence of closing the sequence. Here the state multiplicity can be avoided by changing the flow rate of D_1, at the cost of a slightly increased impurity in the ethanol product. This important conclusion yields the information, that the indirect sequence should not be operated at high D_1 flow rates as far as the specifications of the product compositions are still satisfied. For the direct sequence, however, high D_2 flow rates yield better performance of the sequence.

The above results have been substantiated through simulations on finite column lengths. For both sequences excellent agreement between predic-

tions and simulations is seen.

The thermodynamic description is seen to show great effect on the performance of both sequences. If the plait point is positioned on the water-rich side of the TX boundary the behavior of the sequences are seen to be affected. In the bifurcation diagram representing the direct sequence, a discontinuity arises. In the indirect sequence, the bifurcation parameter interval is narrowed. Thus, the analyses reveal that in design and simulation of heterogeneous azeotropic distillation sequences, significant attention should be focused on the thermodynamics representing the liquid-liquid phase split and the temperature at which this operation is carried out.

It seems, that the indirect sequence is the better choice in the separation of ethanol and water with cyclohexane as entrainer. However, in this sequence operational difficulties may arise from state multiplicity. This issue should be further pursued.

Notation

Variable	Description
B	Bottom product molar flow rate
B_j	Bottom product molar flow rate for column j in a distillation sequence
B (B')	Bottom product composition
B_j	Bottom product composition for column j in a distillation sequence
D (D')	Distillate product molar flow rate
D_j	Distillate product molar flow rate for column j in a distillation sequence
D	Distillate product composition
D_j (D_j')	Distillate product composition for column j in a distillation sequence
E	External feed molar flow rate for a distillation sequence
E	External feed composition for a distillation sequence
E_{OF}	Operationally feasible external feed composition according to Figure 5.6
F	Feed molar flow rate
F	Feed composition
F_{OF}	Operationally feasible feed composition according to Figure 5.6
H	Pure component corner in composition simplex (heavy component)
I	Pure component corner in composition simplex (intermediate component)

Variable	Description
i	Component index
L	Pure component corner in composition simplex (light component)
S	Heavy liquid composition in decanter when overall decanter composition is equal to ternary azeotropic composition
T	Temperature
T	Ternary azeotrope
V	Vapor molar flow rate
V	Overhead vapor composition
V_j	Overhead vapor composition for column j in a distillation sequence
X	Binary azeotrope
$\underline{x}$	Liquid composition
$\boldsymbol{x_B}$	Bottom product composition
$x_{B,i}$	Bottom product mole fraction of component i (i.e. i being cyclohexane, ethanol or water)
$\boldsymbol{x_{B_j}}$	Bottom product composition for column j in a distillation sequence
$x_{B_j,i}$	Bottom product mole fraction of component i for column j in a distillation sequence
$\boldsymbol{x_D}$	Distillate product composition
$x_{D,i}$	Distillate product mole fraction of component i
$\boldsymbol{x_{D_j}}$	Distillate product composition for column j in a distillation sequence
$x_{D_j,i}$	Distillate product mole fraction of component i for column j in a distillation sequence
$\boldsymbol{x_E}$	External feed composition for a distillation sequence
$x_{E,i}$	External feed mole fraction of component i
$\boldsymbol{x_F}$	Feed composition
$x_{F,i}$	Feed mole fraction of component i
Y	Binary azeotrope
$\underline{y}$	Vapor composition
Z	Binary azeotrope

References

Bekiaris, N.; Meski, G. A.; Radu, C. M. and Morari, M. (1993). Multiple Steady States in Homogeneous Azeotropic Distillation. *Ind. Eng. Chem. Res.*, **32**(9), 2023–2038.

Bekiaris, N.; Meski, G. A. and Morari, M. (1996). Multiple Steady States in Heterogeneous Azeotropic Distillation. *Ind. Eng. Chem. Res.*, **35**, 207–237.

Bossen, B. S.; Jørgensen, S. B. and Gani, R. (1993). Simulation, Design, and Analysis of Azeotropic Distillation Operations. *Ind. Eng. Chem. Res.*, **32**, 620–633.

Connemann, M.; Gaube, J.; Karrer, L.; Pfennig, A. and Reuter, U. (1990). Measurement and representation of ternary vapour-liquid-liquid equilibria. *Fluid Phase Equil.*, **60**, 99–118.

Doherty, M. F. and Perkins, J. (1978). On the Dynamics of Distillation Processes I: The Simple Distillation of Multicomponent Non-Reacting Homogeneous Liquid Mixtures. *Chem. Eng. Sci.*, **33**, 281.

Gani, R. and Jørgensen, S. B. (1994). Multiplicity in Numerical Solution of Nonlinear Models: Separation Processes. *Comput. Chem. Eng.*, **18**, 55.

Gani, R.; Ruiz, C. A. and Cameron, I. T. (1986). A Generalized Model for Distillation Columns - I. *Comp. Chem. Eng.*, **10**, 181–198.

Güttinger, T. E. and Morari, M. (1996). Multiple Steady States in Homogeneous Separation Sequences. *Ind. Eng. Chem. Res.*, **35**, 4597–4611.

Güttinger, T. E.; Dorn, C. and Morari, M. (1997). Experimental Study of Multiple Steady States in Homogeneous Azeotropic Distillation Sequences. *Ind. Eng. Chem. Res.*, **36**, 794–802.

Kienle, A. and Marquardt, W. (1991). Bifurcation Analysis and Steady-State Multiplicity of Multicomponent, Non-Equilibrium Distillation Processes. *Chem. Eng. Res.*, **46**, 1757–1769.

Kovach, J. and Seider, W. D. (1987). Heterogeneous Azeotropic Distillation: Experimental and Simulation Results. *AIChE Journal*, **33**, 1300–1314.

Laroche, L.; Bekiaris, N.; Andersen, H. and Morari, M. (1992). The Curious Behavior of Homogeneous Azeotropic Distillation - Implications for Entrainer Selection. *AIChE Journal*, **38**(9), 1309–1328.

Larsen, B. L.; Rasmussen, P. and Fredenslund, A. (1987). A Modified UNIFAC Group-Contribution Model for Prediction of Phase Equilibria and Heats of Mixing. *Ind. Eng. Chem. Res.*, **26**, 2274–2286.

Magnussen, T.; Michelsen, M. and Fredenslund, A. (1979). Azeotropic Distillation Using UNIFAC. In *Inst. Chem. Eng. Symp. Ser. No. 56*, Intl. Symp. on Distillation, Rugby, England.

Müller, D. and Marquardt, W. (1997a). Experimental Verification of Multiple Steady States in Heterogeneous Azeotropic Distillation. *Ind. Eng. Chem. Res.*, **36**(12), 5410–5418.

Müller, D. and Marquardt, W. (1997b). Dynamic Multi–phase Flash Simulation: Global Stability Analysis versus Quick Phase Determination. *Comput. Chem. Eng.*, **21**, S817–S822.

Müller, D.; Marquardt, W.; Hauschild, T.; Ronge, G. and Steude, H. (1997). Experimental Validation of an Equilibrium Stage Model for Three–phase Distillation. *IChemE Symp. Ser.*, **142**, 149–159.

Petlyuk, F. B. and Avet'yan, V. S. (1971). Investigation of the Rectification of Three–component mixtures with Infinite Reflux. *Theor. Found. Chem. Eng.*, **5**, 499–507.

Pham, H. N. and Doherty, M. F. (1990a). Design and Synthesis of Azeotropic Distillation - I. Heterogeneous Phase Diagram. *AIChE Journal*, **45**(7), 1823–1836.

Pham, H. N. and Doherty, M. F. (1990b). Design and Synthesis of Heterogeneous Azeotropic Distillations - II. Residue Curve Maps. *Chem. Eng. Sci.*, **45**(7), 1837–1843.

Rovaglio, M. and Doherty, M. F. (1990). Dynamics of Heterogeneous Azeotropic Distillation Columns. *AIChE Journal*, **36**, 39–52.

Stichlmair, J.; Fair, J. and Bravo, J. (1989). Separation of Azeotropic Mixtures via Enhanced Distillation. *Chem. Eng. Prog.*, **85**, 63.

Widagdo, S. and Seider, W. D. (1996). Azeotropic Distillation. *AIChE Journal*, **42**(1), 96–130.

6

Dynamics of a Heterogeneous Azeotropic Distillation Sequence I

Bifurcation Analysis

This chapter presents a bifurcation analysis performed on a heterogeneous azeotropic distillation sequence suitable for the dehydration of ethanol using cyclohexane as entrainer. The analysis is carried out using a rigorous model implemented in the dynamic simulator DYNSIM (Gani et al. *(1986), Bossen* et al. *(1993)) and the continuation software CONT (Kubicek and Marek (1983), Schreiber (1998)). The parameter chosen as primary bifurcation parameter in the investigation is reflux ratio for the azeotropic distillation column. Multiple steady states are found as were also the case in chapter 5. In the present case the multiple solutions occur in a typical hysteresis scenario. That is stable solutions of high and low product purity coexists, and their basins of attraction are separated by an unstable solution of intermediate purity. The sequence exhibit "state multiplicity" in the obvious operating point for the ∞/∞ case, meaning that for fixed inputs and outputs multiple solutions of the internal column profiles exists (chapter 5). This phenomenon may be seen in the bifurcation analysis as a real eigenvalue moving very close to the imaginary axis, thus resulting in a very slow open loop dynamic behavior in the vicinity of the desired operating point seen from a production viewpoint. This point of tangency signifies where the "state multiplicity" occurs, but also occurs during change of composition profiles. The results from the bifurcation analysis furthermore indicate that complex dynamic behavior is expected to occur in the boundary region of liquid phase splitting.*

6.1 Introduction

Separation of azeotropic mixtures into pure constituents is a commonly encountered task in the chemical process industry. This separation can be facilitated through distillation by adding an entrainer. The resulting ternary system can be categorized as an either homogeneous or heterogeneous system. In industry the application of heterogeneous azeotropic

distillation is by far the most widely used of the two types of separation (see Widagdo and Seider (1996)). Heterogeneous azeotropic distillation is carried out at lower temperatures than homogeneous azeotropic distillation with a heavy entrainer, rendering this separation more effective in terms of energy exploitation. Operation of heterogeneous azeotropic distillation processes however is known to be very difficult due to the very high degree of nonlinearity.

A vast number of studies have been carried out in the research area of distillation behavior. Most research has focused on the static behavior, however within the last four decades an increased interest in the dynamic behavior has been established. The investigations have mainly concentrated on binary distillation or multi component distillation of mixtures with decent behaviors. Within azeotropic distillation and in particular heterogeneous azeotropic distillation the reported results on dynamic behavior are limited.

Dynamics of binary/multicomponent distillation:
One of the first "scriptural works" on distillation dynamics may be the one by Rademaker *et al.* (1975) which is a large collection of research results mainly from the Shell Laboratory.

The dynamic composition response for multicomponent distillation columns was approximated with a two time constant model by Skogestad and Morari (Skogestad and Morari (1987) and Skogestad and Morari (1988)).

A very useful and practical oriented collection of material from Luyben and a number of other heavy contributors to this research area is presented in Luyben (1992). The main focus of this collection is distillation control and control structure selection, but it also covers issues from modelling, identification and simulation (dynamical as well as static) of distillation. It also contains parts on heterogeneous azeotropic distillation.

Azeotropic distillation:
Widagdo and Seider (1996) made an exhaustive review, which excellently presents the major results within the research field of azeotropic distillation until then.

Matsuyama and Nishimura (1977) classified ternary vapor liquid equilibria systems into 113 groups. Doherty and Perkins (1978) clearly interpreted the mathematical theory of the complex equilibrium properties of azeotropic mixtures. They used residue curves to describe distillation processes. Hilmen *et al.* (1999) presented a qualitative representation of all physically occurring ternary mixtures, by combining only four elementary topological cells.

Steady state multiplicities in heterogeneous azeotropic distillation have been demonstrated in a number of simulation studies. Magnussen *et al.* (1979) simulated multiple steady states for the Ethanol-Water-Benzene system. The same did Kovach and Seider (1987a), Kovach and Seider (1987b) in a study, where they used homotopy-continuation methods for simulating several heterogeneous azeotropic distillation systems and tracking steady state solution paths in parametric studies. Widagdo *et al.* (1989) predicted multiple steady states in the separation of a five component mixture of sec-butanol, water, di-sec-butyl-ether (entrainer), methyl-ethyl-ketone and 1-butene (impurities). Gani and Jørgensen (1994) showed simulated results indicating 'internal state' multiplicity for heterogeneous azeotropic distillation of the Ethanol-Water-Benzene system.

Dynamics of azeotropic distillation:
Also in the subject of azeotropic distillation some investigations on the dynamic behavior have been presented. Prokopakis and Seider (1983) simulated homogeneous azeotropic distillation towers dynamically. Gani *et al.* (1986) developed a generalized model suitable for performing startup calculations as well as azeotropic separation simulations. A modified version of this model (Bossen *et al.* (1993)) presents the model formulation of the work in this chapter. Andersen *et al.* (1991) made dynamic simulations of homogeneous azeotropic distillation separating a mixture of acetone, heptane and toluene.

Rovaglio and Doherty (1990) simulated the dynamics of heterogeneous azeotropic distillation, where the system used was ethanol water and benzene. In a later study, Widagdo *et al.* (1992) observed underdamped oscillations in a dynamic simulation of the heterogeneous azeotropic distillation, separating sec-butanol from water using di-sec-butyl-ether as entrainer (also methyl-ethyl-ketone and 1-butene were present in mixture separated). Bossen *et al.* (1993) simulated the separation of several mixtures (both homogeneous and heterogeneous systems) through steady state as well as dynamic simulation. Simulations of the ethanol-water-cyclohexane system have been performed by Müller *et al.* (1997), Müller and Marquardt (1997a).

Recent studies by Lee *et al.* (1999) predict the occurrence of limit cycles in homogeneous azeotropic distillations. They performed continuation and simulated the sustained oscillations with a CMO model, and reproduced them by simulations with a more rigorous model in ASPEN PLUS/DYNAMICS. The mixture studied was methanol, methyl butyrate and toluene.

A recent interesting work by Vadapalli and Seider (2001) presents a generalized framework for tracing steady state solution paths by extending

a process simulator (ASPEN PLUS) with an add-in continuation subroutine. They present test results of the framework on an adiabatic CSTR problem as well on homogeneous azeotropic distillation. They also tested the framework on heterogeneous azeotropic distillation, however the results are not displayed in their article.

Experimental studies of azeotropic distillation:
Experimental investigations regarding azeotropic distillation have mainly concentrated on the static phenomena. Steady state multiplicities have for homogeneous azeotropic distillation been experimentally verified by: Güttinger *et al.* (1997). Steady state multiplicity for heterogeneous azeotropic distillation have through experiments been verified by Kovach and Seider (1987a), Müller *et al.* (1997), Müller and Marquardt (1997b), where the latter also in a dynamic experiment showed the hysteresis effect due to the multiple steady states

Current study:
In the present work the heterogeneous azeotropic separation of ethanol and water using cyclohexane as an entrainer is considered. This system has three minimum boiling binary azeotropes (saddle points) and one minimum boiling ternary azeotrope (unstable node). The ternary- as well as one of the binary azeotropes are heterogeneous. The three pure component corners constitute stable nodes. In figure 6.1 the composition simplex is displayed with specification of residue curves and the two liquid phase boundary (binodal curve).

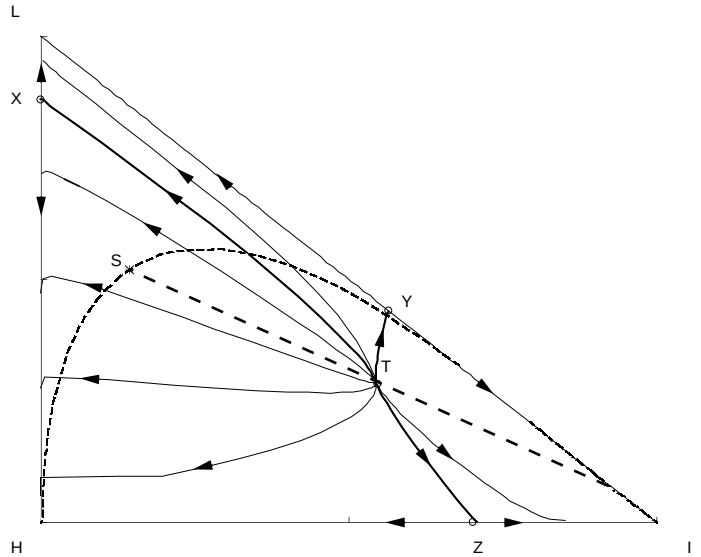

Figure 6.1. Residue curve diagram of the Ethanol(L)-Water(H)-Cyclohexane(I) system using modified UNIFAC (Larsen *et al.* (1987)). The binary azeotropes are given by X, Y, and Z. S is the the water-rich end point of the tie line going through the ternary azeotrope T.

A two-column distillation sequence suitable for this separation is considered. This sequence is termed the 'direct' sequence. For the direct sequence the external feed is introduced directly to the azeotropic column. A steady state analysis has previously been carried out in Chapter 5. This analysis was carried out on this and one additional process configuration (an 'indirect' sequence) with the additional approximations of infinite reflux and column length (Petlyuk and Avet'yan (1971), Bekiaris *et al.* (1993), Bekiaris *et al.* (1996)). One of the conclusions from that analysis was that the 'indirect' sequence appeared to be the better alternative for separating ethanol from water with cyclohexane as entrainer from a static analysis viewpoint. One may therefore argue: Why such great interest in the 'direct' distillation sequence, a sequence that provide such complex behavior and possible operational problems? The answer to that is that the 'direct' sequence is occurring quite frequently in the process industry, and thus from an industrial point of view is very interesting. From an academic point of view the 'direct' sequence is also very interesting, since an extensive analysis of this sequence may provide fundamental understanding and reveal until now undiscovered dynamic phenomena of the complex behavior of heterogeneous azeotropic distillation.

Also experimental investigations indicate that complex dynamic phenomena may appear for the direct sequence (Müller *et al.* (1997) and Müller and Marquardt (1997b)). Finally, before results on the dynamic behavior of the two types of sequences are available, it is not possible to recommend a preferred alternative. Therefore the aim of this chapter is to extend the analysis in chapter 5 to a "finite" case (finite number of trays and finite reflux). Furthermore the aim is to reveal possible complex nonlinear dynamics and practical implications of the complex static phenomena predicted through the static ∞/∞ analysis (chapter 5). The investigations in this chapter are carried out using a pseudo arc-length continuation method on a rigorous model.

First, the background, with a brief introduction to bifurcation analysis and a description of the investigated process, is given. Then follows a 1-parameter bifurcation analysis and the main results from this investigation. Subsequently, dynamics during change in composition profile types is elaborated on. Next, results are given for the case when changes in the number of liquid phases occur. Subsequently the predicted dynamics close to optimal operation is described. After this a comparison of the results obtained through continuation and the predictions obtained through the ∞/∞ analysis (see chapter 5) is outlined. In conclusion a discussion and the major conclusions of this work are given.

6.2 Background

6.2.1 Bifurcation Analysis

Consider a finite dimensional non linear time invariant (FDNLTI) system of the form:

$$\dot{x} = f(x, \alpha), \quad x \in \mathbb{R}^n, \quad \alpha \in \mathbb{R}^k, \tag{6.1}$$

where f is a smooth function of (x, α). Here $\alpha = (\alpha_1, \alpha_2, ..., \alpha_k)$, where α_1 is the bifurcation parameter and $\alpha_2, ...\alpha_k$ are auxiliary parameters (i.e. inputs). A bifurcation analysis of this system means construction of its one-parameter bifurcation diagram, in particular, studying the dependence of equilibria and limit cycles on the parameter, as well as locating and analyzing possible bifurcations (Kuznetsov (1998)).

Types of Bifurcations
A huge number of different bifurcations have been derived and described theoretically. Examples of contributions within the theoretical field are Guckenheimer and Holmes (1983), Wiggins (1990). A more application oriented approach has been given by Kuznetsov (1998). In the chemical engineering literature a number of bifurcations from the theoretical field has been found occurring in 'real life'. Some of the more common bifurcations reported within the chemical engineering literature are fold bifurcations and Hopf bifurcations. The two types of bifurcations can be described as follows:

- *Fold bifurcation:* This bifurcation is characterized by a real eigenvalue crossing the imaginary axis, and thus changing the stability of the steady state.
- *Hopf bifurcation:* A Hopf bifurcation is characterized by the emergence/disappearence of a periodic solution. The characteristics of this bifurcation is the migration of a complex pair of eigenvalues from the negative to the positive half of the complex plane. Furthermore, Hopf bifurcations are divided into supercritical and subcritical Hopf bifurcations.

where the eigenvalues are the roots of the characteristic polynomial:

$$p(\lambda) = \det(A - \lambda I) \tag{6.2}$$

Here A is the Jacobian matrix evaluated at the equilibrium point $y^0 = (x^0, \alpha^0)$:

$$A = \left.\frac{\partial f}{\partial y}\right|_{y=y^0}, \quad y = (x, \alpha) \tag{6.3}$$

where the equilibrium point satisfies:

$$\dot{x} = f(x, \alpha) = 0 \tag{6.4}$$

Within chemical engineering, various bifurcations have been reported in reacting systems: Fold bifurcations have been found to occur in CSTR reactors, see Balakotaiah and Luss (1981) and Balakotaiah and Luss (1983). Fold and Hopf bifurcations (as well as more exotic bifurcations) have been found in fixed bed reactors with recycle (Recke and Jørgensen (1997)). For binary distillation processes, fold bifurcation have been simulated (Nielsen (1990)), theoretically explained (Jacobsen and Skogestad (1991)) and experimentally verified (Kienle *et al.* (1995), Koggersbøl *et al.* (1996)). According to the many observations of steady state multiplicity described above, fold bifurcations also occur in azeotropic distillation. Recent interesting studies reveal that Hopf bifurcations may occur in homogeneous azeotropic distillation, Lee *et al.* (1999).

Performing Continuation The task of performing continuation of azeotropic distillation systems is difficult. One of the main reasons for this is the large numerical differences in states and the presence of limit points (azeotropes), which when evaluating the Jacobian numerically may introduce unreliable or at best inaccurate results. In the case of heterogeneous azeotropic distillation, the discrete introduction and deletion of a second liquid phase, results in a discontinuous Jacobian matrix. This applies not only for the decanter, but also for the movement of the interface between trays having one and two liquid phases. These discrete events may give rise to problems when integrating with a standard Newton-type method, as pointed out by Widagdo *et al.* (1992). Furthermore carrying out continuations are very time consuming, since in the current implementation, the extended Jacobian is evaluated numerically. Details on the methods used in CONT and on performing continuation with CONT can be found in Kubicek and Marek (1983) and Schreiber (1998).

6.2.2 ∞/∞ analysis

The ∞/∞ analysis was presented by Petlyuk and Avet'yan (1971) and Bekiaris *et al.* (1993) for single homogeneous azeotropic distillation columns and by Bekiaris *et al.* (1996) for single heterogeneous azeotropic distillation columns. As previously mentioned the ∞/∞ analysis, builds on the assumptions of infinite column length and reflux rate. Under the assumption of ∞/∞ conditions all feasible column profiles may be determined. These profiles contain at least one singular point. Bekiaris *et al.* (1993) defines three allowable profile types to which the feasible column profiles belong. These are:

- *Type I:* The top composition of the column is that of an unstable node. The bottom composition can be situated anywhere *inside* a distillation region.
- *Type II:* The bottom composition is that of a stable node. The top composition can be situated anywhere *inside* a distillation region.
- *Type III:* The column profile runs along the boundaries and contains at least one of the saddle points.

Using these three allowable profile types, the feasible regions of the process variables are traced while varying a key process variable (the bifurcation parameter) within its definition range.

6.2.3 "Direct" Distillation Sequence

In the current work, a distillation sequence suitable for the heterogeneous azeotropic dehydration of ethanol, using cyclohexane as the entrainer is considered. The distillation sequence is containing an azeotropic distillation column (separating ethanol from the mixture), a dehydrating column (separating water) and a decanter (separating the water-rich phase from the cyclohexane-rich phase). The sequence is termed the '*direct*' sequence, since the external feed is introduce directly into the azeotropic distillation column. This sequence is presented in Figure 6.2.

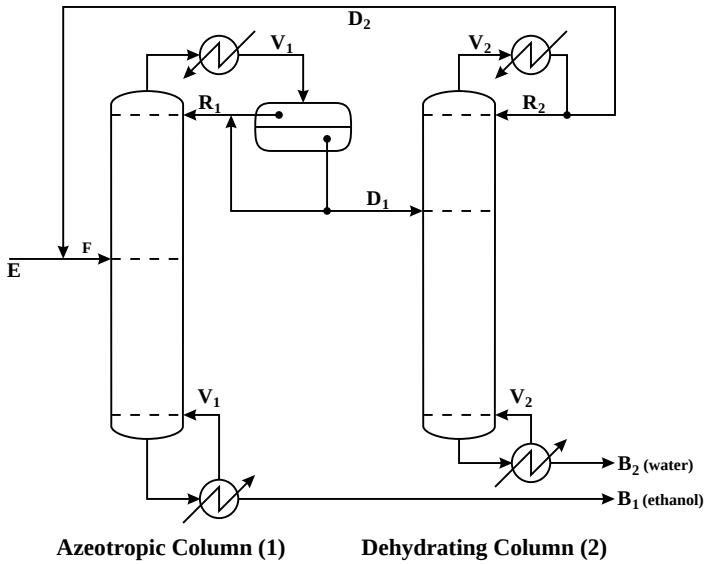

Figure 6.2. Flowsheet of the 'direct' sequence.

The process is found frequently in the chemical industry (European patent EP 0 001 681 A1). The direct sequence is operated with a feed composition near the binary azeotrope between ethanol and water.

An example analysis is carried out. This analysis is performed with:

- External feed:
  Flow rate: $E = 100$ moles/hr
  $\boldsymbol{x_E} = (x_{E,cyclohexane}, x_{E,ethanol}, x_{E,water}) = (0.05, 0.7, 0.25)$.
  External feed introduced at saturation conditions.
- 27 trays in each column
- Azeotropic column feed on tray 13 (counted from the top).
- Dehydrating column feed on tray 5 (see Figure 6.2).
- Constant vapor flow rates in the two columns of 400 moles/hr (yielding $V/E = 4$).
- Recycle flow rate, D_2, is fixed at 15 moles/hr.
- Constant pressure: 1 atm.
- Decanter operated at boiling point temperature.

It is assumed, that there is no pressure gradient in the columns and in the streams. The modified UNIFAC VLE model description used in the rigorous model, according to Larsen *et al.* (1987), as well as the parameters used are given in appendix B. The model implementation was carried out using the rigorous distillation models in the dynamic simulator DYNSIM developed by Gani and coworkers (Gani *et al.* (1986), Bossen *et al.*

(1993)). The integration of the continuation equations, as well as the model equations, was performed through methods in the solver library of the software package CONT developed by Kubicek and Marek (1983) and Schreiber (1998). The continuation equations were solved by an Adams-Bashforth method (up to 4th order). The model equations were solved by the Gear method as implemented in the LSODE package (Hindmarsh (1983), Radhakrishnan and Hindmarsh (1993)). Solution of the equations were obtained using numerically evaluated jacobiants.

6.3 Example Analyses: 1-parameter Bifurcation Analysis

As outlined above, the recycle flow rate, D_2, is fixed at $15 moles/hr$. The background for choosing this relatively small recycle rate is that it is equivalent to the rate used in the initial ∞/∞ analysis (see chapter 5) and thus the static results are comparable. However the definition sets for the parameters of interest, namely B_1 and D_1, is not entirely the same in the two analyses:

Definition Sets The decanter operates at the boiling point, and not at 298 K as was the case in chapter 5. The reason for this change was due to better convergence properties when running the continuations. This however changes the definition set of the bifurcation parameters slightly. A shortcut method for finding the definition set was presented in section 5.4.1.1. An evaluation of the geometric constructions for this method (see appendix D) gives the following definition set:

$$\begin{aligned} B_1 &\in [0; 100\, moles/hr] \\ D_2 &\in [13.3; 67.3\, moles/hr] \end{aligned}$$

In comparison, the definition set in chapter 5 - in the case where the decanter operates at 298 K - may be evaluated similarly, yielding:

$$\begin{aligned} B_1 &\in [0; 100\, moles/hr] \\ D_2 &\in [12.2; 51.6\, moles/hr] \end{aligned}$$

The definition sets above are quite different from the set derived in section 5.4.1.1. The reason for that is that a different (realistic) feed composition was used in section 5.4.1.1. As will materialize from the continuation, the definition set of B_1, with decanter operating at the boiling point temperature (listed above), corresponds to the following range of reflux ratio:

$$L_1/D_1 \in [2.60; 28.9]$$

The change in definition sets combined with the choice of recycle rate for the example analysis, implies exceptionally slow dynamics for some

range of reflux ratio around optimal purity of ethanol product, as shall be seen later. The combination may also result in branches of steady state solutions separated from each others. These issues will be discussed later.

6.3.1 Continuation of Steady States

In figure 6.3 the bifurcation diagram obtained from the continuation with CONT is given. As can be seen from this figure multiple steady state solutions occur in a typical hysteresis scenario. That is stable solutions of high and low product purity coexists, and their basins of attraction are separated by an unstable solution of intermediate purity. However the performed continuation did not result in a continuous range of solutions, but rather fragmentary ranges of solutions.

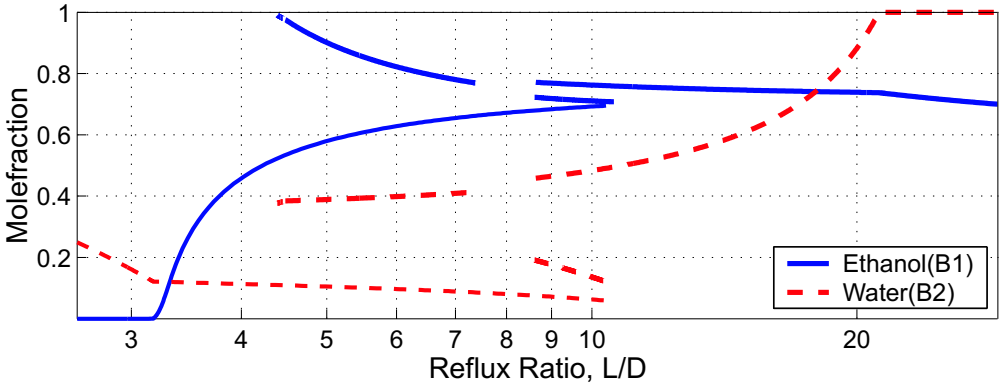

Figure 6.3. Transition of product purities (solid: ethanol purity of ethanol product, dashed: water purity of water product).

In subsections 6.3.2–6.3.4 below, continuation results of the different steady state branches are described, by following the three branches of the ethanol product purity in figure 6.3 (ethanol mole fraction of B_2) with low, medium or high ethanol purity.

6.3.2 Lower Steady State Branch

The steady state branch with the low ethanol product purity is equivalent to the branch derived from steps 1 to 2 in the ∞/∞ analysis of chapter 5. Figure 6.4 displays the transition of product purities, the magnitude of the realpart of the rightmost eigenvalue, as well as the liquid composition profiles for both distillation columns along this branch. As can be seen from this figure the branch starts at a reflux ratio, L/D, of 2.602, where the composition of the product from column 2 corresponds to the external feed composition. The figure also illustrates at a reflux ratio of 3.176 that the composition profile type of the azeotropic column changes according to section C.1 from a type II to a type III profile. During this shift the realpart of the rightmost eigenvalue passes a maximum (without changing

sign). The lower steady state branch terminates when the decanter overall liquid composition reaches the region of liquid splitting (limited by the binodal curve). This happens at a reflux ratio of 10.379.

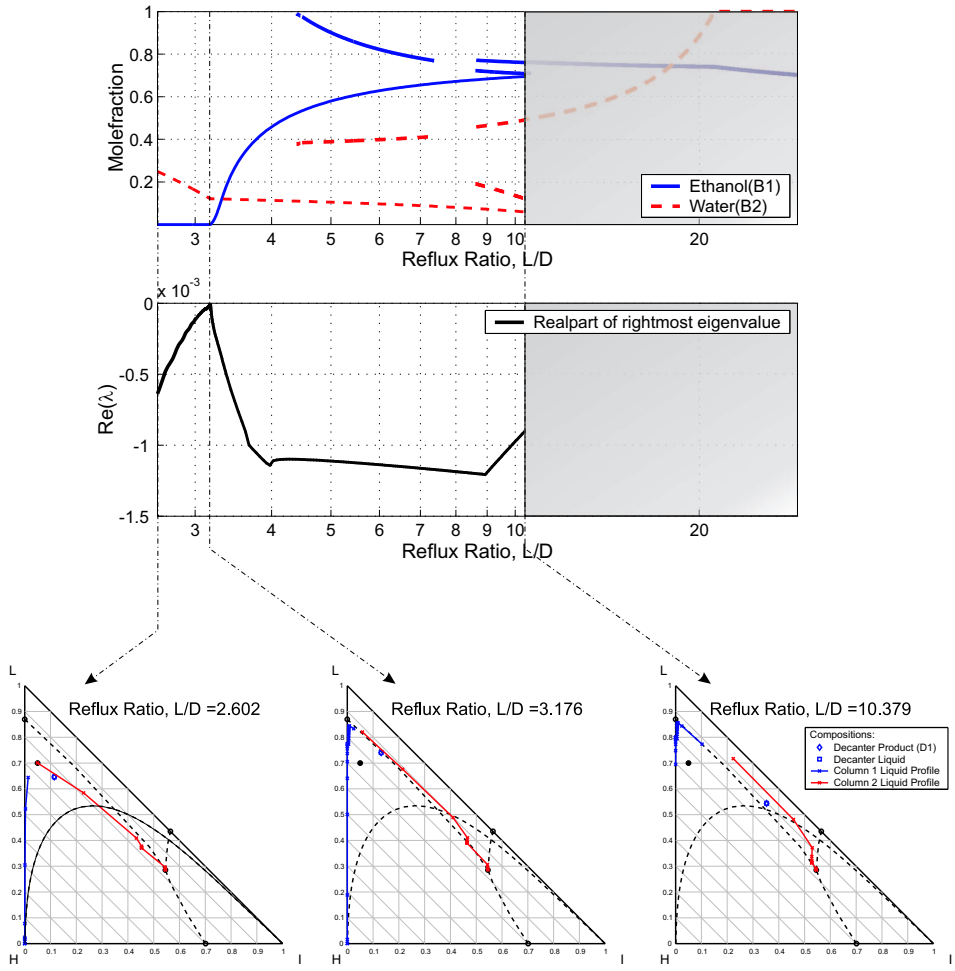

Figure 6.4. Transition of product purities (top figure - solid: ethanol purity of ethanol product, dashed: water purity of water product), realpart of rightmost eigenvalue on the lower branch (middle figure) and liquid composition profiles in the composition simplex for 3 particular reflux ratio values (bottom figure)on the lower branch.

6.3.3 Middle Steady State Branch

The middle steady state branch corresponds to the branch derived from step 3 in the ∞/∞ analysis. In the range where multiple steady states exist, this branch represents the solutions with medium ethanol product purity. Since continuation from the lower steady state branch to the middle steady state branch was not immediately feasible, an initial starting point on the middle steady state branch was obtained by implementing a P-controller. This P-control controlled the decanter composition by manipulating the reflux ratio. Once a steady state was obtained, the con-

troller was disconnected and continuation was started from this stationary point. In figure 6.5 the change of product purities and the real part of the rightmost eigenvalue has been plotted against the reflux ratio, together with liquid composition profiles for both distillation columns within this branch. It is seen that the continuation covers a reflux ratio range of 8.608 to 10.590, in which one eigenvalue has positive real part, thus rendering this stationary solution unstable.

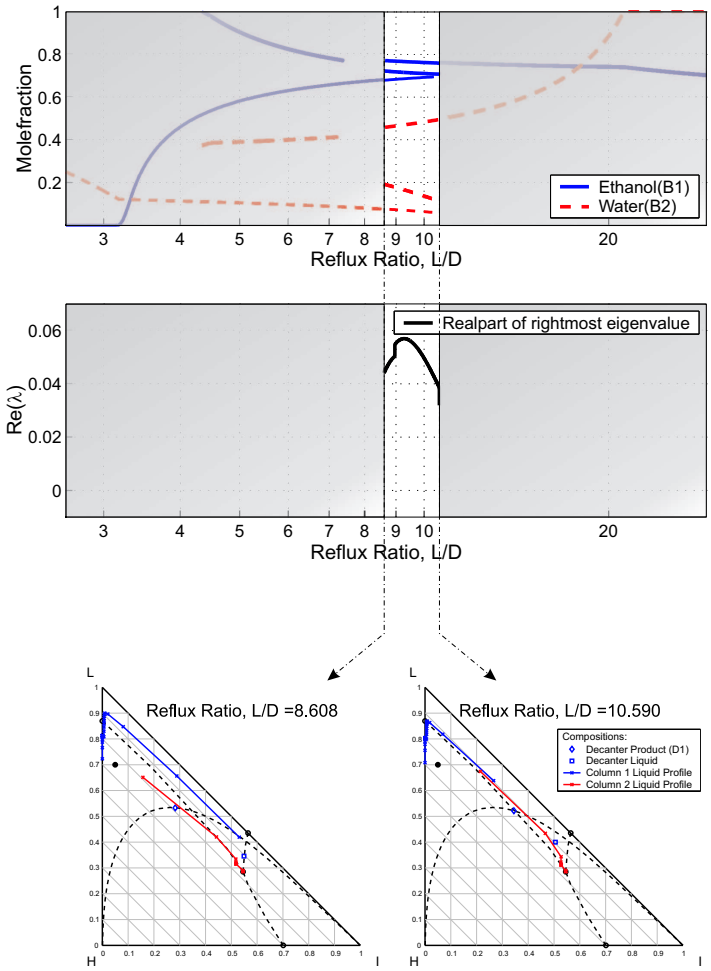

Figure 6.5. Transition of product purities (top figure - solid: ethanol purity of ethanol product, dashed: water purity of water product), realpart of rightmost eigenvalue on the middle branch (middle figure) and liquid composition profiles in the composition simplex for 2 particular reflux ratio values (bottom figure)on the middle branch.

6.3.4 Upper Steady State Branch

The upper steady state branch corresponds to the branch derived from steps 4 to 8 in the ∞/∞ analysis. This branch corresponds to the static solutions with high ethanol product purity. It is seen that the continuation results of this branch are somewhat fragmented.

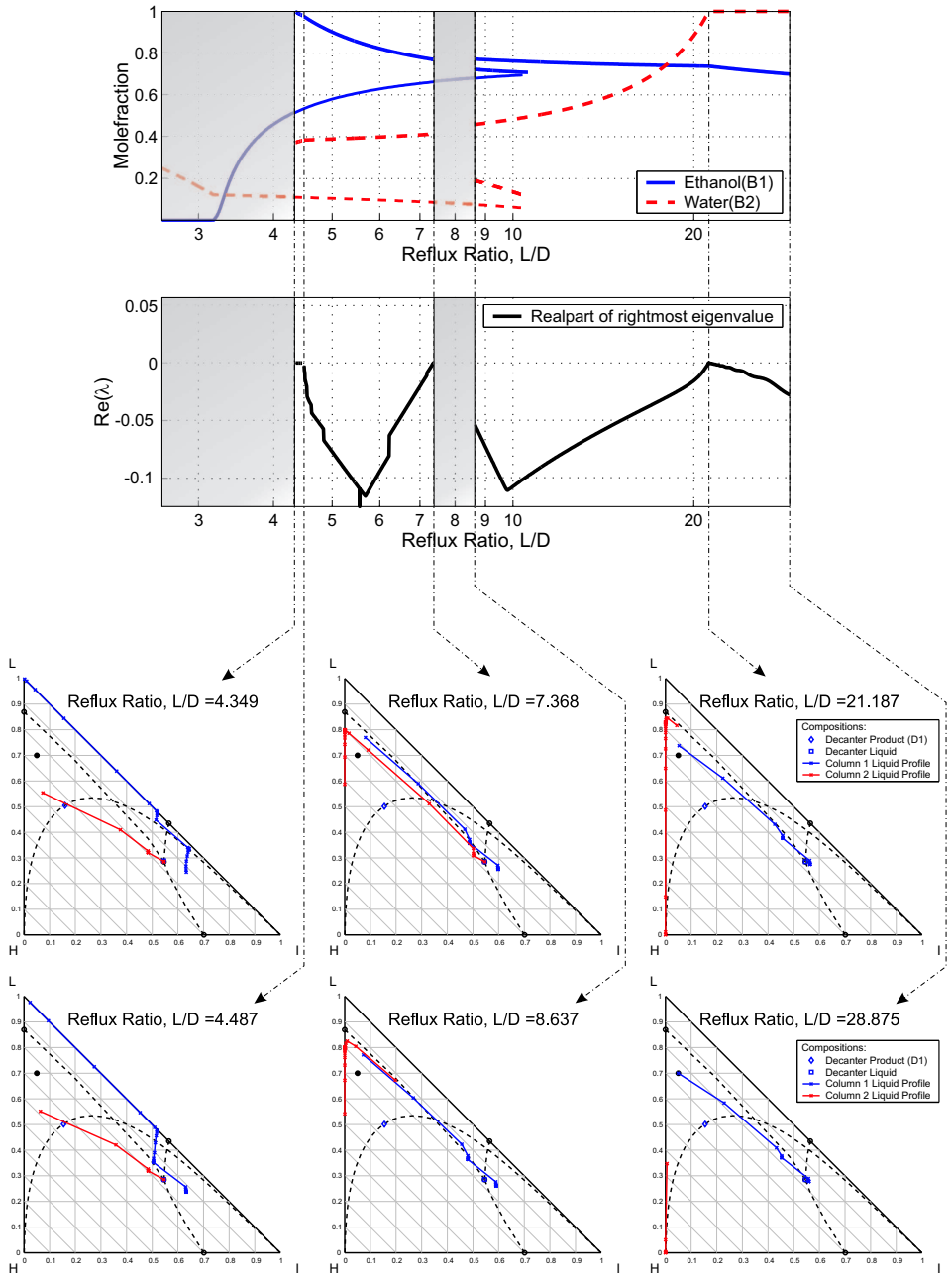

Figure 6.6. Transition of product purities (top figure - solid: ethanol purity of ethanol product, dashed: water purity of water product), realpart of rightmost eigenvalue on the upper branch (middle figure) and liquid composition profiles in the composition simplex for 6 particular reflux ratio values (bottom figure)on the upper branch.

The reflux ranges of 4.349–4.446, 4.487–7.368 and 8.637–28.875 are covered. The termination of this branch is reached, when the water product flow rate reaches zero, and thus the ethanol product reaches the composition of the external feed. This happens for a reflux ratio of 28.875.

6.4 Dynamics at Changes in Composition Profile Type

An interesting aspect is the dynamic behavior during changes of composition profile type (according to the ∞/∞ analysis). Figure 6.7 below shows a series of eigenvalue plots at different values of the reflux ratio. It illustrates the right most eigenvalues during a change in composition profile type occurring between steps 1 and 2 (see figure C.2) for the direct sequence. As can be seen from this figure one real eigenvalue is moving towards zero when the bifurcation parameter (reflux ratio) is approaching the point where a change in composition profile from type II to III is occurring. The eigenvalue does not cross the imaginary axis. This implies that open loop dynamics is very slow during change in composition profile. This observation is also physically plausible, since the change in composition profile is always accompanied by at least one end-composition reaching either a small vicinity of an azeotrope or a distillation boundary, thus resulting in the inclusion of at least one additional pinch point within the composition profile during profile change. To keep the record straight: by "open loop" is meant standard (L, V) configuration with level and pressure control loops closed (perfect control), but composition control loops open.

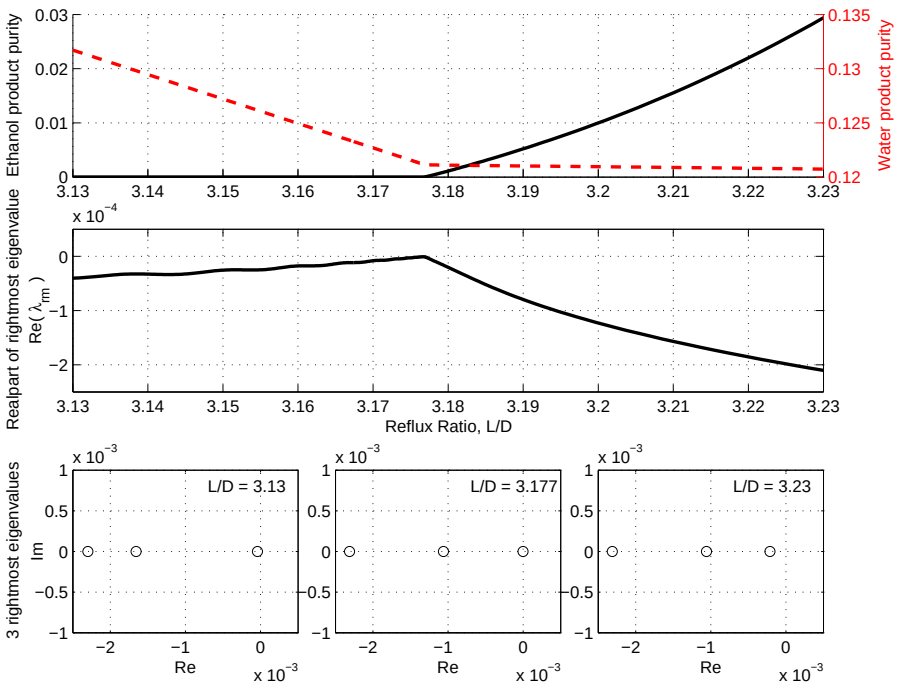

Figure 6.7. Transition of product purities (top - solid: ethanol purity of ethanol product, dashed: water purity of water product), realpart of rightmost eigenvalue (middle) and location of 3 rightmost eigenvalues (bottom) during a change in composition profile occurring between step 1 and step 2

6.5 Dynamics at Change in Number of Phases

In the situation where the number of phases changes, i.e. for that particular value of the bifurcation parameter where the number of liquid phases in the decanter changes from 1 to 2, the function f in equation 6.1 is not C^1 and thus not possible to linearize. The notion of eigenvalues for this particular value of the bifurcation parameter looses its meaning. The consequence is therefore also that a standard Newton based continuation method fails with the discrete introduction and deletion of a second liquid phase, since the Jacobian matrix is discontinuous. The function f however is still C^0.

It is important to note that the overall composition profiles do not change in the limit where the number of liquid phases in the decanter changes. For the direct sequence the change in number of liquid phases occurs between step 2 and 3 (see figure C.2). In figure 6.8 below, the ethanol product purity and the right most eigenvalue have been plotted for reflux ratios close to the singular point where the number of liquid phases changes. It is seen that the medium ethanol product purity steady state branch (black dashed) as expected is unstable, since the real part of the right most eigenvalue is positive. It is also seen that the lower ethanol product purity steady state branch (blue solid) is stable, since the right most eigenvalue is negative. Moreover, et is evident that the unstable steady state branch

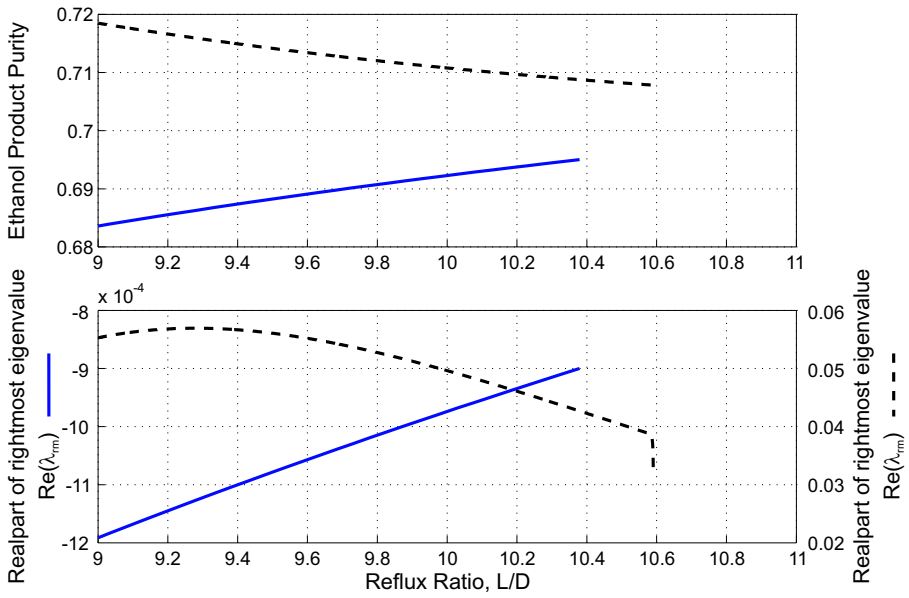

Figure 6.8. Transition of ethanol product purity (top - ethanol purity of ethanol product - blue solid: one stable liquid phase, black dashed: liquid phase splitting occurring in decanter, real part of rightmost eigenvalue (bottom) during a change in the number of phases in the decanter (occurring between step 2 and step 3)

goes beyond the extent of the stable steady branch. The implication of this observation is that the two steady state branches of figure 6.8 can not be connected via only one simple fold bifurcation, but necessarily have to be connected through more complex bifurcation(s). In chapter 7 this region of the bifurcation diagram is investigated further.

6.6 Dynamics close to optimal operation

In the obvious operating point i.e. were optimal purity of the ethanol product is reached, it was seen in chapter 5 that state multiplicity occurs in the case with infinite number of trays and infinite reflux. This happens during step 4 of the ∞/∞ analysis. It was also predicted that a fold bifurcation occurred close to the state multiplicity. The fold bifurcation occurs in the changes between steps 3 and 5 according to the ∞/∞ analysis.

Unfortunately it was not possible to perform the continuation around the fold bifurcation at optimal ethanol product purity. It was however possible to get very close to were the bifurcation occurs. Figure 6.9 shows the development of the rightmost eigenvalues for values of the reflux ratio close to optimal purity of the ethanol product. It is seen that the right

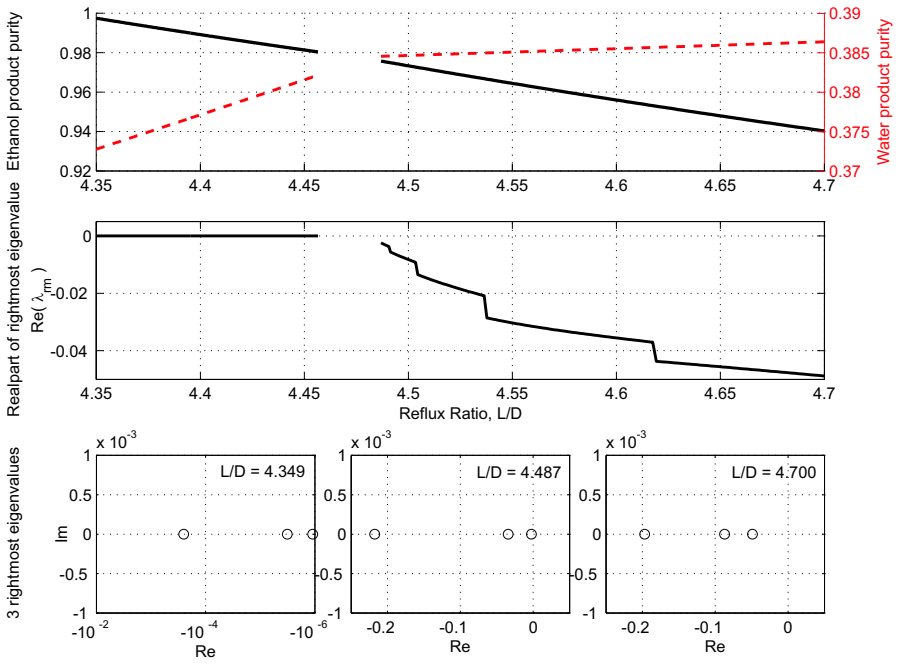

Figure 6.9. Transition of product purities (top - black: ethanol purity of ethanol product, red: water purity of water product, solid/dashed: lower/middle branch respectively), real part of rightmost eigenvalue (middle) and location of 3 rightmost eigenvalues (bottom) during step 5 and a part of step 6

most eigenvalue is very close to zero (-1e-6) in the near vicinity of optimal purity of the ethanol product – Do note that the eigenvalue plot of reflux ratio $L/D = 4.349$ has a logarithmic scale of the real axis (bottom left corner of figure 6.9). It is furthermore observed that the three right most eigenvalues are real (imaginary part of zero) for the values of reflux ratio displayed. The implications of the numerically very small eigenvalue observed, is that close to optimal ethanol product purity the open loop dynamics of the system is exceptionally slow. The reason for this is to be found in the way the decanter is operated, and can be qualitatively explained through ∞/∞ considerations: The decanter operates at boiling point temperature conditions, instead of 298 K as was the case in chapter 5. This changed the definition set of B_1 and D_2 compared to 5. The change results in the decanter composition moving very close to the ternary azeotrope, when the state multiplicity (optimal ethanol product purity) occurs. The implication therefore is that the azeotropic column contains 'close' to three pinch points where the state multiplicity occur: the bottom composition is located in the pure component corner of ethanol (L), the decanter composition is located very close to the ternary azeotrope (T), and the column composition profile contain one additional pinch point (either X or Y) immediately before and after the state multiplicity. Thus the dynamics has to be slow.

6.7 Comparison to ∞/∞ predictions

The results from the ∞/∞ analysis carried out on the direct sequence in chapter 5 are summarized in table 6.1 together with the results for the continuations.

Table Notes:

$^{\diamondsuit}$ "Steady State Solution" refers to the steady state solution traced in the continuation: sS = stable steady state; uS = unstable steady state.

† "Continuation" refers to what reflux ratio ranges (on the individual branches) continuation have been performed for. The performed continuations only cover continuation of the static solution within each reflux ratio segment.

$^{\heartsuit}$ "Multiplicity" occurring according to ∞/∞ predictions: OM = step in which Output Multiplicity occurs; SM = step in which State Multiplicity occurs.

$^{\maltese}$ A bifurcation is expected quite close to a reflux ratio of 10.379. The reasons for that are that the total decanter composition lies very close to the binodal curve for this reflux ratio, and because the ∞/∞ analysis predicts that the distillate composition and the overhead

Continuation			**∞/∞ predictions**				
Reflux Ratio Azeotropic Column	Steady State Solution$^{\diamond}$	Continuation†	Step	Type,Pinch		Multi-plicity$^{\heartsuit}$	Branch
				Azeo. Col.	Dehyd. Col.		
α=2.602	sS	✓	Init	II, H	I, T		Lower
2.602<α<3.176	-	✓	1	II, H	I, T		
3.176<α<10.379$^{\clubsuit}$	-	✓	2	III, X	I, T	OM	
⋮ ♠	⋮		-	-	-		
⋮ ♠	⋮		3	III, X	I, T	OM	Middle
10.590>α>8.608	uS	✓	-	-	-		
8.608>α>α_f	-		-	-	-		
$\alpha=\alpha_f$	-		4	II, L	I, T	OM,SM	Upper
α_f<α<4.349	sS		5	III, Y	I, T	OM	
4.349<α<4.46	-	✓	-	-	-		
4.46<α<$\alpha_{5\to6}$*	-		-	-	-		
$\alpha_{5\to6}$<α<4.487*	-		6	I, T	I, T	OM	
4.487<α<7.368	-	✓	-	-	-		
7.368<α<$\alpha_{6\to7}$*	-		-	-	-		
$\alpha_{6\to7}$<α<8.64*	-		7	I, T	III, X	OM	
8.637<α<21.187	-	✓	-	-	-		
21.187<α<28.875	-	✓	8	I, T	II, H		
α=28.875	-	✓	Final	I, T	II, H		

Table 6.1. Summary of results from continuation and ∞/∞ predictions of the direct sequence. See text for detailed description.

vapor composition splits and move in separate directions, when the total decanter composition enters the liquid split region.

♠ As described above, the lower and middle branches can not be connected via only one simple fold bifurcation, but necessarily have to be connected through more complex bifurcation(s).

* $\alpha_{5\to6}$ and $\alpha_{6\to7}$ correspond to the reflux ratio values were the composition profiles shift, according to the ∞/∞ predictions, from step 5 to 6 and 6 to 7 respectively.

As already pointed out the continuation did not result in a continuous range of solutions, but rather fragmentary ranges of solutions. It is seen from table 6.1 that continuation was not possible for any of the composition profile shifts where a type I profile was transformed into a type III profile (or vice versa). Also continuation was not possible around the 'internal state' multiplicity/fold predicted to occur between step 3 and 5.

6.8 Discussion

Continuation of state multiplicity / upper fold bifurcation With a little effort continuation around the internal state multiplicity / fold bifurcation may be possible within the current setup, if recycle is increased or for an alternative feed composition. From the ∞/∞ analysis it is seen that the transition from step 3 to 5 involves composition profile type shift: III $\rightarrow$ II $\rightarrow$ III in the azeotropic column. This type of transition as is also obvious from the results in table 6.1 does normally not constitute a problem within the current setup.

Variation of recycle flow rate In the analysis, the recycle flow rate, D_2, was fixed at 15 moles/hr. It will be very interesting to examine the dynamic behavior for higher and more production relevant recycle flow rates. The determination of a suitable recycle flow rate, D_2, is a trade off between having a wider high purity branch of the ethanol product, where the dynamics is faster (high recycle flow rate), and having reduced energy consumption, where the dynamics is very slow (low recycle flow rate). This trade off obviously needs to be subject to the fulfillment of product purity requirements.

Method of continuation A possible improvement of the current setup would be an extension to the continuation method, by adding a stiff integration method for the integration of continuation equations, but more important add an exact integration method for the model equations, were integration is carried out as usual when the number of liquid phases does not change, until exactly the limit were an additional liquid phase appears or disappears, then the integration is restarted with the new number of liquid phases.

6.9 Conclusions

In this chapter, a bifurcation analysis has been performed on a heterogeneous azeotropic distillation sequence suitable for the dehydration of ethanol using cyclohexane as entrainer. The sequence contains an azeotropic column with a decanter and a dehydrating column. The external feed is entered directly to the azeotropic column – thus the sequence is termed the 'direct' sequence. The analysis is carried out using rigorous models implemented in a dynamic simulator integrated with continuation software. The continuation method used is arc-length continuation. The parameter chosen as primary bifurcation parameter in the investigation is reflux ratio for the azeotropic distillation column. The existence of multiple steady states was verified within the 'direct' sequence. In the present

case the multiple solutions occur in a typical hysteresis scenario. That is stable solutions of high and low product purity coexists, and their basins of attraction are separated by an unstable solution of intermediate purity.

The sequence exhibit "state multiplicity" in the obvious operating point for the ∞/∞ case, meaning that for fixed inputs and outputs multiple solutions of the internal column profiles exists (chapter 5). It was not possible to perform the continuation around the state multiplicity and the expected fold bifurcation at optimal ethanol product purity for the chosen combination of feed composition and recycle flow rate. It was however possible to get very close to were the bifurcation occurs. It is concluded that the phenomenon of "state multiplicity" may be seen in the bifurcation analysis as a real eigenvalue moving very close to the imaginary axis, thus resulting in a very slow open loop dynamic behavior in the vicinity of the obvious operating point. This point of tangency signifies where the "state multiplicity" occurs, but also occurs during change of composition profiles.

The results from the bifurcation analysis furthermore indicate that complex dynamic behavior is expected to occur in the boundary region of liquid phase splitting. By “more complex” dynamic behavior is meant that the two branches, lower ethanol product purity branch and medium ethanol product purity branch, can not be connected via only one simple fold bifurcation, but necessarily have to be connected through more complex bifurcation(s).

Notation

Variable	Description
A	Jacobian matrix (defined in equation 6.3)
B_j	Bottom product molar flow rate for column j in distillation sequence
D	Distillate product molar flow rate
D_j	Distillate product molar flow rate for column j in distillation sequence
D_j	Distillate product composition for column j in distillation sequence
E	External feed molar flow rate for distillation sequence
f	Smooth function (equation 6.1)
H	Pure component corner in composition simplex (heavy component)
I	Pure component corner in composition simplex (intermediate component)
L	Reflux molar flow rate
L_j	Reflux molar flow rate for column j in distillation sequence

Variable	Description
L	Pure component corner in composition simplex (light component)
p	Characteristic polynomial (equation 6.2)
S	Heavy liquid composition in decanter when overall decanter composition is equal to ternary azeotropic composition
T	Ternary azeotrope
V	Vapor molar flow rate
x	State vector
$\dot{x}$	Time derivative of state vector
X	Binary azeotrope
$\boldsymbol{x_E}$	External feed composition for distillation sequence
$x_{E,i}$	External feed mole fraction of component i
Y	Binary azeotrope
y	Extended state vector ($y = (x, \alpha)$)
y^0	Equilibrium point ($y^0 = (x^0, \alpha^0)$)
Z	Binary azeotrope
α	Vector of bifurcation parameter(s) and auxiliary parameters (i.e. inputs)
α_n	Bifurcation parameter ($n = 1$), auxiliary parameters ($n = 2, ..., k$)
∂	Partial derivative
λ	Vector of eigenvalues

References

Andersen, H. W.; Laroche, L. and Morari, M. (1991). Dynamics of Homogeneous Azeotropic Distillation Columns. *Ind. Eng. Chem. Res.*, **30**, 1846–1855.

Balakotaiah, V. and Luss, D. (1981). Analysis of the Multiplicity Patterns of a CSTR. *Chem. Eng. Comm.*, **13**, 111–132.

Balakotaiah, V. and Luss, D. (1983). Multiplicity Features of Reacting Systems. Dependence of Steady States of a CSTR on the Residence Time. *Chem. Eng. Sci.*, **38**, 1709–1721.

Bekiaris, N.; Meski, G. A.; Radu, C. M. and Morari, M. (1993). Multiple Steady States in Homogeneous Azeotropic Distillation. *Ind. Eng. Chem. Res.*, **32**(9), 2023–2038.

Bekiaris, N.; Meski, G. A. and Morari, M. (1996). Multiple Steady States in Heterogeneous Azeotropic Distillation. *Ind. Eng. Chem. Res.*, **35**, 207–237.

Bossen, B. S.; Jørgensen, S. B. and Gani, R. (1993). Simulation, Design, and Analysis of Azeotropic Distillation Operations. *Ind. Eng. Chem. Res.*, **32**, 620–633.

Doherty, M. F. and Perkins, J. (1978). On the Dynamics of Distillation Processes I: The Simple Distillation of Multicomponent Non-Reacting Homogeneous Liquid Mixtures. *Chem. Eng. Sci.*, **33**, 281.

Gani, R. and Jørgensen, S. B. (1994). Multiplicity in Numerical Solution of Nonlinear Models: Separation Processes. *Comput. Chem. Eng.*, **18**, 55.

Gani, R.; Ruiz, C. A. and Cameron, I. T. (1986). A Generalized Model for Distillation Columns - I. *Comp. Chem. Eng.*, **10**, 181–198.

Guckenheimer, J. and Holmes, P. (1983). *Nonlinear Oscillations, Dynamical Systems, and Bifurcations of Vector Fields*, volume 42 of *Springer Series in Applied Mathematical Sciences*. Springer Verlag. ISBN 3-540-90819-6. (Sixth printing 2001).

Güttinger, T. E.; Dorn, C. and Morari, M. (1997). Experimental Study of Multiple Steady States in Homogeneous Azeotropic Distillation Sequences. *Ind. Eng. Chem. Res.*, **36**, 794–802.

Hilmen, E. K.; Kiva, V. N. and Skogestad, S. (1999). Analysis of Closed Multivessel Batch Distillation of Ternary Azeotropic Mixtures using Elementary VLE Cells. *Comp. Chem. Engng.*, **23**(Suppl), 347–350.

Hindmarsh, A. C. (1983). ODEPACK, A Systematized Collection of ODE Solvers. *IMACS Transactions on Scientific Computation*, **1**, 55–64. in Scientific Computing, R.S. Stepleman et al. (Eds.), North-Holland, Amsterdam.

Jacobsen, E. W. and Skogestad, S. (1991). Multiple Steady States in Ideal Two–Product Distillation. *AIChE Journal*, **37**, 499–511.

Kienle, A.; Groebel, M. and Gilles, E. D. (1995). Multiplicities and instabilities in binary distillation - Theoretical and experimental results. *Chem. Eng. Sci.*, **50**, S2691–S2703.

Koggersbøl, A.; Andersen, T. R.; Bagterp, J. and Jørgensen, S. B. (1996). An Output Multiplicity in Binary Distillation : Experimental Verification. *Comput. Chem. Eng.*, **20**, S835–S840.

Kovach, J. and Seider, W. D. (1987a). Heterogeneous Azeotropic Distillation: Experimental and Simulation Results. *AIChE Journal*, **33**, 1300–1314.

Kovach, J. and Seider, W. D. (1987b). Heterogeneous Azeotropic Distillation - Homotopy-Continuation Methods. *Comput. Chem. Eng.*, **11**(6), 593–605.

Kubicek, M. and Marek, M. (1983). *Computational Methods in Bifurcation Theory and Dissipative Structures*. Springer Series in Computational Physics. Springer-Verlag, Inc., New York. ISBN 0-387-12070-X.

Kuznetsov, Y. A. (1998). *Elements of Applied Bifurcation Theory*. Springer-Verlag, Inc., New York. ISBN 0-387-98382-1.

Larsen, B. L.; Rasmussen, P. and Fredenslund, A. (1987). A Modified UNIFAC Group-Contribution Model for Prediction of Phase Equilibria and Heats of Mixing. *Ind. Eng. Chem. Res.*, **26**, 2274–2286.

Lee, M.; Dorn, C.; Meski, G. A. and Morari, M. (1999). Limit Cycles in Homogeneous Azeotropic Distillation. *Ind. Eng. Chem. Res.*, **38**, 2021–2027.

Luyben, W. L., editor (1992). *Practical Distillation Control*. Van Nostrand Reinhold, New York. ISBN 0-442-00601-2.

Magnussen, T.; Michelsen, M. and Fredenslund, A. (1979). Azeotropic Distillation Using UNIFAC. In *Inst. Chem. Eng. Symp. Ser. No. 56*, Intl. Symp. on Distillation, Rugby, England.

Matsuyama, H. and Nishimura, H. (1977). Topological and Thermodynamic Classification of Ternary Vapor-Liquid Equilibria. *J. Chem. Eng. Japan*, **10**(3), 181–187.

Müller, D. and Marquardt, W. (1997a). Dynamic Multi–phase Flash Simulation: Global Stability Analysis versus Quick Phase Determination. *Comput. Chem. Eng.*, **21**, S817–S822.

Müller, D. and Marquardt, W. (1997b). Experimental Verification of Multiple Steady States in Heterogeneous Azeotropic Distillation. *Ind. Eng. Chem. Res.*, **36**(12), 5410–5418.

Müller, D.; Marquardt, W.; Hauschild, T.; Ronge, G. and Steude, H. (1997). Experimental Validation of an Equilibrium Stage Model for Three–phase Distillation. *IChemE Symp. Ser.*, **142**, 149–159.

Nielsen, C. S. (1990). *Multivariable Identification and Control of an Experimental Distillation Column with Heat Pump*. Ph.D. thesis, Department of Chemical Engineering, Technical University of Denmark.

Petlyuk, F. B. and Avet'yan, V. S. (1971). Investigation of the Rectification of Three–component mixtures with Infinite Reflux. *Theor. Found. Chem. Eng.*, **5**, 499–507.

Prokopakis, G. J. and Seider, W. D. (1983). Dynamic Simulation of Azeotropic Distillation Towers. *AIChE. J.*, **29**(6), 1017–1029.

Rademaker, O.; Rijnsdorph, J. E. and Maarleveld, A. (1975). *Dynamics and Control of Continuous Distillation Units*. Elsevier Scientific Publishing Company, Amsterdam. ISBN 0-444-41234-4.

Radhakrishnan, K. and Hindmarsh, A. C. (1993). Description and Use of LSODE, the Livermore Solver for Ordinary Differential Equations. LLNL Report UCRL-ID-113855.

Recke, B. and Jørgensen, S. B. (1997). Non-linear Dynamics of a Fixed Bed Reactor with Recycle. *Fractals and Chaos in Chemical Engineering*, pages 652–663. Proceedings of the International CFIC 96 Conference. Rome, Italy 2 - 5 September 1996. ISBN 981-02-3165-2.

Rovaglio, M. and Doherty, M. F. (1990). Dynamics of Heterogeneous Azeotropic Distillation Columns. *AIChE Journal*, **36**, 39–52.

Schreiber, I. (1998). Description of CONT - program for construction of parameter dependence of stationary or periodic solutions of ordinary differential or difference equations.

Skogestad, S. and Morari, M. (1987). The Dominant Time Constant for Distillation Columns. *Comp. Chem. Engng.*, **11**(6), 607–617.

Skogestad, S. and Morari, M. (1988). Understanding the Dynamic Behavior of Distillation Columns. *Ind. Eng. Chem. Res.*, **27**(10), 1848–1862.

Vadapalli, A. and Seider, J. D. (2001). A Generalized Framework for Computing Bifurcation Diagrams Using Process Simulation Programs. *Comp. Chem. Engng.*, **25**, 445–464.

Widagdo, S. and Seider, W. D. (1996). Azeotropic Distillation. *AIChE Journal*, **42**(1), 96–130.

Widagdo, S.; Seider, W. D. and Sebastian, D. H. (1989). Bifurcation Analysis in Heterogeneous Azeotropic Distillation. *AIChE Journal*, **35**(9), 1457–1464.

Widagdo, S.; Seider, W. D. and Sebastian, D. H. (1992). Dynamic Analysis of Heterogeneous Azeotropic Distillation. *AIChE Journal*, **38**(8), 1229–1242.

Wiggins, S. (1990). *Introduction to Applied Non-linear Dynamical Systems and Chaos*. Springer-Verlag, New York.

7

Dynamics of a Heterogeneous Azeotropic Distillation Sequence II

Dynamic Simulation

The present chapter extends the bifurcation analysis of the heterogeneous azeotropic distillation sequence, carried out in Part I of this work. The investigations in this chapter are performed via rigorous dynamic simulation. The sequence investigated is the 'direct' sequence suitable for the dehydration of ethanol using cyclohexane as entrainer. The dynamic simulations of this sequence are carried out using rigorous models implemented in the dynamic simulator DYNSIM (Gani et al. *(1986), Bossen* et al. *(1993)). Reflux ratio is chosen as the parameter of variation. The results from the simulations reveal that sustained oscillations occur in the 'direct' sequence in the region close to and beyond the boundary of liquid phase splitting within the decanter. This is the first reported occurrence of limit cycles in the literature within heterogeneous azeotropic distillation. The oscillation reported here exists within a reflux ratio range of 9.5–11.88838. The results indicate clearly that the stable periodic solution is bounded by a cyclic fold bifurcation and a 'blue sky' catastrophe (global bifurcation). The implication of the latter global bifurcation is that the period time increases for increasing parameter of variation. As the parameter of variation increases towards the bifurcation point and the period time of the limit cycle tends to infinity, the amplitude of the solution remains bounded. The occurrence and implications of the limit cycle on operation is discussed. A comparison of the results obtained here with the results of the ∞/∞ analysis of the direct sequence carried out in chapter 5 is given.*

7.1 Introduction

A commonly encountered task in the chemical process industry is the separation of azeotropic mixtures into pure constituents. This separation can be facilitated through distillation by adding an entrainer. The resulting ternary system can be categorized as an either homogeneous or heterogeneous system. In industry the application of heterogeneous azeotropic

distillation is by far the most widely used of the two types of separation (Widagdo and Seider (1996)). Heterogeneous azeotropic distillation is carried out at lower temperatures than homogeneous azeotropic distillation with a heavy entrainer, rendering this separation more energy efficient. Operation of heterogeneous azeotropic distillation processes however is known to be potentially difficult due to the very high degree of nonlinearity.

A considerable effort has been put into the research area of distillation behavior. A brief overview of some major contributions within the research field of distillation dynamic behavior was given in part I (chapter 6) of this work. The reader is referred to this overview.

In the present work the heterogeneous azeotropic separation of ethanol and water using cyclohexane as an entrainer is considered. This system has three minimum boiling binary azeotropes (saddle points) and one minimum boiling ternary azeotrope (unstable node). The ternary- as well as one of the binary azeotropes are heterogeneous. The three pure component corners constitute stable nodes. In figure 7.1 the composition simplex is displayed with specification of residue curves and the two liquid phase boundary (binodal curve).

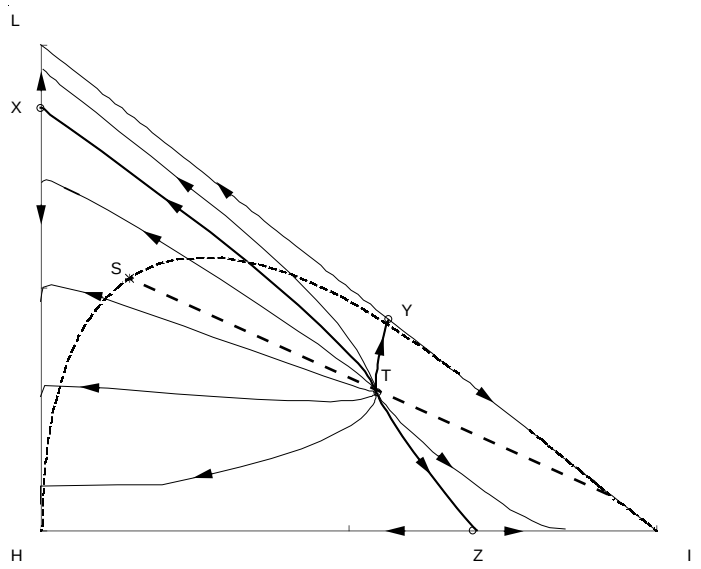

Figure 7.1. Residue curve diagram of the Ethanol(L)-Water(H)-Cyclohexane(I) system using modified UNIFAC (Larsen *et al.* (1987)). The binary azeotropes are given by X, Y, and Z. S is the the water-rich end point of the tie line going through the ternary azeotrope T.

A two-column distillation sequence suitable for this separation is considered. This sequence is termed the 'direct' sequence. For the direct sequence the external feed is introduced directly to the azeotropic column.

The flowsheet of the distillation sequence is sketched in figure 7.2

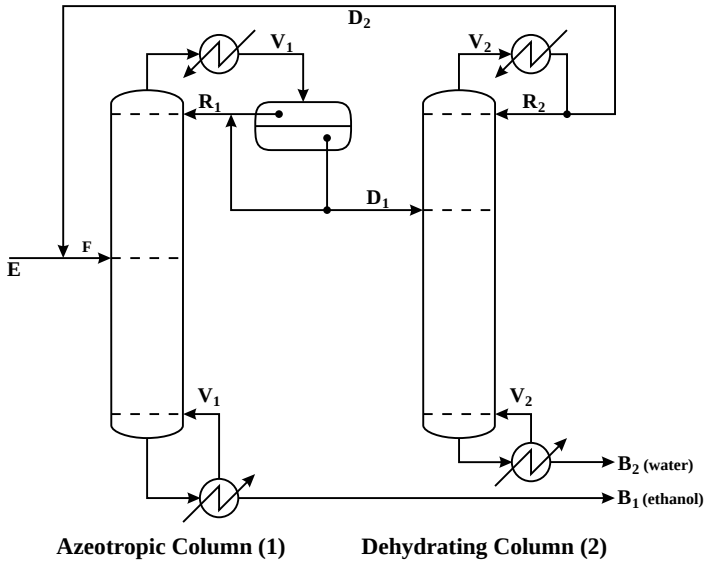

Figure 7.2. Flowsheet of the 'direct' sequence.

A steady state analysis has previously been carried out in chapter 5. This analysis was carried out on this and one additional process configuration (an 'indirect' sequence) with the additional approximations of infinite reflux and column length (Petlyuk and Avet'yan (1971), Bekiaris *et al.* (1993), Bekiaris *et al.* (1996)). The ∞/∞ analysis predicted output and internal state multiplicity for the direct sequence. The static solutions were verified through steady state simulations on a sequence with finite column lengths. The results from the ∞/∞ analysis of the direct sequence were extended by a bifurcation analysis in chapter 6 using arc-length continuation. Output multiplicity was verified again. Another main conclusion of this chapter was that more complex dynamic behavior is expected to occur in the boundary region of liquid phase splitting for the decanter (and possibly also in this region further down the trays of the azeotropic column). By "more complex" dynamic behavior is meant that the two branches, lower ethanol product purity branch and medium ethanol product purity branch, can not be connected via only one simple fold bifurcation, but necessarily have to be connected through more complex bifurcation(s), or not be connected at all.

Experimental investigations indicate that complex dynamic phenomena may appear for the direct sequence (Müller *et al.* (1997) and Müller and Marquardt (1997)) in this particular operating range. Therefore the aim of this chapter is to extend the results of the direct sequence from chapter 5 and 6, with the objective of revealing the complex nonlinear dynamics and practical implications predicted in chapter 6. The investigations in this chapter are performed via rigorous dynamic simulation.

First, in section 7.2, the simulation model references are given together with the plant design and operational parameters for the simulations. Then follows the dynamic simulation results in section 7.3. The investigations starts in the region close to and beyond the boundary of the liquid phase splitting. In section 7.3.1 the results of a simulation within this region shows that a limit cycle appears. Subsequently section 7.3.2 describes the sustained oscillation observed, expanding the extent of the solution, and discussing the feasible as well as the most likely terminations of this range of solutions. Section 7.3.3 discuss the observed limit cycle implications on operation. Then follows a degrees of freedom analysis for the decanter in section 7.3.4. In section 7.4 the results of the dynamic behavior investigations are compared with the results from the ∞/∞ analysis of chapter 5. Finally a discussion and the conclusions of this work are given.

7.2 Simulation Model and Parameters

The design and operational parameters for simulating the direct sequence are:

- External feed:
  Flow rate: $E = 100$ moles/hr
  $\boldsymbol{x_E} = (x_{E,cyclohexane}, x_{E,ethanol}, x_{E,water}) = (0.05, 0.7, 0.25)$.
  External feed introduced at saturation conditions.
- 27 trays in each column
- Azeotropic column feed on tray 13 (counted from the top).
- Dehydrating column feed on tray 5.
- Constant vapor flow rates in the two columns of 400 moles/hr.
- Recycle flow rate, D_2, is fixed at 15 moles/hr.
- Constant pressure: 1 atm.
- Decanter operated at boiling point temperature.
- Reflux ratio initial value of 10.379

The simulations are carried out using a rigorous model implemented in the dynamic simulator DYNSIM (Gani *et al.* (1986), Bossen *et al.* (1993)). The reader is referred to these articles for the detailed model description and assumptions. The solver used for simulating the system of ordinary differential equations is the Livermore Solver for Ordinary Differential Equations (LSODE) from the ODEPACK (Hindmarsh (1983), Radhakrishnan and Hindmarsh (1993)).The modified UNIFAC VLE model description is used in the rigorous model (see appendix B).

7.3 Simulation Results

7.3.1 Dynamics at Change in Number of Phases

As was explained in part I (chapter 6) in the situation where the number of phases changes, i.e. for that particular value of the bifurcation parameter where the number of liquid phases in the decanter (or elsewhere in the system) changes from 1 to 2 (or vice versa), the function f in equation 6.1 is C^0 but not C^1. Simulation results in this chapter where the two phase region is crossed thus must be carefully validated and interpreted, since no other guarantee for correctness can be given.

In order to investigate the dynamics when a change in the number of liquid phases in the decanter occur, the sequence was simulated dynamically for a decanter composition initially very close to the liquid split boundary (reflux ratio of 10.379). A small step increase in the reflux ratio (10.379→10.5) was applied at time, t=500 hr. The result from this simulation is seen in figure 7.3.

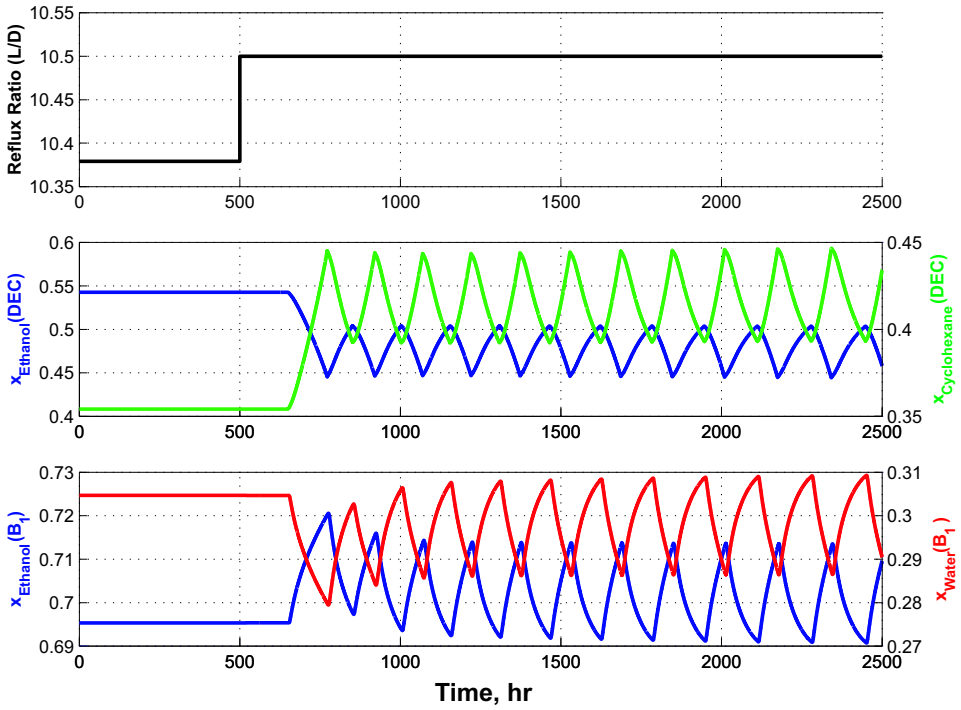

Figure 7.3. Dynamic simulation for a step in the reflux ratio (upper). Transition of ethanol product composition (middle). Transition of water product composition (lower). Green: cyclohexane molefraction; blue: ethanol molefraction; red: water molefraction.

As can be seen from figure 7.3 the system starts oscillating, after the step change is applied. The oscillations eventually ends up in a limit cycle.

7.3.2 Sustained Oscillations

In order to facilitate the understanding of this phenomena (realizing that 165 states may be hard to visualize or comprehend) the upper part of figure 7.4 sketch a small section of the bifurcation diagram.

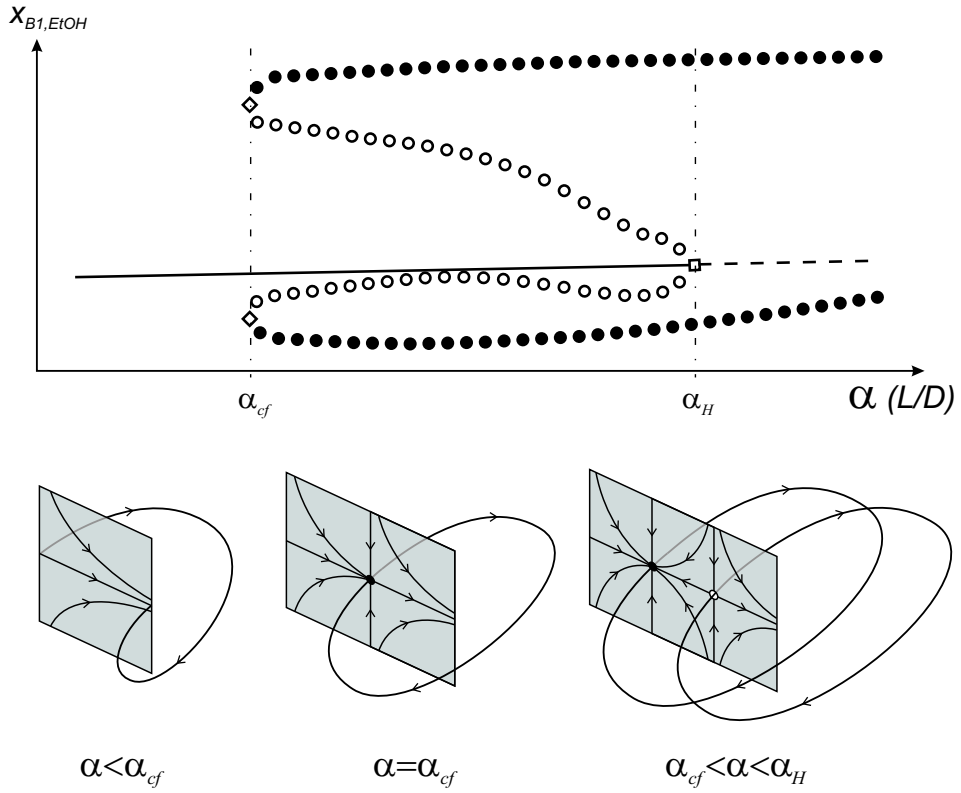

Figure 7.4. Schematic representation of the Hopf bifurcation and the cyclic fold bifurcation occuring at the lower ethanol product purity branch. **Upper part:** Solid line: stable steady states. Dashed line: unstable steady states. Open square: Hopf bifurcation. Open circles: unstable periodic solution. Open diamonds: Cyclic fold bifurcation. Solid circles: stable periodic solution. **Lower part:** Poincaré maps of the cyclic fold bifurcation, visualized with time drawn perpendicular to the maps.

It is seen that for increasing reflux ratio, α (L/D), a subcritical Hopf bifurcation is occurring (square) from the lower stable steady state branch at a reflux ratio of α_H. The figure furthermore shows a predicted cyclic fold of the periodic solution occurring at a lower reflux ratio of α_{cf}.

In other words for:

- $\alpha < \alpha_{cf}$, a stable steady state exists
- $\alpha = \alpha_{cf}$, a stable steady state and an unstable periodic solution exist
- $\alpha_{cf} < \alpha < \alpha_H$, a stable steady state, an unstable periodic solution and a stable periodic solution exist
- $\alpha_H \leq \alpha$, an unstable steady state and a stable periodic solution exist

within the small section of the bifurcation diagram.

Below the bifurcation diagram in figure 7.4, the Poincaré map of a cyclic fold is displayed. The Poincaré map is a possible way of mapping continuous-time dynamical systems defined by differential equations in discrete time. It also allows the mapping of high dimensional systems into only a few dimensions. The map projects $(x, \dot{x})$ whenever time, t, is a multiple of $T = 2\pi/\omega_f$. T and ω_f are the period time and frequency (of the forcing used) respectively. The dimension drawn perpendicular to the Poincaré map in figure 7.4 visualizes the time, t. Starting from high reflux ratios it is seen that for $\alpha_{cf} < \alpha < \alpha_H$ a stable and a saddle fixed point exist. Decreasing the reflux ratio from here, eventually leads to the collision of the two fixed points. This happens for $\alpha = \alpha_{cf}$, where only one fixed point exists. Decreasing the reflux ratio further results in the disappearance of the fixed point ($\alpha < \alpha_{cf}$). The steady states are in the interest of simplicity not shown within the Poincaré map, since for time invariant systems (in our case the FDNLTI system defined by equation 6.1), fixed points of limit cycles do not appear differently from steady state fixed points.

As already mentioned the discrete introduction and deletion of a second liquid phase (giving a discontinuous Jacobian matrix), result in failure when trying to track the periodic solution with a 'standard' Newton based continuation method. The solutions are here found through simulation. Figure 7.5 shows the steady states obtained through continuations (see chapter 6) as well as the periodic solutions obtained through simulations in a narrow neighborhood around the fold bifurcation occurring at low ethanol product purity.

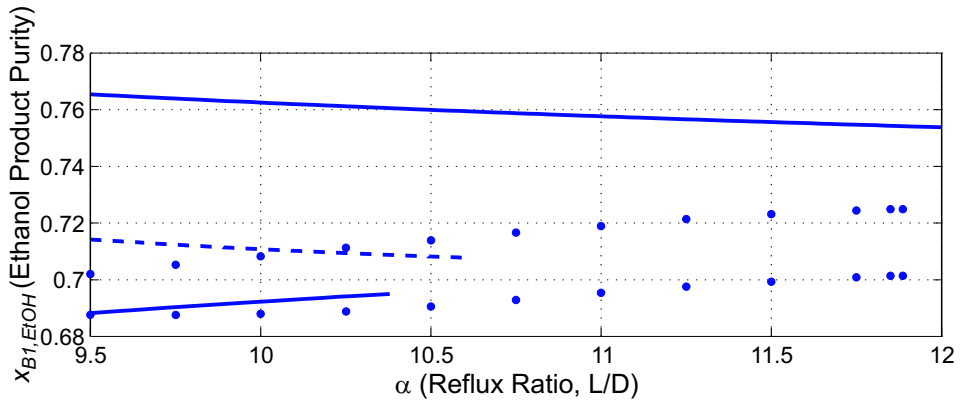

Figure 7.5. Section of bifurcation diagram: Transition of ethanol product purity. Solid lines: stable stationary solutions found by continuation. Dashed lines: unstable stationary solutions found by continuation. Solid circles: stable periodic solutions found by simulation.

It is seen that the limit cycle is simulated for a reflux ratio range of 9.5 to 11.888. The amplitude of the oscillations increases for low reflux ratios, but remains bounded and apparently constant as the reflux ratio is increased towards 11.888.

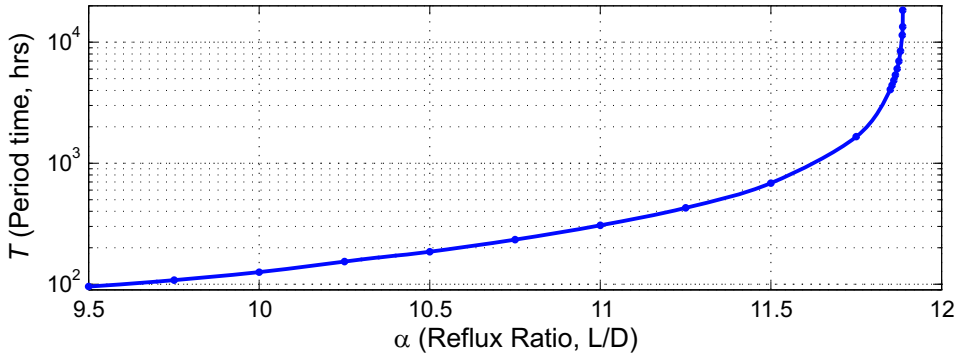

Figure 7.6. Period time, T, of the limit cycle vs. bifurcation parameter, α (reflux ratio, L/D), found by simulation).

In figure 7.6 the period time for the oscillation has been mapped against the reflux ratio, L/D. From this figure, it is seen that the period time for small values of the reflux ratio, close to the cyclic fold bifurcation, is 'small' (around 100 hrs for a reflux ratio of 9.5). When the reflux ratio is increased, the period time increases and eventually rises drastically just before the termination of the stable periodic solution (note the logarithmic axis). The simulations point to a termination of the stable periodic solution between a reflux ratio of 11.888 and 11.890. The simulation for a reflux ratio of 11.888 showed a period time of 18882 hours.

How the stable periodic solution terminates is somewhat unclear. There are at least three possibilities:

1. The stable periodic solution terminates in a global bifurcation – a *"blue sky" catastrophe*. Here the period time increases for increasing α. As α increases towards the bifurcation point, α^*, the period time T tends to infinity while the amplitude of the solution remains bounded. The limit cycle disappears discontinuously for $\alpha > \alpha^*$, causing the system to settle on a stable stationary solution 'far' from the limit cycle.

2. The stable periodic solution terminates in a global bifurcation – a *"SNIPER"* bifurcation (Saddle-Node Infinite PERiod). The period time increases for increasing α. As α increases towards the bifurcation point, α^*, the period time T tends to infinity while the amplitude of the solution remains bounded. The limit cycle disappears discontinuously for $\alpha > \alpha^*$, causing the system to settle on a stable stationary solution close to where the limit cycle spent most of the period time.

3. The stable periodic solution terminates in another cyclic fold with a very, very long period time. The cyclic fold causes the periodic solution to become unstable again. The unstable periodic solution terminates somewhere else possibly in a Hopf bifurcation.

The difference between the first two and the latter termination is that for values of α close to α^*, ($\alpha < \alpha^*$), the limit cycle spends most of the period time close to a stationary solution in case of a 'blue sky' or a 'SNIPER' bifurcation, whereas this is not the case for a cyclic fold.

Figure 7.7 shows the stable oscillatory behavior of the ethanol mole fraction in the decanter for four different values of the bifurcation parameter, α (reflux ratio, L/D): 9.5; 10.75; 11.75 and 11.888. The oscillations are plotted against the number of cycles, N_{Cycles}, of period time, T_P. It is seen for low reflux ratio values (9.5 and 10.75) that the cycles seem more regular or 'sinusoidal' in nature. However, as the reflux ratio is increased (11.75 and 11.888) and the period time increases drastically, it is clear that the ethanol mole fraction in the decanter remains nearly constant during most of the cycle time – the system spends most of the time along the trajectory, inside the liquid-liquid region, near the point/boundary (binodal curve) were a change in the number of liquid phases occur in the decanter.

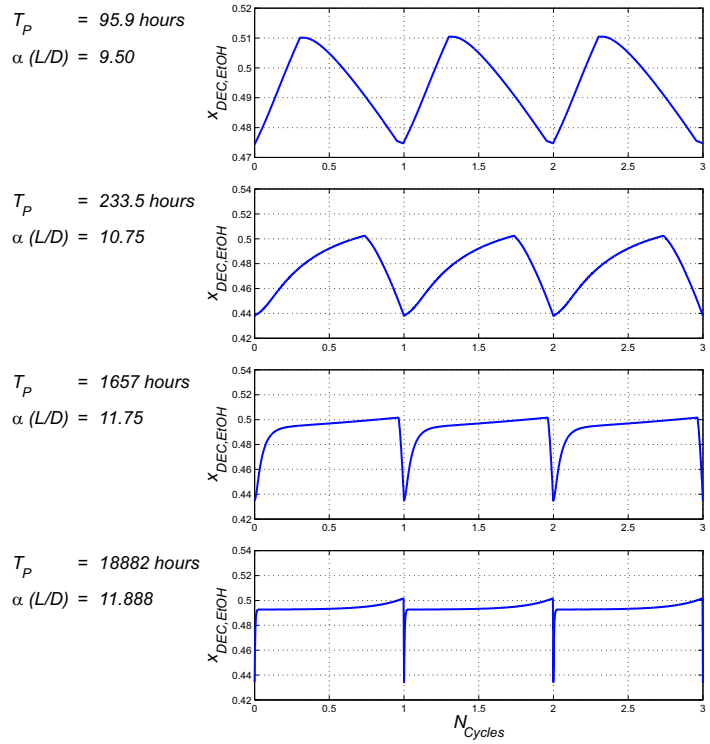

Figure 7.7. Sustained oscillations for four different values of the bifurcation parameter, α (reflux ratio, L/D). Ethanol mole fraction in decanter vs. time in number of cycles, N_{Cycles}, of period time, T_P.

Besides the difference in how the system settles after the limit cycle disappears, the difference between a 'blue sky' and a 'SNIPER' bifurcation may also be seen in the way the period time grows close to the bifurcation point. For a 'blue sky' the period time T of the solution grows as $\ln|\alpha - \alpha^*|$ as $\alpha \to \alpha^*$. For a 'SNIPER' the period time T grows as $(|\alpha - \alpha^*|)^{-1/2}$ as $\alpha \to \alpha^*$, which is more quickly than the logarithmic form, Kaas-Petersen and Scott (1988).

Of the three alternatives, indications point towards a 'blue sky' bifurcation. The reasons for that are:

- Close to were the periodic solution ceases to exist, the system remains nearly constant most of the time during a cycle, where the decanter composition resides inside the liquid-liquid region, near the point/boundary (binodal curve) were a change in the number of liquid phases occur in the decanter (not shown) – ruling out alternative 3.

- After the limit cycle disappears, the system 'jumps' to the equilibrium point on the upper ethanol product purity branch, settling with a decanter composition close to the ternary azeotrope well inside the liquid-liquid region (not shown) – ruling out alternative 2.

Figure 7.8 displays the implications of a 'blue sky' (bs) catastrophe on the phase plane. For $\alpha < \alpha_{bs}$ a stable periodic solution exists together with two unstable stationary solutions. As alpha is increased, the periodic solution comes closer and closer to the unstable stationary solution, x_0 (saddle point), and the system spends most of the time along the trajectory near to x_0. The period time T tends to infinity as α increases towards α_{bs}. For $\alpha = \alpha_{bs}$ the stable periodic solution coincide with x_0 resulting in a homoclinic orbit to the saddle point, x_0. Increasing α further, $\alpha_{bs} < \alpha$, the periodic solution has disappeared and the two unstable stationary solutions still exist.

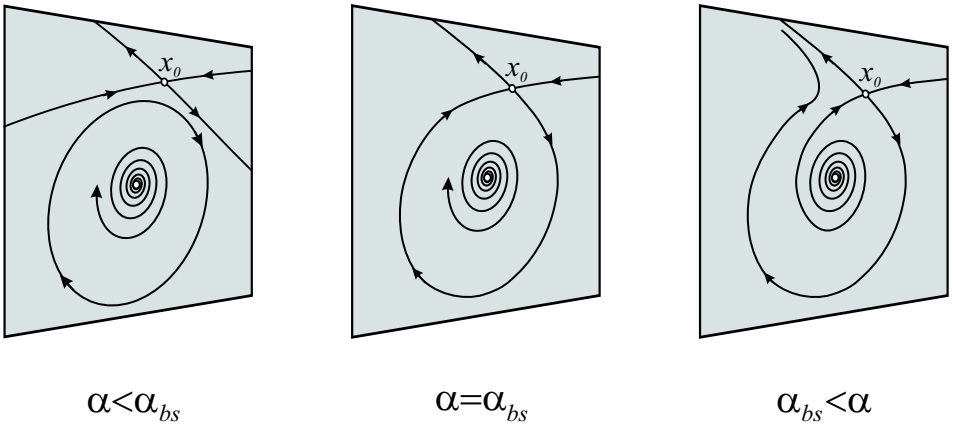

Figure 7.8. Phase plane diagrams of "blue sky" disappearance of a limit cycle (Thompson and Stewart (1986)). $\alpha < \alpha_{bs}$ a stable periodic solution exist together with two unstable stationary solutions. $\alpha = \alpha_{bs}$ the stable periodic solution coincide with the unstable stationary solution (saddle point) resulting in a homoclinic orbit to the saddle point. $\alpha_{bs} < \alpha$ the periodic solution has disappeared and the two unstable stationary solutions still exist.

Assuming now, that the limit cycle disappears in a 'blue sky' bifurcation, the termination (bifurcation) point, α_{bs}, may be determined more accurately by maximizing the linear fit of $-\ln|\alpha - \alpha_{bs}|$ vs. T_P for large values of the period time, T_P. This optimization (not shown) results in a reflux ratio value $\alpha_{bs} = 11.88838$ at the bifurcation point.

7.3.3 Limit Cycle Implications on Operation

It is clear that the limit cycle does not lie close to the obvious operating point with maximum ethanol product purity. However, it may still have significant impact on the operation. The implication of a subcritical Hopf bifurcation is that a stable stationary solution coexist with a stable periodic solution. This can be troublesome in some scenarios, since the periodic solution may be present, and attracts the system after a certain disturbance or setpoint change. Once the system starts oscillating (due to a disturbance or a set point change) it may be hard to get rid of the

oscillation again, because of hysteresis effect.
Such a scenario is illustrated in figure 7.9, were the operation (for some reason – perhaps because of a "catastrophic" jump from the obvious operating point on the upper ethanol product purity branch) is located on the lower ethanol product purity branch, and were the aim is to go to the upper high ethanol product purity branch. Here initially the azeotropic distillation column is operated with a reflux ratio of 9.75. In an attempt to obtain higher purity of the ethanol product by forcing the system to go to the high purity branch, the reflux ratio is increased to 11.0 ($t = 2500$ hrs). The system starts oscillating, and eventually ends up with cycles of period $T_P = 306$ hrs . As a consequence of the oscillations most likely and intuitively obvious the engineer, operator or perhaps an 'intelligent control system' will (eventually) reduce the reflux ratio to the original reflux ratio of 9.75, with the purpose of stabilizing the system to a steady state. This happens at $t = 7500$ hrs. However the oscillations still remains, but have now become much faster (stable period of $T_P = 100$). The amplitude of this new and faster oscillation is almost as large as the previous oscillation. By reducing the reflux ratio further to 8.0 (at $t = 12500$ hrs) the oscillations eventually stops and the system settles at a stable steady state, with an even lower ethanol product purity than originally.

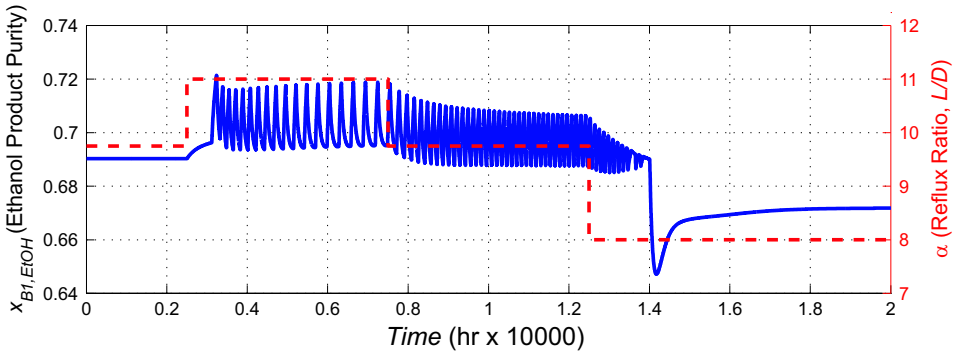

Figure 7.9. Operational implication of a subcritical Hopf bifurcation. Ethanol product purity and reflux ratio. Solid: Ethanol product purity. Dashed: Reflux ratio (L/D) set point.

7.3.4 Degrees of Freedom Analysis for Decanter

Since the simulated limit cycle is closely related to the crossing of the binodal curve for the composition of the decanter, and thus a discrete appearence/dissapearence of a second liquid phase within this unit, a degree of freedom analysis for the condenser/decanter arrangement is appropriate. The analysis is divided into two: one section with Vapor-Liquid-Equilibrium (VLE) conditions and one section with Vapor-Liquid-Liquid-Equilibrium (VLLE) conditions. Figure 7.10 schematically displays the operation for the two cases as simulated within this work.

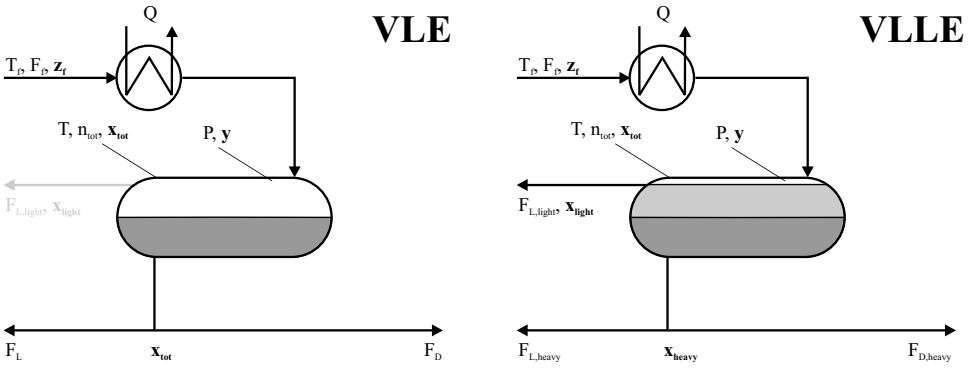

Figure 7.10. Decanter operation at VLE conditions and VLLE conditions

VLE conditions:

For VLE conditions the condenser/decanter arrangement basically reduces to a total dynamic condenser with two liquid product streams:

Total mass balance:

$$\frac{dn_{tot}}{dt} = F_f - F_L - F_D \tag{7.1}$$

Component balances:

$$\frac{d\left(n_{tot}x_{tot,i}\right)}{dt} = F_f z_{f,i} - \left(F_L + F_D\right)x_{tot,i} \qquad i = 1,2 \tag{7.2}$$

Energy balance:

$$c_{p,tot}\frac{d\left(n_{tot}T\right)}{dt} = c_{p,f}F_f T_f - c_{p,tot}\left(F_L + F_D\right)T + Q \tag{7.3}$$

Vapor-liquid equilibrium relationship:

$$y_i = f_i\left(x_{tot,1}, x_{tot,2}, x_{tot,3}, T, P\right) \qquad i = 1,2,3 \tag{7.4}$$

Mole fraction summations (consistency constraints):

$$\sum_{i=1}^{3} y_i = 1 \qquad and \qquad \sum_{i=1}^{3} x_{tot,i} = 1 \tag{7.5}$$

The equation set above adds up to:

- Number of equations: 9
- Constants (4): $c_{p,tot}$, $c_{p,f}$
- Externally specified (4): T_f, F_f, $z_{f,i}$ $i = 1,2$
- Unspecified (12): n_{tot}, F_L, F_D, P, T, Q, and $x_{tot,i}$, y_i $i = 1,2,3$

The dynamic degrees of freedom for the condenser/decanter arrangement are thus equal to:

$$12 - 9 = 3$$

These may be used for control of e.g.: P, n_{tot} and F_L/F_D.

VLLE conditions:

When the decanter composition enters the region of liquid splitting, a light phase starts building up. Eventually this phase reaches a level, where it is decanted (stream $F_{L,light}$ in figure 7.10).

Total mass balance:

$$\frac{dn_{tot}}{dt} = F_f - (F_{L,light} + F_{L,heavy} + F_{D,heavy}) \tag{7.6}$$

Component balances:

$$\begin{aligned} \frac{d(n_{tot}x_{tot,i})}{dt} &= F_f z_{f,i} - (F_{L,light}x_{light,i} \\ &\quad +(F_{L,heavy} + F_{D,heavy})x_{heavy,i}) \qquad i = 1,2 \end{aligned} \tag{7.7}$$

Energy balance:

$$\begin{aligned} c_{p,tot}\frac{d(n_{tot}T)}{dt} &= c_{p,f}F_f T_f - (c_{p,light}F_{L,light}T \\ &\quad +c_{p,heavy}(F_{L,heavy} + F_{D,heavy})T) + Q \end{aligned} \tag{7.8}$$

Vapor-liquid equilibrium relationship:

$$y_i = f_i\left(x_{tot,1}, x_{tot,2}, x_{tot,3}, T, P\right) \qquad i = 1,2,3 \tag{7.9}$$

Liquid-liquid equilibrium relationship:

$$x_{light,i} = g_{light,i}\left(x_{tot,1}, x_{tot,2}, x_{tot,3}, T, P\right) \qquad i = 1,2,3 \tag{7.10}$$

$$x_{heavy,i} = g_{heavy,i}\left(x_{tot,1}, x_{tot,2}, x_{tot,3}, T, P\right) \qquad i = 1,2,3 \tag{7.11}$$

Mole fraction summations (consistency constraints):

$$\sum_{i=1}^{3} y_i = 1 \quad , \quad \sum_{i=1}^{3} x_{light,i} = 1 \quad and \quad \sum_{i=1}^{3} x_{heavy,i} = 1 \tag{7.12}$$

The equation set for VLLE conditions adds up to:

- Number of equations: 16
- Constants (4): $c_{p,tot}$, $c_{p,f}$, $c_{p,light}$, $c_{p,heavy}$

- Externally specified (4): $T_f,\ F_f,\ z_{f,i} \quad i = 1, 2$

- Unspecified (19): n_{tot}, $F_{L,light}$, $F_{L,heavy}$, $F_{D,heavy}$, P, T, Q and $x_{tot,i}$, $x_{light,i}$, $x_{heavy,i}$, $y_i \quad i = 1, 2, 3$

The dynamic degrees of freedom for the condenser/decanter under VLLE conditions are thus equal to:

$$19 - 16 = 3$$

May be used for control of e.g.: $P,\ n_{heavy}$(via Lever rule) and reflux ratio: $(F_{L,light} + F_{L,heavy})\,/F_{D,heavy}$

Do note that it is not possible to manipulate reflux freely, if only one (light) liquid phase is returned to the azeotropic column. The reflux flow is in that case set by the liquid phase split. In the simulations the light phase is decanted as soon as the total decanter composition enters the liquid split region (with a $(F_{L,light} + F_{L,heavy})/F_{D,heavy}$ ratio corresponding to the liquid phase split within the decanter).

7.4 Comparison to ∞/∞ predictions

The ∞/∞ analysis presented in chapter 5 uses the assumptions of infinite column lengths and infinite reflux. The method originally developed by Petlyuk and Avet'yan (1971) and Bekiaris *et al.* (1993),Bekiaris *et al.* (1996) operates with three feasible profile types:

- *Type I:* The top composition of the column is that of an unstable node. The bottom composition can be situated anywhere *inside* a distillation region.

- *Type II:* The bottom composition is that of a stable node. The top composition can be situated anywhere *inside* a distillation region.

- *Type III:* The column profile runs along the boundaries and contains at least one of the saddle points.

Using the three allowable profile types above, the feasible regions of the process variables can be traced while varying a key process variable (in this case the reflux ratio) within its definition range.

Continuation / Simulation					**∞/∞ predictions**				
Reflux Ratio Azeotropic Column	Solutions Neighbor-hood$^{\diamondsuit}$	Expected Bifurca-tion Type	Continuation†	Simulation‡	Step	Type,Pinch		Multi-plicity$^{\heartsuit}$	Branch
						Azeo. Col.	Dehyd. Col.		
α=2.602	sS		✓	✓	Init	II, H	I, T		Lower
2.602<α<3.176	-		✓	✓	1	II, H	I, T		
3.176<α<α_{cf}	-		✓	✓	2	III, X	I, T	OM	
α=α_{cf}	sS,uP	cyclic fold	✓	✓	-	-	-		
α_{cf}<α<9.5	sS,uP,sP		✓	✓	-	-	-		
9.5<α<10.379‡	-		✓	✓	-	-	-		
10.379<α<α_H‡	-		✓	✓	-	-	-		
α=$\alpha_H$$^{\ddagger,\maltese}$	uS,sP	Hopf		✓	-	-	-		
α_H<α<11.888‡	-			✓	-	-	-		
α_{bs}=α=11.888$^{\clubsuit}$	uS,HO	blue sky		✓	-	-	-		
11.888<α<α_{df}	uS				-	-	-		
α=$\alpha_{df}$$^{\spadesuit}$	uS	degen.fold			-	-	-		
α_{df}>α>11.888	uS				3	III, X	I, T	OM	Middle
α_{bs}=α=11.888$^{\clubsuit}$	uS,HO	blue sky			-	-	-		
11.888>α>10.590	uS				-	-	-		
10.590>α>8.608	-		✓	✓	-	-	-		
8.608>α>α_f	-				-	-	-		
α=α_f	-	fold			4	II, L	I, T	OM,SM	Upper
α_f<α<4.349	sS				5	III, Y	I, T	OM	
4.349<α<4.46	-		✓	✓	-	-	-		
4.46<α<$\alpha_{5\to6}$*	-				-	-	-		
$\alpha_{5\to6}$<α<4.487*	-				6	I, T	I, T	OM	
4.487<α<7.368	-		✓	✓	-	-	-		
7.368<α<$\alpha_{6\to7}$*	-				-	-	-		
$\alpha_{6\to7}$<α<8.64*	-				7	I, T	III, X	OM	
8.637<α<21.187	-		✓	✓	-	-	-		
21.187<α<28.875	-		✓	✓	8	I, T	II, H		
α=28.875	-		✓	✓	Final	I, T	II, H		

Table 7.1. Summary of results from continuation, simulations and ∞/∞ predictions of the direct sequence. See text for detailed description.

Table Notes:

$\diamondsuit$ "Solutions Neighborhood" refers to neighborhood solutions to the static solution of each steady state branch (including the static solution itself). sS = stable steady state; uS = unstable steady state; sP = stable periodic solution; uP = unstable periodic solution; HO = homoclinic orbit.

† "Continuation" refers to what reflux ratio ranges (on the individual branches) continuation have been performed for. The performed continuations only cover continuation of the static solution within each reflux ratio segment.

‡ "Simulation" refers to what reflux ratio ranges (on the individual branches) simulation have been carried out for. The performed simulations cover simulation of the static solution for each reflux ratio segment, except the unstable static solution for the reflux ratio range: 10.379–11.888. Simulation has also been carried out for the stable limit cycle in the reflux ratio range: 9.5–11.888.

$\heartsuit$ "Multiplicity" occurring according to ∞/∞ predictions: OM = step in which Output Multiplicity occurs; SM = step in which State Multiplicity occurs.

$\maltese$ It is quite conceivable from the composition profiles of figure 6.4 that the expected Hopf bifurcation occurring at α_H is close to 10.379, since the total decanter composition lies very close to the binodal curve for this reflux ratio, and because this bifurcation is related (somehow) to the entering of the decanter composition into the two liquid phase region.

$\clubsuit$ A more exact location of the blue sky catastrophe has been determined to be 11.88838, according to the preceding sections.

$\spadesuit$ Presumably a degenerated fold occur at $\alpha = \alpha_{df}$, in which one real eigenvalue changes sign (resulting in three positive eigenvalues after the fold instead of only two).

* $\alpha_{5\to6}$ and $\alpha_{6\to7}$ correspond to the reflux ratio values were the composition profiles shift, according to the ∞/∞ predictions, from step 5 to 6 and 6 to 7 respectively.

7.5 Discussion

7.5.1 ∞/∞ analysis

Even though ∞/∞ predictions are a strong tool in short cut analysis of the static behavior, it is obvious from the dynamic analysis carried out here, that a lot of information still needs to be established - stability of stationary solutions, possible periodic behavior, stability of periodic solutions, etc.

7.5.2 Solver Method

The solver LSODE used for our purpose is a general purpose code with adaptive step-size selection. In the preceding simulations we have relied on the code to select very small step sizes near the change in the number of liquid phases (i.e. points were the system is not differentiable). It may (or may not) introduce an error to the integration in that particular step were the discontinuity of the jacobian occurs, which may (or may not) be of significant importance to the solution. The local error here however is large, and thus the solver should take very small steps near the discontinuity. But the numerical methods used here assumes that several derivatives are available when integrating the system. Thus in order to substantiate the existence of the periodic solution further it would be beneficial to choose a solver with an event location capability. This type of solver has an event function $g(t, x)$ associated with the ODE's. The solver automatically detects when the function g changes sign, stops the integration, finds the root $g(t^*, x^*) = 0$, and restarts the integration with the new set of differential equations from (t^*, x^*). In the present case the event function should reflect the phase stability check for the decanter i.e. when a change in the number of liquid phases in the decanter occurs. Examples of solvers with this capability include: LSODAR (Hindmarsh (1983) and Petzold (1983)) – a variant of LSODE, RADAU5 of Hairer and Wanner (1996) as well as DDASRT (a variant of DASSL) of Brenan *et al.* (1996).

7.5.3 Phase Stability Check

The determination of wether one or two liquid phases exist for a given ternary mixture is evaluated through a phase stability check. A phase stability check typically involves an analysis of the Gibbs energy. The method developed and implemented by Baker and Michelsen (Baker *et al.* (1982), Michelsen (1982a) and Michelsen (1982b)) is generally accepted to be the most reliable approach. This check however is quite 'expensive' in terms of computer time (remember that many repeated checks need to be evaluated in each integration step). The implementation of phase stability test in DYNSIM uses a shortcut method. DYNSIM initially calculates the

heterogeneous liquid boiling surface bounded by the binodal curve. If a given composition lies within this surface the liquid is heterogeneous and a liquid split calculation is performed.

Even though this shortcut method may introduce a small inaccuracy to the numerical solution (compared to a 'full' phase stability check) close to were VLE-VLLE transition points are located, it is believed that the shortcut does not affect the fact that a periodic solution exist for the investigated system, since the qualitative topology of the composition simplex with residue curves, separatrices and binodal curve remains intact.

7.5.4 Decanter Operation

It is clear from the results, that the simulated limit cycle is closely related to the emergence/disappearence of a second liquid phase within the decanter. All of the cycles simulated showed decanter compositions of both heterogeneous and homogeneous conditions through one stable cycle. It is also clear from the above degree of freedom analysis that the design and operation of the decanter is of great importance to the limit cycle. Both existence of the limit cycle as well as the period time and propagation of the cycle may be highly influenced by this. This is an issue, which needs to be explored further. Müller and Marquardt (1997) report in their experimental validation of steady state multiplicity, that operation on the unstable branch was not possible in the experimental setup they used. The reason for that was, due to very long settling times for the decanter when operated heterogeneously different from normal operating conditions (i.e. were the decanter composition is close to the ternary azeotrope). This observation implies that experimental validation of the proposed limit cycle within this chapter may render infeasible, since it may be clouded by kinetic phenomena. Decanter dimensions and operating conditions for the sequence in an experimental setup must be designed accordingly.

It is evident however, that the simulated limit cycle is different in nature from the limit cycle found by Lee *et al.* (1999) in homogeneous azeotropic distillation, since the limit cycle found in the present work includes both heterogeneous as well as homogeneous operation of the decanter.

7.5.5 Simulation Model

A verification of the simulations with a simpler model (i.e. CMO) may prove to be beneficial, in order to establish the origin and reason(s) for the periodic solution. A simpler model formulation also reduce the computational effort (which is relatively high for a detailed rigorous model like the one used in this work). The drawback of course may be that a simplification will omit momentous dynamic characteristics and result in

wrong or inaccurate findings and interpretations.

When validated with an appropriate solver method as described in section 7.5.2, it may also be desirable to perform tests with commercial available dynamic simulators such as ASPEN PLUS/DYNAMICS, in order to substantiate the predicted behavior in other industrially applied, prevailing simulators.

The simulations of the sustained oscillations are furthermore proposed to be verified with other thermodynamic model representations (i.e. NRTL model) and with U-V flash calculations instead of the P-T flash calculation used in the accomplished simulations.

7.6 Conclusions

An investigation of the dynamics within a heterogeneous azeotropic distillation sequence, suitable for the dehydration of ethanol using cyclohexane as entrainer, has been carried out. The present chapter extends the bifurcation analysis, carried out in Part I of this work. The sequence investigated is termed the 'direct' sequence. The dynamic simulations carried out in this chapter uses rigorous models implemented in the dynamic simulator DYNSIM (Gani *et al.* (1986), Bossen *et al.* (1993)). Reflux ratio was chosen as the parameter of variation.

The results from the simulations reveal that sustained oscillations occur in the 'direct' sequence. These oscillations occur in the region close to and beyond the boundary of liquid phase splitting within the decanter. The simulated limit cycle is different in nature from the limit cycle found by Lee *et al.* (1999) in homogeneous azeotropic distillation, since the limit cycle found in the present work includes both heterogeneous as well as homogeneous operation of the decanter.

The results indicate clearly that the stable periodic solution is bounded by a cyclic fold bifurcation and a 'blue sky' catastrophe (global bifurcation). The implication of the latter global bifurcation is that the period time increases for increasing parameter of variation. As the parameter of variation increases towards the bifurcation point, the period time of the limit cycle tends to infinity while the amplitude of the solution remains bounded. The oscillation reported was simulated within a reflux ratio range of 9.5–11.88838. The implications of the limit cycle on operation was investigated. The hysteresis phenomena was simulated. A comparison of the results obtained here with the results of the ∞/∞ analysis of the direct sequence carried out in chapter 5 was given.

It is concluded that the simulated limit cycle is closely related to the

emergence/disappearence of a second liquid phase within the decanter. It is evident that further investigations are necessary in order to substantiate the existence of the limit cycle, as well as to clear up the origin and physical reasons for the occurrence of the limit cycle.

Notation

Variable	Description
$c_{p,f}$	Constant pressure heat capacity of feed to decanter
$c_{p,light}$	Constant pressure heat capacity of light liquid phase in decanter
$c_{p,heavy}$	Constant pressure heat capacity of heavy liquid phase in decanter
$c_{p,tot}$	Constant pressure heat capacity of decanter liquid
D	Distillate product molar flow rate
D_j	Distillate product molar flow rate for column j in distillation sequence
E	External feed molar flow rate for distillation sequence
f	Smooth function (equation 6.1)
f_i	Vapor-liquid equilibrium function for component i (equations 7.4 and 7.9)
F_D	Distillate flow rate from decanter
$F_{D,heavy}$	Distillate flow rate of heavy liquid phase from decanter
F_f	Feed flow rate to decanter
F_L	Reflux flow rate from decanter
$F_{L,light}$	Reflux flow rate of light liquid phase from decanter
$F_{L,heavy}$	Reflux flow rate of heavy liquid phase from decanter
g	Event function (section 7.5.2)
$g_{light,i}$	Liquid-liquid equilibrium function for component i in light liquid phase (equation 7.10)
$g_{heavy,i}$	Liquid-liquid equilibrium function for component i in heavy liquid phase (equation 7.10)
H	Pure component corner in composition simplex (heavy component)
I	Pure component corner in composition simplex (intermediate component)
L	Reflux molar flow rate
L	Pure component corner in composition simplex (light component)
n_{heavy}	Mass holdup of heavy liquid phase in decanter
n_{tot}	Total mass holdup of decanter
N_{Cycles}	Number of cycles
P	Pressure in decanter
Q	Heat removal in condenser

Variable	Description
S	Heavy liquid composition in decanter when overall decanter composition is equal to ternary azeotropic composition
t	Time
t^*	Root to event function (section 7.5.2)
T	Ternary azeotrope
T	Temperature in decanter
T, T_P	Period time
T_f	Temperature of feed to decanter
x	State vector
x^*	Root to event function (section 7.5.2)
x_0	State vector at stationary solution
$\dot{x}$	Time derivative of state vector
X	Binary azeotrope
$\boldsymbol{x_E}$	External feed composition for distillation sequence
$x_{E,i}$	External feed mole fraction of component i
$x_{light,i}$	Decanter light liquid phase mole fraction of component i
$x_{heavy,i}$	Decanter heavy liquid phase mole fraction of component i
$x_{tot,i}$	Decanter overall mole fraction of component i
y_i	Decanter gas phase mole fraction of component i
Y	Binary azeotrope
$z_{f,i}$	Mole fraction of component i in feed to decanter
Z	Binary azeotrope
α^*	Bifurcation point
α_m	Bifurcation parameter value at point m. When m contains numbers (i.e. $m =$ '$5 \rightarrow 6$'), α_m corresponds to the bifurcation parameter value where a step transition occur according to the ∞/∞ predictions in chapter 5 (i.e. change from step 5 to step 6). When m is a string, α_m corresponds to the bifurcation parameter value where a bifurcation occur (cf = cyclic fold, H = Hopf, bs = blue sky, df = degenerate fold, f = fold).
ω_f	Frequency

References

Baker, L. E.; Pierce, A. C. and Luks, K. D. (1982). Gibbs Energy Analysis of Phase Equilibria. *Soc. Pet. Eng. J.*, **22**, 731–742.

Bekiaris, N.; Meski, G. A.; Radu, C. M. and Morari, M. (1993). Multiple Steady States in Homogeneous Azeotropic Distillation. *Ind. Eng. Chem. Res.*, **32**(9), 2023–2038.

Bekiaris, N.; Meski, G. A. and Morari, M. (1996). Multiple Steady States

in Heterogeneous Azeotropic Distillation. *Ind. Eng. Chem. Res.*, **35**, 207–237.

Bossen, B. S.; Jørgensen, S. B. and Gani, R. (1993). Simulation, Design, and Analysis of Azeotropic Distillation Operations. *Ind. Eng. Chem. Res.*, **32**, 620–633.

Brenan, K. E.; Campbell, S. L. and Petzold, L. R. (1996). *Numerical Solutions of Initial–Value Problems in Differential–Algebraic Equations*, volume 14 of *Classics in Applied Mathematics*. SIAM Society for Industrial & Applied Mathematics. ISBN 0-89871-353-6.

Gani, R.; Ruiz, C. A. and Cameron, I. T. (1986). A Generalized Model for Distillation Columns - I. *Comp. Chem. Eng.*, **10**, 181–198.

Hairer, E. and Wanner, G. (1996). *Solving Ordinary Differential Equations II. Stiff and Differential Algebraic Problems*, volume 14 of *Springer Series in Computational Mathematics*. Springer Verlag, Berlin, second edition. ISBN 3-54-060452-9.

Hindmarsh, A. C. (1983). ODEPACK, A Systematized Collection of ODE Solvers. *IMACS Transactions on Scientific Computation*, **1**, 55–64. in Scientific Computing, R.S. Stepleman et al. (Eds.), North-Holland, Amsterdam.

Kaas-Petersen, C. and Scott, S. K. (1988). Homoclinic Orbits in a Simple Chemical Model of an Autocatalytic Reaction. *Physica D*, **32**, 461–470. Elsevier Science Publishers B.V. North-Holland Physics Publishing Division.

Larsen, B. L.; Rasmussen, P. and Fredenslund, A. (1987). A Modified UNIFAC Group-Contribution Model for Prediction of Phase Equilibria and Heats of Mixing. *Ind. Eng. Chem. Res.*, **26**, 2274–2286.

Lee, M.; Dorn, C.; Meski, G. A. and Morari, M. (1999). Limit Cycles in Homogeneous Azeotropic Distillation. *Ind. Eng. Chem. Res.*, **38**, 2021–2027.

Michelsen, M. L. (1982a). The Isothermal Flash Problem. Part I. Stability. *Fluid Phase Equilib.*, **9**, 1–19.

Michelsen, M. L. (1982b). The Isothermal Flash Problem. Part II. Phase Split Calculations. *Fluid Phase Equilib.*, **9**, 21–40.

Müller, D. and Marquardt, W. (1997). Experimental Verification of Multiple Steady States in Heterogeneous Azeotropic Distillation. *Ind. Eng. Chem. Res.*, **36**(12), 5410–5418.

Müller, D.; Marquardt, W.; Hauschild, T.; Ronge, G. and Steude, H. (1997). Experimental Validation of an Equilibrium Stage Model for Three–phase Distillation. *IChemE Symp. Ser.*, **142**, 149–159.

Petlyuk, F. B. and Avet'yan, V. S. (1971). Investigation of the Rectification of Three–component mixtures with Infinite Reflux. *Theor. Found. Chem. Eng.*, **5**, 499–507.

Petzold, L. R. (1983). Automatic Selection of Methods for Solving Stiff and Nonstiff Systems of Ordinary Differential Equations. *SIAM J. Sci. Stat. Comput.*, **4**, 136–148.

Radhakrishnan, K. and Hindmarsh, A. C. (1993). Description and Use of LSODE, the Livermore Solver for Ordinary Differential Equations. LLNL Report UCRL-ID-113855.

Thompson, J. M. and Stewart, H. B. (1986). *Nonlinear Dynamics and Chaos*. John Wiley and Sons, New York. ISBN 0-471-90960-2. (Seventh printing 1991).

Widagdo, S. and Seider, W. D. (1996). Azeotropic Distillation. *AIChE Journal*, **42**(1), 96–130.

8

Optimal Heat Distribution in Distillation

In this chapter investigations regarding optimal placement and duty distribution of internal heat exchangers in distillation columns have been carried out based on simulations. In particular the effect of adding 2, 4 and 19 internal heat exchangers to a 19 tray distillation column separating 2-propanol and methanol was studied. It is concluded that the minimum entropy production placement of the heat exchangers depends strongly on the degree of separation. The optimum is however rather flat, which indicates that optimal placement for a nominal operating point may remain nearly optimal in terms of entropy production even for significant changes in feed and product compositions. When compared to a conventional column run under the same operating conditions, entropy production for an optimally operating column with four thermally active stages (4TA) is reduced by 25 % as compared to 37 % for a column with six thermally active stages (6TA) column and 49 % for a column in which all the trays are equipped with heat exchangers.

8.1 Introduction

In spite of its relatively low energy efficiency (typically a few percent), distillation is still one of the most widely used separation techniques in the chemical industry. This is illustrated by the fact that distillation accounts for more than 3 % of the total energy dissipation in the USA, Mix *et al.* (1978), Humphrey and Siebert (1992). Energy consumption attributed to distillation has been reported as high as 5-6 % within the industrialized countries by Pilavachi (1996).

An immense amount of work has been carried out in the field of heat integration within distillation trains. Most of this work had the purpose of minimizing the use of external utilities in heat exchanger networks. The major tool for this work has been pinch-analysis which can minimize the external duties when integrating conventional columns, Linnhoff *et al.* (1982).

From a 2nd law efficiency point of view, conventional distillation performs very poorly in general. One way of improving this efficiency is to distribute the heat added and removed over the distillation column via heat exchangers. Various methods for optimizing the 2nd law efficiency (minimizing the entropy production, minimizing the exergy loss) for distillation process design have previously been suggested: equipartition of entropy production, Tondeur and Kvaalen (1987); equipartition of forces (EOF), Ratkje *et al.* (1995); equal thermodynamic distance (ETD), Salamon and Nulton (1998).

Assuming a distillation column with N stages and a heat exchanger on each stage, all methods predict that the entropy production in the column, ΔS_{HX}, goes to zero as N goes to infinity (see appendix). In the limit of "large" (but finite) N, the predictions however diverge. This divergence has been outlined in the coffee cup example of Salamon *et al.* (2000).

From economical/engineering point of view, an issue that needs to be addressed is how well can one do with only a few more thermally active stages compared to conventional columns. Optimal tray locations for 4 thermally active stages (condenser, 1 heat exchanger in rectifying section, 1 heat exchanger in stripping section and reboiler = 4 thermally active stages = "4TA") have previously been investigated by Koijer *et al.* (1999), and Siragusa *et al.* (2000).

8.2 Economic vs. Thermodynamic Optimum

The net heat input to a distillation column, $Q_{net,input} = Q_{added} - Q_{removed} = h_D + h_B - h_F$, for a specified separation is practically constant. This is true for binary distillation, and applies also to a large extent to multi component distillation with specified product concentrations. The amount of high grade energy added to a distillation column is however not constant, but depends on the sizing and design as well as the operation of the column.

The "true thermodynamic optimum" minimizes the entropy production or, equivalently, the exergy cost. This is carried out by minimizing the quality of the heat input to the column and at the same time maximize the quality of the heat output. This makes it necessary to add heat exchangers on each plate. Possible design procedures for such processes can include the approaches of EOF or ETD. For industrial applications where the objective is operating at the economical optimum, one can imagine using a "Poor man's" ETD/EOF column. Since the introduction of internal heat exchange on trays both affect capital investment and possibly also separation efficiency the economic design optimum is likely to be an approximation to an ETD/EOF distillation column with only a few extra

heat exchangers. In this chapter a "6TA" column is investigated, i.e., a column which is equipped with an additional 4 internal heat exchangers. In the following section the model used in the simulations is described. The results are compared to a conventional column, a 4TA column as well as a column where each plate is equipped with a heat exchanger. Finally the optimal results are discussed.

8.3 Entropy Production in Distillation

Figure 8.1 illustrates the thermodynamic transitions in distillation:

1. Temperature equilibration of the feed from the feed temperature to an arbitrary reference temperature (e.g. the boiling point of the low boiling component)

2. unmixing of the ideal feed mixture to the two products D and B at the reference temperature and

3. temperature equilibration from the reference temperature to the product temperatures (e.g. saturated liquid).

From a thermodynamic efficiency point of view, it is most interesting to look at the entropy production due to internal irreversibilities, ΔS_{irrev}. If

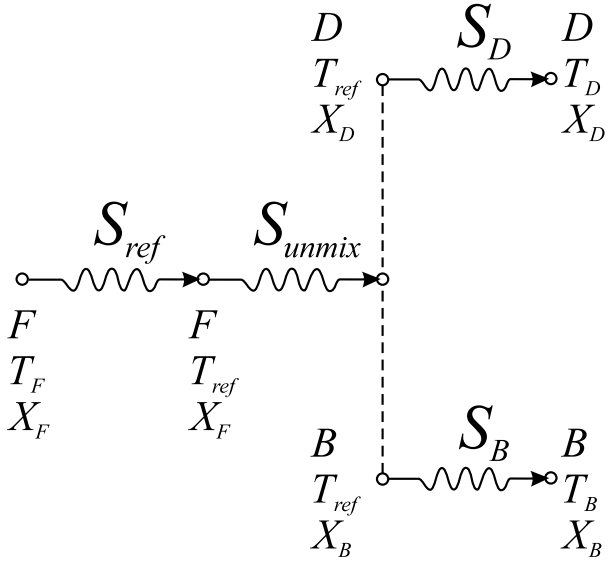

Figure 8.1. Thermodynamic transitions in distillation.

the subpaths traveled within figure 8.1 are reversible changes ΔS_{irrev} can

be expressed as:

$$\begin{aligned} \Delta S_{irrev} &= \Delta S_{HX} - \Delta S_{rev} \\ &= \Delta S_{HX} - (\Delta S_{ref} + \Delta S_{unmix} + \Delta S_D + \Delta S_B) \end{aligned} \tag{8.1}$$

The change of entropy in the universe for a distillation column can with the given assumption be formulated as:

$$\Delta S_u = \Delta S_{HX} + \Delta S_{unmix} + \Delta S_D + \Delta S_B \tag{8.2}$$

Where ΔS_{HX} is the entropy change carried by heat exchange on the TA-plates, in the reboiler and in the condenser:

$$\Delta S_{HX} = \sum_{j=1}^{N_T} \frac{q_j}{T_j} + \frac{q_D}{T_D} + \frac{q_B}{T_B} \tag{8.3}$$

ΔS_{unmix} is the entropy change of reversible unmixing in the separation. ΔS_D and ΔS_B are the entropy changes due to cooling and heating the distillate respectively the bottom product. Detailed explanations of performing entropy calculations have been outlined in Brown and Siragusa (2000).

8.4 Simulation Model

The simulation model consists of a distillation column with 19 ideal stages, a partial reboiler (1 ideal stage) and a total condenser, separating methanol and 2-propanol. A schematic of the 6TA distillation column model can be seen in figure 8.2.
The vapor-liquid equilibrium model used is Soave-Redlich-Kwong. Feed and product specifications are given in table 8.1.

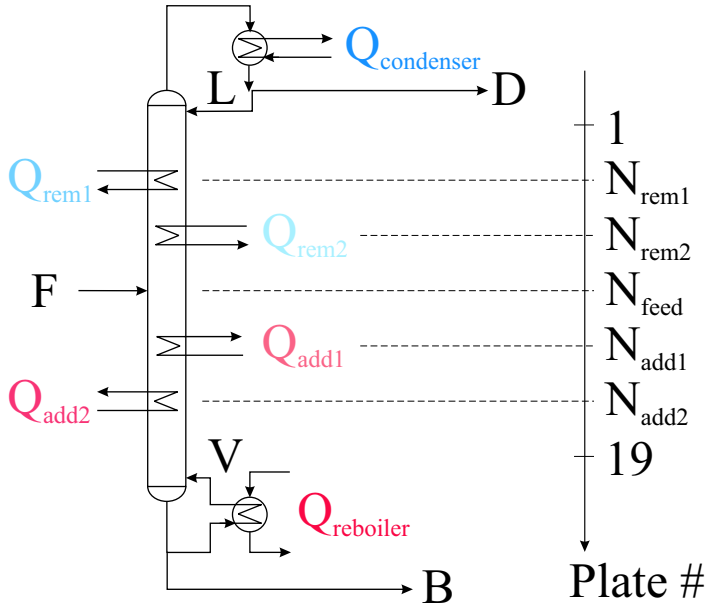

Figure 8.2. The 6TA distillation column.

Specification	Value	Unit
X_F	50	mole % MeOH
X_D	95	mole % MeOH
X_B	5	mole % MeOH
F	1	Mole

Table 8.1. Feed and product specifications. Specification Value Unit.

The model was implemented in Matlab®. The procedure for minimizing the entropy production for each specified set of TA-positions was rather simple:

1. Make an initial guess at the duties of the intermediate TA-plates (using simplex method)
2. Make an initial guess for the condenser duty (using secant method)
3. Carry out balancing of column by plate to plate calculation, finding the reboiler duty and optimal feed plate location
4. If balancing is not converging goto (2) otherwise
5. Evaluate entropy production
6. If convergence of entropy production not obtained (minimum entropy production) goto (1), otherwise
7. Repeat the procedure for new TA-plate positions.

8.5 Results

An entropy minimization of the 6TA column was carried out for different TA plate positions. The initially investigated integer-parameter space is given in table 8.2.

TA plate #	Parameters
N_{rem1}	2:4
N_{rem2}	2:8
N_{add1}	11:14
N_{add2}	14:17

Table 8.2. Investigated parameter space.

In figure 8.3 a plot has been made over the performed entropy minimization. For each heat exchanger combination in the stripping section, the entropy change carried by heat exchange is plotted as a surface against the heat exchanger combinations in the rectifying section. It is seen that

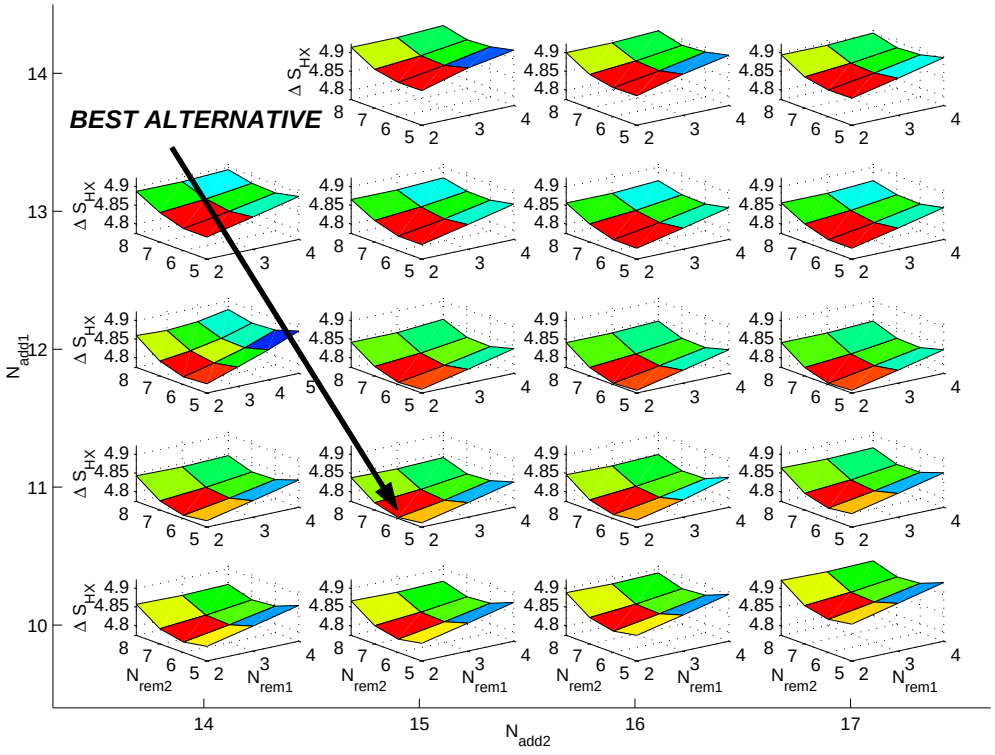

Figure 8.3. Minimum entropy production [J/(mol K)] for investigated thermally active tray positions. Main x-axis: lowest positioned heat exchanger (N_{add2}). Main y-axis: highest positioned heat exchanger in stripping section (N_{add1}). Minor x-axes: highest positioned heat exchanger in rectifying section (N_{rem1}). Minor y-axes: lowest positioned heat exchanger in rectifying section (N_{rem2}). Minor z-axes entropy change carried by heat exchange (ΔS_{HX}).

the optimal combination for minimum entropy production within the investigated parameter space is: $[N_{rem1}, N_{rem2}, N_{add1}, N_{add2}] = [2, 6, 12, 17]$. As can be seen from figure 8.3, the minimum entropy change does not take place at an interior point but rather it lies on the boundary of the set of allowed parameter values. Thus it was decided to expand the parameter range to also include the tray one position ($N_{rem1} = 1$). This was not originally included because it corresponds to a model column which differs significantly from the one shown in figure 8.2; with $N_{rem1} = 1$, no reflux is used from the condenser.

In figure 8.4 it is shown that the entropy production is reduced significantly when $N_{rem1} = 1$ is used in combination with the best TA plate choices in the stripping section.

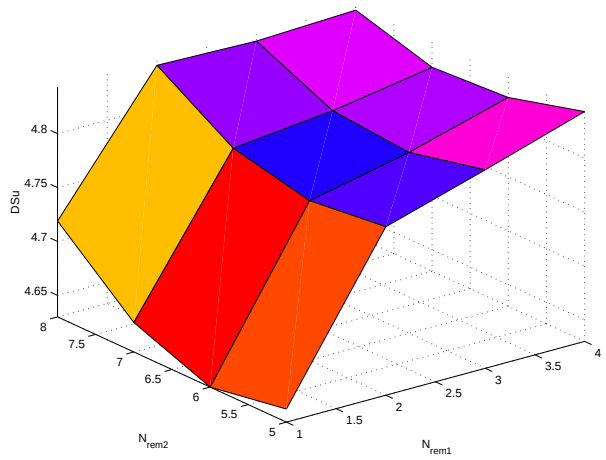

Figure 8.4. Entropy change [J/(mol K)] carried by heat exchange, ΔS_{HX} , for $[N_{add1}, N_{add2}]$=[11,15].

Table 8.3 shows the heat input of high grade heat, the net heat input (constant), the entropy change carried by heat exchange and the entropy production due to internal irreversibilities.

Column Type	Absolute Heat Input [kJ/mole feed]	Net Heat Input [J/mole feed]	ΔS_{HX} [J/mole K]	ΔS_{irrev} [J/mole K]
Conventional	50.0	419	5.64	2.71
4TA (optimal)	54.0	419	4.95	2.02
6TA (optimal)	57.1	419	4.63	1.70
ETD ("optimal")[1]	62.5	419	4.31	1.38

Table 8.3. Comparison of absolute heat input, entropy change carried by heat exchange and entropy production due to internal irreversibilities for conventional, 4TA, 6TA and ETD column cases.

8.6 Conclusions

The overall integration of heat integrated (4TA, 6TA,...) distillation columns will increase the resolution of the temperature interval for supplied/removed heats and lower the need for external utilities, provided that the new higher cooling temperatures and lower heating temperatures can be made use of elsewhere in a given plant. It is shown that in order to perform the separation at the minimum entropy production it is necessary to add 8 % and 14 % more heat in the stripping section for the 4TA and the 6TA column respectively when compared to the conventional case (table 8.3). It is also shown that entropy production can be significantly reduced by adding only 2 extra heat exchangers, namely 25 % compared to conventional distillation. The reduction in entropy change carried by internal irreversibillities for the addition of 4 extra heat exchangers is 37 %. The optimal tray locations for the thermally active trays are for the 6TA: 1 , 6 , 11 and 15. In comparison, the 4TA optimal placements are trays 4 and 17. The optimum is rather flat, which indicates that optimal placement of TA's for a nominal operating point may remain nearly optimal in terms of entropy production for even significant changes in feed and product compositions.

8.7 Discussion

It would be more reasonable to investigate the true optimum for a "symmetric" column. The column would be more "symmetric" if the condenser was partial instead of total. In the present simulation model the reboiler constitutes an equilibrium stage whereas the condenser does not. A thermodynamically improved structure would be a deflegmator which only condenses the necessary reflux followed by a total condenser which condenses only the distillate product stream. With the present setup a significant amount of entropy is produced by entering the subcooled reflux which also have a different composition to the top tray. One important aspect yet to be analyzed is operability and control of thermally integrated columns.

Notation

Variable	Description
Q	Heat
D	Distillate
B	Bottom product
F	Feed
x	Molar ratio
T	Temperature

Variable	Description
ref	Reference state
h	Enthalpy
S	Entropy
$irrev$	Irreversibility
HX	Heat exchange
rev	Reversible
$unmix$	Unmixing
N	Thermally Active tray location #
$addi$	The iŠth addition
$remj$	The jŠth removal
Δ	Change

References

Brown, D. and Siragusa, G. (2000). Calculating total entropy production for a distillation process. *Manuscript in prep.*.

Humphrey, J. L. and Siebert, A. F. (1992). Separation technologies. An opportunity for energy savings. *Chem. Eng. Prog.*, **88**(3), 32–41.

Koijer, G. M.; Kjelstrup, S.; van der Koi, H. J.; Gross, B.; Knoche, K. F. and Andersen, T. R. (1999). Positioning Heat Exchangers in Binary Tray Distillation using Isoforce Operation. In *Proceedings for ECOS'99 (PEC 99-15)*, ECOS'99, Tokyo, Japan.

Linnhoff, B.; Townsend, D. W.; Boland, D.; Hewitt, G. F.; Thomas, B. E. A.; Guy, A. R. and Marsland, R. H. (1982). *A User Guide on Process Integration for the Efficient Use of Energy*. The Institution of Chemical Engineers, Rugby England. ISBN 0.

Mix, T. J.; Dweck, J. S.; Weinberg, M. and Armstrong, R. (1978). Energy Conservation in Distillation. *Chem. Eng. Prog.*, **74**(4), 49–55.

Pilavachi, P. A. (1996). Systems Modelling as a Design Tool for Energy Efficiency-Research within the European Union. *Comp. Chem. Engng.*, **20**(Suppl), 467–472.

Ratkje, S. K.; Sauar, E.; Hansen, E.; Lien, K. M. and Hafskjold, B. (1995). Analysis of entropy production rates for design of distillation columns. *Ind. Eng. Chem. Res.*, **34**, 3001–3007.

Salamon, P. and Nulton, J. (1998). The geometry of separation processes: A horse-carrot theorem for steady flow systems. *Europhys. Lett.*, **42**, 571–576.

Salamon, P.; Nulton, J. D.; Siragusa, G.; Andersen, T. R. and Limon, A. (2000). Principles of Control Thermodynamics. *Submitted for publication in Energy (PEC 00-17)*.

Siragusa, G.; Andresen, B. and Salamon, P. (2000). Optimal heat integration on a 19 plate distillation column, utilizing two additional heat exchangers. *Manuscript in prep.*.

Tondeur, D. and Kvaalen, E. (1987). Equipartition of entropy production: an optimal criterion for transfer and separation processes. *Ind. Eng. Chem. Res.*, **36**, 50–56.

9

Conclusions and Suggestions to Further Work

This chapter sums up the major conclusions of this work. The conclusions are divided into sections according to the chapters they were stated.
Finally suggestions to further work on the research topics within this thesis are given.

9.1 Summary of Conclusions

Chapter 4: Experimental Validation of Input Multiplicity in Binary Distillation – Influence on Control Structure Selection
Steady state multiplicities are known to occur within multicomponent distillation. Also in simple binary distillation output multiplicities have been reported and experimentally verified. The phenomena of steady state multiplicity in distillation have received only limited interest within the process design community.

In this chapter, the occurrence of the input multiplicity predicted and simulated by Koggersbøl (1995), was experimentally verified. The demonstration was carried out on an experimental semi-industrial sized energy integrated distillation facility separating methanol from isopropanol. The multiplicity is related to the binary mixture thermodynamics properties and distillation properties, and implies that separation goes through a maximum when the boil up is increased keeping all other inputs constant. The input multiplicity was verified well within the feasible operating window.

Three experiments were carried out. The results from these experiments clearly verify the existence of the proposed input multiplicity. The influence of variations in tray efficiency due to entrainment on the input multiplicity was discussed. It is concluded that entrainment effects on the tray efficiencies is likely to shift the optimum separation somewhat towards lower vapor flow rates.

The practical relevance of these findings is that a suitable control configuration and strategy can be selected to reduce the possibility of performance degradation due to this phenomenon. The findings also show that attention from the process design community should be drawn to this field of research, since it is driven by changes in operability and stability resulting in performance reducing behavior which is brought about by these phenomena.

Chapter 5: Steady State Multiplicities in Heterogeneous Azeotropic Distillation Sequences

The steady state behaviour of two heterogenous azeotropic distillation sequences designed to separate ethanol and water using cyclohexane as the entrainer has been investigated assuming infinitely long column sections and infinite reflux. Both sequences contain an azeotropic and a dehydrating column; in the direct sequence the feed is entered directly to the azeotropic column, while in the indirect sequence the feed enters first the dehydrating column, which then also is used as a concentrator. The two sequences exhibit very different steady state behavior despite the similarity of the two sequences. The direct sequence exhibits output and state multiplicity, whereas the indirect sequence, only exhibits state multiplicity. Thus, the position of the decanter within the sequence is of great importance. The conclusions of this chapter are not restricted to one single operating point but relevant for all realistic operating points.

In the direct sequence the output multiplicity persists throughout the operationally feasible parameter space. Increasing recycle flow rates improves the product quality and eliminates a trade-off between the two product purities. For both of the investigated sequences state multiplicity prevails close to the optimal operating point.

The state multiplicity of the direct sequence is a consequence of the state multiplicity of the single column as found computationally by Gani and Jørgensen (1994) and analyzed by Bekiaris *et al.* (1996). The state multiplicity of the indirect sequence occurs as a consequence of closing the sequence. Here the state multiplicity can be avoided by changing the flow rate of D_1, at the cost of a slightly increased impurity in the ethanol product purity. This important conclusion yields the information, that the indirect sequence should not be operated at high D_1 flow rates as far as the specifications of the product compositions are still satisfied. For the direct sequence, however, high D_2 flow rates yield better performance of the sequence.

The results have been substantiated through simulations on finite column lengths. For both sequences excellent agreement between predictions and simulations is seen.

The thermodynamic description is seen to show great effect on the performance of both sequences. If the plait point is positioned on the water-rich side of the TX boundary the behavior of the sequences are seen to be affected. In the bifurcation diagram representing the direct sequence, a discontinuity arises. In the indirect sequence, the bifurcation parameter interval is narrowed. Thus, the analyses reveal that in design and simulation of heterogeneous azeotropic distillation sequences, significant attention should be focused on the thermodynamics representing the liquid-liquid phase split and the temperature at which this operation is carried out.

It seems from a static viewpoint, that the indirect sequence is the better choice in the separation of ethanol and water with cyclohexane as entrainer. However, in this sequence operational difficulties may arise from state multiplicity and from dynamic effects.

Chapter 6: Dynamics of Heterogeneous Azeotropic Distillation Sequences, Part I – Bifurcation Analysis
In this chapter, a bifurcation analysis has been performed on a heterogeneous azeotropic distillation sequence suitable for the dehydration of ethanol using cyclohexane as entrainer. The sequence contains an azeotropic column with a decanter and a dehydrating column. The external feed is entered directly to the azeotropic column – thus the sequence is termed the 'direct' sequence. The analysis is carried out using rigorous models implemented in a dynamic simulator integrated with continuation software. The continuation method used is arc-length continuation. The parameter chosen as primary bifurcation parameter in the investigation is reflux ratio for the azeotropic distillation column. The existence of multiple steady states was verified within the 'direct' sequence. In the present case the multiple solutions occur in a typical hysteresis scenario. That is stable solutions of high and low product purity coexists, and their basins of attraction are separated by an unstable solution of intermediate purity.

The sequence exhibit "state multiplicity" in the obvious operating point for the ∞/∞ case, meaning that for fixed inputs and outputs multiple solutions of the internal column profiles exists (chapter 5). It was not possible to perform the continuation around the state multiplicity and the expected fold bifurcation at optimal ethanol product purity for the chosen combination of feed composition and recycle flow rate. It was however possible to get very close to were the bifurcation occurs. It is concluded that the phenomenon of "state multiplicity" may be seen in the bifurcation analysis as a real eigenvalue moving very close to the imaginary axis, thus resulting in a very slow open loop dynamic behavior in the vicinity of the obvious operating point. This point of tangency signifies where the "state

multiplicity" occurs, but also occurs during change of composition profiles.

The results from the bifurcation analysis furthermore indicate that complex dynamic behavior is expected to occur in the boundary region of liquid phase splitting. By "more complex" dynamic behavior is meant that the two branches, lower ethanol product purity branch and medium ethanol product purity branch, can not be connected via only one simple fold bifurcation, but necessarily have to be connected through more complex bifurcation(s).

Chapter 7: Dynamics of Heterogeneous Azeotropic Distillation Sequences, Part II – Dynamic Simulation

This chapter extends the bifurcation analysis, carried out in Part I of this work. The dynamic simulations carried out on the 'direct sequence' in this chapter uses rigorous models implemented in the dynamic simulator DYNSIM (Gani *et al.* (1986), Bossen *et al.* (1993)). Reflux ratio was chosen as the parameter of variation.

The results from the simulations reveal that sustained oscillations occur in the 'direct' sequence. These oscillations occur in the region close to and beyond the boundary of liquid phase splitting within the decanter. The simulated limit cycle is different in nature from the limit cycle found by Lee *et al.* (1999) in homogeneous azeotropic distillation, since the limit cycle found in the present work includes both heterogeneous as well as homogeneous operation of the decanter.

The results indicate clearly that the stable periodic solution is bounded by a cyclic fold bifurcation and a 'blue sky' catastrophe (global bifurcation). The implication of the latter global bifurcation is that the period time increases for increasing parameter of variation. As the parameter of variation increases towards the bifurcation point, the period time of the limit cycle tends to infinity while the amplitude of the solution remains bounded. The oscillation reported was simulated within a reflux ratio range of 9.5–11.88838. The implications of the limit cycle on operation was investigated. The hysteresis phenomena was simulated. A comparison of the results obtained here with the results of the ∞/∞ analysis of the direct sequence carried out in chapter 5 was given.

It is concluded that the simulated limit cycle is closely related to the emergence/disappearence of a second liquid phase within the decanter. It is concluded that further investigations are necessary in order to substantiate the existence of the limit cycle, as well as to clear up the origin and physical reasons for the occurrence of the limit cycle.

Chapter 8: Optimal Heat Distribution in Distillation
This chapter investigates optimal placement and duty distribution of internal heat exchangers in distillation columns. The effect of adding 2, 4 and 19 internal heat exchangers to a 19 tray distillation column separating 2-propanol and methanol was studied. The overall integration of heat integrated (4TA, 6TA,...) distillation columns will increase the resolution of the temperature interval for supplied/removed heats and lower the need for external utilities, provided that the new higher cooling temperatures and lower heating temperatures can be made use of elsewhere in a given plant. It is shown that in order to perform the separation at the minimum entropy production it is necessary to add 8 % and 14 % more heat in the stripping section for the 4TA and the 6TA column respectively when compared to the conventional case. It is also shown that entropy production can be significantly reduced by adding only 2 extra heat exchangers, namely 25 % compared to conventional distillation. The reduction in entropy change carried by internal irreversibillities for the addition of 4 extra heat exchangers is 37 %. The optimal tray locations for the thermally active trays are for the 6TA: 1 , 6 , 11 and 15. In comparison, the 4TA optimal placements are trays 4 and 17. The optimum is rather flat, which indicates that optimal placement of TA's for a nominal operating point may remain nearly optimal in terms of entropy production for even significant changes in feed and product compositions.

It is concluded that it would be more reasonable to investigate the true optimum for a "symmetric" column. The column would be more "symmetric" if the condenser was partial instead of total. In the present simulation model the reboiler constitutes an equilibrium stage whereas the condenser does not. A thermodynamically improved structure would be a deflegmator which only condenses the necessary reflux followed by a total condenser which condenses only the distillate product stream. With the present setup a significant amount of entropy is produced by entering the subcooled reflux which also have a different composition to the top tray.

9.2 Suggestions to Further Work

Below follows suggestions to future work that may be undertaken within three main subjects of this thesis:

Experimental validation of input multiplicity in heat integrated binary distillation – Influence on control structure selection

Entrainment Effects: In order to quantify the effect of entrainment on the input multiplicity experimentally, it is suggested to carry out the entire experiment (operating conditions of experiment III) with bottom pressure controlled.

Verification of Instability: Experimental verification of the stability/instability predicted for the two different pressure control schemes, when composition control loops are closed. It is suggested to perform two dynamic experiments with top pressure controlled: 1) At low vapor flow rate switch to two point composition control and verify stability, and 2) at high vapor flow rates switch to two point composition control and verify instability.

Analysis of nonlinear dynamic behavior in heterogeneous azeotropic distillation sequences

Explore state multiplicity / upper fold bifurcation: With a little effort continuation around the internal state multiplicity / fold bifurcation for the 'direct sequence' may be possible within the current setup, if recycle is increased or if an alternative feed composition is chosen.

Variation of recycle flow rate: It will be very interesting to examine the dynamic behavior for higher and more production relevant recycle flow rates (i.e. where product purity requirements for both product are satisfied).

Variation of feed composition: Another interesting aspect is how the dynamic behavior changes with variations in feed composition. In particular it will be relevant to perform the continuation for a more realistic feed composition.

Method of continuation: A great improvement to the current setup would be to extend the continuation method, by adding a solver for the model equations with an event location capability, hereby making it possible to integrate exact when the number of liquid phases changes. Some possible candidates are: LSODAR (Hindmarsh (1983) and Petzold (1983)), RADAU5 of Hairer and Wanner (1996) as well as DDASRT of Brenan *et al.* (1996).

Phase Stability Check: In order to obtain a more exact model formulation, it may be necessary to include a 'full' phase stability check involving

an analysis of the Gibbs energy. The method developed and implemented by Baker and Michelsen (Baker *et al.* (1982), Michelsen (1982a) and Michelsen (1982b)) is a good candidate.

Substantiate existence of periodic solution: It is evident that further investigations are necessary in order to substantiate the existence of the limit cycle, as well as to clear up the origin and physical reasons for the occurrence of the limit cycle. This however can not be undertaken before having improved the continuation method and model formulation as described above.

Explore the trajectory of periodic solution: When/if verified with the proposed improvements above, the trajectory and termination of the periodic solution should be explored. Also it may be interesting to see if a simpler model (i.e. CMO) will represent the periodic solution. A simpler model may prove to be beneficial, in order to establish the origin and reason(s) for the periodic solution.

Experimental validation: When/if verified with the proposed improvements above, the limit cycle should also be experimentally validated. This however may be difficult or infeasible, due to kinetic phenomena as explained in chapter 7.

Comparison to other sequence: In order to finally determine which sequence ('direct' or 'indirect') is the preferred separation, similar continuation and dynamic simulation analyses have to be carried out for the 'indirect' sequence.

Optimal design and duty distribution in heat integrated distillation with internal heat exchangers

Investigate "symmetric" column: It will be interesting to investigate the true optimum for a "symmetric" column. The column is termed "symmetric" if the condenser is partial instead of total.

Prediction of optimal duty distribution: For minimum entropy production good prediction methods of optimal duty distribution exist for large fully energy integrated (near reversible) distillation columns. When implementing only a few internal heat exchangers compared to conventional distillation, these prediction methods does not predict the true optimum very well. Thus modifications/improvements to these methods are needed in the more realistic cases.

Operability and control: One important aspect yet to be analyzed is operability and control of thermally integrated columns. Continuation methods may be an appropriate approach to reveal the nonlinear dynamical behavior and the operational implications.

References

Baker, L. E.; Pierce, A. C. and Luks, K. D. (1982). Gibbs Energy Analysis of Phase Equilibria. *Soc. Pet. Eng. J.*, **22**, 731–742.

Bekiaris, N.; Meski, G. A. and Morari, M. (1996). Multiple Steady States in Heterogeneous Azeotropic Distillation. *Ind. Eng. Chem. Res.*, **35**, 207–237.

Bossen, B. S.; Jørgensen, S. B. and Gani, R. (1993). Simulation, Design, and Analysis of Azeotropic Distillation Operations. *Ind. Eng. Chem. Res.*, **32**, 620–633.

Brenan, K. E.; Campbell, S. L. and Petzold, L. R. (1996). *Numerical Solutions of Initial–Value Problems in Differential–Algebraic Equations*, volume 14 of *Classics in Applied Mathematics*. SIAM Society for Industrial & Applied Mathematics. ISBN 0-89871-353-6.

Gani, R. and Jørgensen, S. B. (1994). Multiplicity in Numerical Solution of Nonlinear Models: Separation Processes. *Comput. Chem. Eng.*, **18**, 55.

Gani, R.; Ruiz, C. A. and Cameron, I. T. (1986). A Generalized Model for Distillation Columns - I. *Comp. Chem. Eng.*, **10**, 181–198.

Hairer, E. and Wanner, G. (1996). *Solving Ordinary Differential Equations II. Stiff and Differential Algebraic Problems*, volume 14 of *Springer Series in Computational Mathematics*. Springer Verlag, Berlin, second edition. ISBN 3-54-060452-9.

Hindmarsh, A. C. (1983). ODEPACK, A Systematized Collection of ODE Solvers. *IMACS Transactions on Scientific Computation*, **1**, 55–64. in Scientific Computing, R.S. Stepleman et al. (Eds.), North-Holland, Amsterdam.

Koggersbøl, A. (1995). *Distillation Column Dynamics, Operability and Control*. Ph.D. thesis, Technical University of Denmark, Lyngby Denmark.

Lee, M.; Dorn, C.; Meski, G. A. and Morari, M. (1999). Limit Cycles in Homogeneous Azeotropic Distillation. *Ind. Eng. Chem. Res.*, **38**, 2021–2027.

Michelsen, M. L. (1982a). The Isothermal Flash Problem. Part I. Stability. *Fluid Phase Equilib.*, **9**, 1–19.

Michelsen, M. L. (1982b). The Isothermal Flash Problem. Part II. Phase Split Calculations. *Fluid Phase Equilib.*, **9**, 21–40.

Petzold, L. R. (1983). Automatic Selection of Methods for Solving Stiff and Nonstiff Systems of Ordinary Differential Equations. *SIAM J. Sci. Stat. Comput.*, **4**, 136–148.

A

Experimental Results

This appendix summarizes the results obtained during the three input multiplicity experiments carried out in 2000. Initially a short description of the experiments is given (A.1). Also in this section the filenames for the dynamic experimental data from the MOdular Data Acquisition and Control system (MODAC) is given as well as file names and time ranges specification of the individual steady states obtained during the experiments. Then follows section A.2 where a range of relevant plots of dynamical data recorded during the experiments are displayed. After that steady state measurement mean values and standard deviations for the measurements are listed (section A.3). Samples taken out during the different operating conditions in the experiments were analyzed on a gas chromatograph. The results and standard deviations from the determinations are listed in section A.4. Finally the composition determinations and the external flow rates have been reconciled in order to obtain consistent data sets. The results from the data reconciliation are listed in section A.5.

A.1 Description of Input Multiplicity Experiments

Three input multiplicity experiments have been carried out. The three experiments differed in the feed flow rates. The feed flow rate set points for the three experiments are given in table A.1. Column top pressure was

Name	February 2000 experiment	October 2000 experiment	November 2000 experiment
Feed flow rate set point [tons/hr]	0.066	0.070	0.110

controlled in all three experiments. Set point for this loop was 100 kPa. At the end of the final experiment the pressure control was changed such that the bottom pressure was controlled. The concentration profile was fixed at tray 15 in the experiments. Set point for the methanol concentration on this tray was $x_{MeOH,15,set} = 0.75$. The boil up was varied in the three experiments, and operating points were recorded for a boil up rate range of: 0.4 to 1.1 tons/hr.

A.1.1 Experiment, Feb. 14th 2000 - Feb. 18th 2000

The first input multiplicity experiment was carried out from February 14th 2000 to February 18th 2000. During this experiment, lasting 89 hrs, 7 steady states were obtained, at which the distillate, the bottom product and the feed flow where sampled for off–line analysis on a gas chromatograph. The filenames for the dynamic experimental data from the MOdular Data Acquisition and Control system (MODAC) is given in table A.1. File names and time ranges specification of the individual steady states obtained during this experiment is given in table A.2.

MODAC file name	MODAC time range (hr)
d140200f.dat	0–8.4
d150200b.dat	0–0.6
d150200d.dat	0–0.2
d150200e.dat	0–0.2
d150200f.dat	0–48.1
d170200b.dat	0–7.7
d170200c.dat	0–24.1

Table A.1. File names (for experimental data) and time ranges specification for the entire input multiplicity experiment, February 14th 2000 - February 18th 2000.

Steady State	MODAC file name	MODAC time (hr)	Time (hr) since experiment start
SS1	d150200f.dat	23.5–24.5	33.0–34.0
SS2	d150200f.dat	39.3–40.3	48.8–49.8
SS3	d150200f.dat	45.8–46.8	55.3–56.3
SS4	d170200b.dat	3.4–4.4	61.0–62.0
SS5	d170200c.dat	3.7–4.7	69.0–70.0
SS6	d170200c.dat	10.4–11.4	75.7–76.7
SS7	d170200c.dat	18.0–19.0	83.3–84.3

Table A.2. File names (for experimental data) and time ranges specification of the individual steady states obtained in the input multiplicity experiment, February 14th 2000 - February 18th 2000.

A.1.2 Experiment, Oct. 27th 2000 - Oct. 31st 2000

The second experiment was performed from October 27th 2000 to October 31st 2000. During the 114 hrs lasting experiment, 7 steady states were obtained, at which the distillate, the bottom product and the feed flow where sampled for off–line gas chromatography analysis.

MODAC file name	MODAC time range (hr)
d271000b.dat	0–0.3
d271000c.dat	0–1.0
d271000d.dat	0–0.3
d271000e.dat	0–1.1
d271000f.dat	0–5.1
d271000g.dat	0–5.4
d271000i.dat	0–0.6
d271000j.dat	0–8.5
d281000a.dat	0–30.2
d291000a.dat	0–13.3
d291000b.dat	0–7.1
d301000a.dat	0–11.8
d301000b.dat	0–13.8
d311000a.dat	0–13.3
d311000b.dat	0–0.2
d311000c.dat	0–2.3

Table A.3. File names (for experimental data) and time ranges specification for the entire input multiplicity experiment, October 27th 2000 - October 31st 2000.

Steady State	MODAC file name	MODAC time (hr)	Time (hr) since experiment start
SS1	d281000a.dat	6.25–8.25	28.4–30.4
SS2	d281000a.dat	28.0–30.0	50.2–52.2
SS3	d291000a.dat	10.0–12.0	62.4–64.4
SS4	d301000a.dat	0.3–2.3	73.1–75.1
SS5	d301000b.dat	2.75–4.75	87.3–89.3
SS6	d311000a.dat	2.1–3.6	100.5–102.0
SS7	d311000a.dat	11.0–13.0	109.4–111.4

Table A.4. File names (for experimental data) and time ranges specification of the individual steady states obtained in the input multiplicity experiment, October 27th 2000 - October 31st 2000.

A.1.3 Experiment, Nov. 14th 2000 - Nov. 19th 2000

From November 14th 2000 to November 19th 2000 the third and last experiment was carried out. This experiment lasted 115 hrs. 9 steady states were obtained, at which the distillate, the bottom product and the feed flow where sampled for off–line analysis on a gas chromatograph.

MODAC file name	MODAC time range (hr)
d141100a.dat	0–7.0
d141100b.dat	0–43.2
d161100a.dat	43.2–43.9
d161100b.dat	0–9.1
d161100c.dat	0–1.0
d161100e.dat	0–42.3
d181100a.dat	0–10.7
d191100a.dat	0–1.1

Table A.5. File names (for experimental data) and time ranges specification for the entire input multiplicity experiment, November 14th 2000 - November 19th 2000.

Steady State	MODAC file name	MODAC time (hr)	Time (hr) since experiment start
SS1	d141100b.dat	10.5–12.5	17.5–19.5
SS2	d141100b.dat	24.8–26.8	31.8–33.8
SS3	d141100b.dat	38.5–40.5	45.5–47.5
SS4	d161100b.dat	6.4–8.4	57.3–59.3
SS5	d161100e.dat	11.0–13.0	72.0–74.0
SS6	d161100e.dat	18.7–20.7	79.7-81.7
SS7	d161100e.dat	28.7–30.7	89.7–91.7
SS8	d161100e.dat	40.1–42.1	101.1–103.1
SS9	d181100a.dat	5.6–7.6	108.9–110.9

Table A.6. File names (for experimental data) and time ranges specification of the individual steady states obtained in the input multiplicity experiment, November 14th 2000 - November 19th 2000.

A.2 Dynamic data

A.2.1 Experiment, Feb. 14th 2000 - Feb. 18th 2000

Comments to dynamic data: As can be seen from figure A.1 the distillate flow rate, D (FM_4), is somewhat aggressively controlled. The fast fluctuations however, does not have any significant impact on the column separation performance at "steady state", as long as the reflux rate, L (FM_6), is maintained constant. The reason for that is that the condenser is total (providing a total condensed overhead product with constant composition and temperature) to the "decanter" which functions as a reflux drum, providing surge volume to protect the column in case of upsets or failures. It can be seen from the figure that V has a relatively smooth trajectory and remains constant during "steady states" (since $V \gg D$ it follows that $L \approx V$).

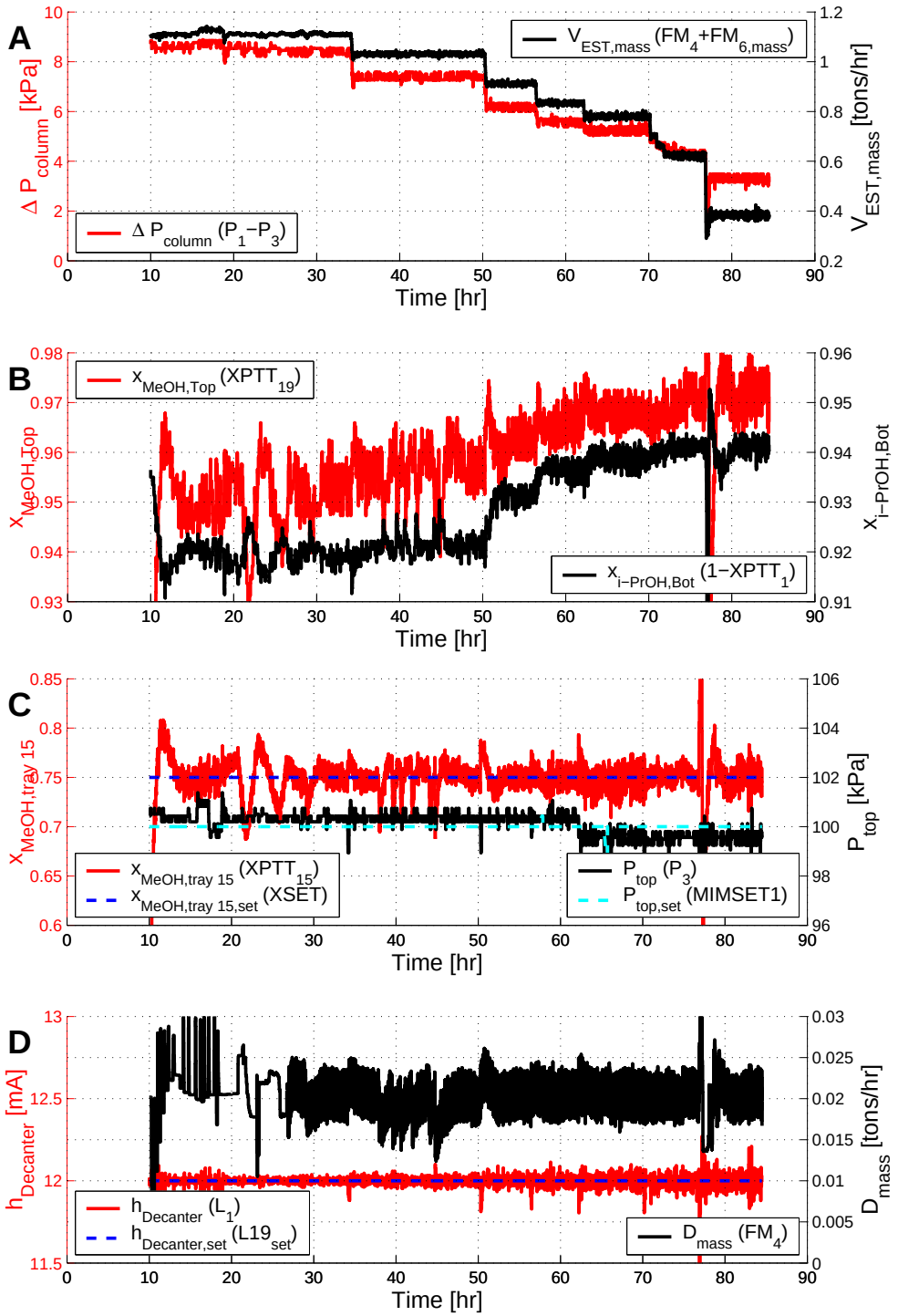

Figure A.1. Dynamic data from input multiplicity experiment, Feb. 14th 2000 - Feb. 18th 2000. Top pressure controlled. **A:** Column pressure drop (ΔP_{column}) and estimated boilup ($V_{EST,mass}$). **B:** Estimated product purities ($x_{MeOH,Top}$ and ($x_{PrOH,Bot}$)). **C:** Estimated composition on tray 15 ($x_{MeOH,tray15}$), setpoint to tray 15 composition controller ($x_{MeOH,tray15,set}$), column top pressure (P_{top}) and setpoint to column top pressure controller ($P_{top,set}$). **D:** Decanter level ($h_{Decanter}$), setpoint to decanter level controller ($h_{Decanter,set}$) and distillate flow rate (D_{mass}).

A.2.2 Experiment, Oct. 27th 2000 - Oct. 31st 2000

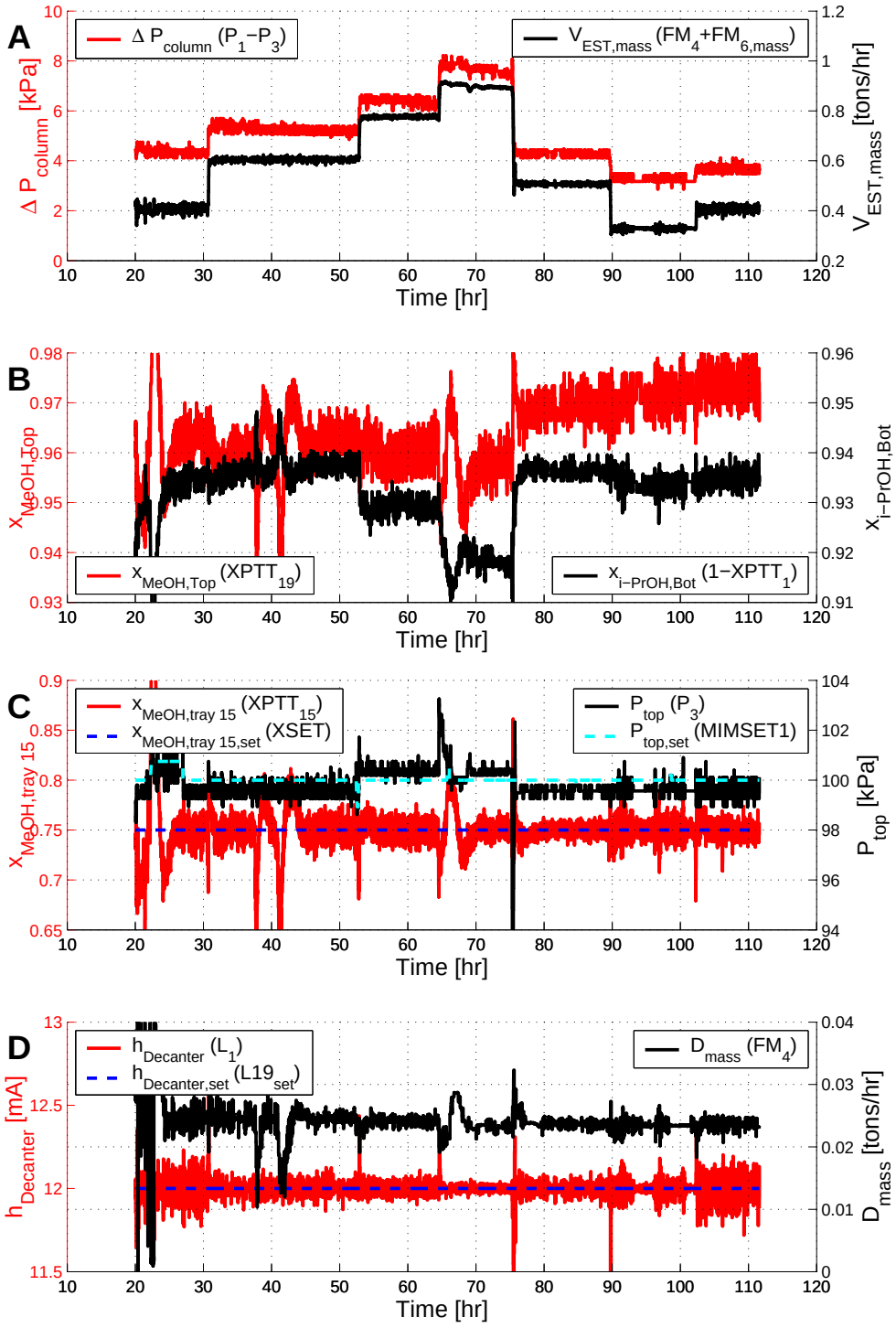

Figure A.2. Dynamic data from input multiplicity experiment, Oct. 27th 2000 - Oct. 31st 2000. Top pressure controlled. **A:** Column pressure drop (ΔP_{column}) and estimated boilup ($V_{EST,mass}$). **B:** Estimated product purities ($x_{MeOH,Top}$ and ($x_{PrOH,Bot}$)). **C:** Estimated composition on tray 15 ($x_{MeOH,tray15}$), setpoint to tray 15 composition controller ($x_{MeOH,tray15,set}$), column top pressure (P_{top}) and setpoint to column top pressure controller ($P_{top,set}$). **D:** Decanter level ($h_{Decanter}$), setpoint to decanter level controller ($h_{Decanter,set}$) and distillate flow rate (D_{mass}).

A.2.3 Experiment, Nov. 14th 2000 - Nov. 19th 2000

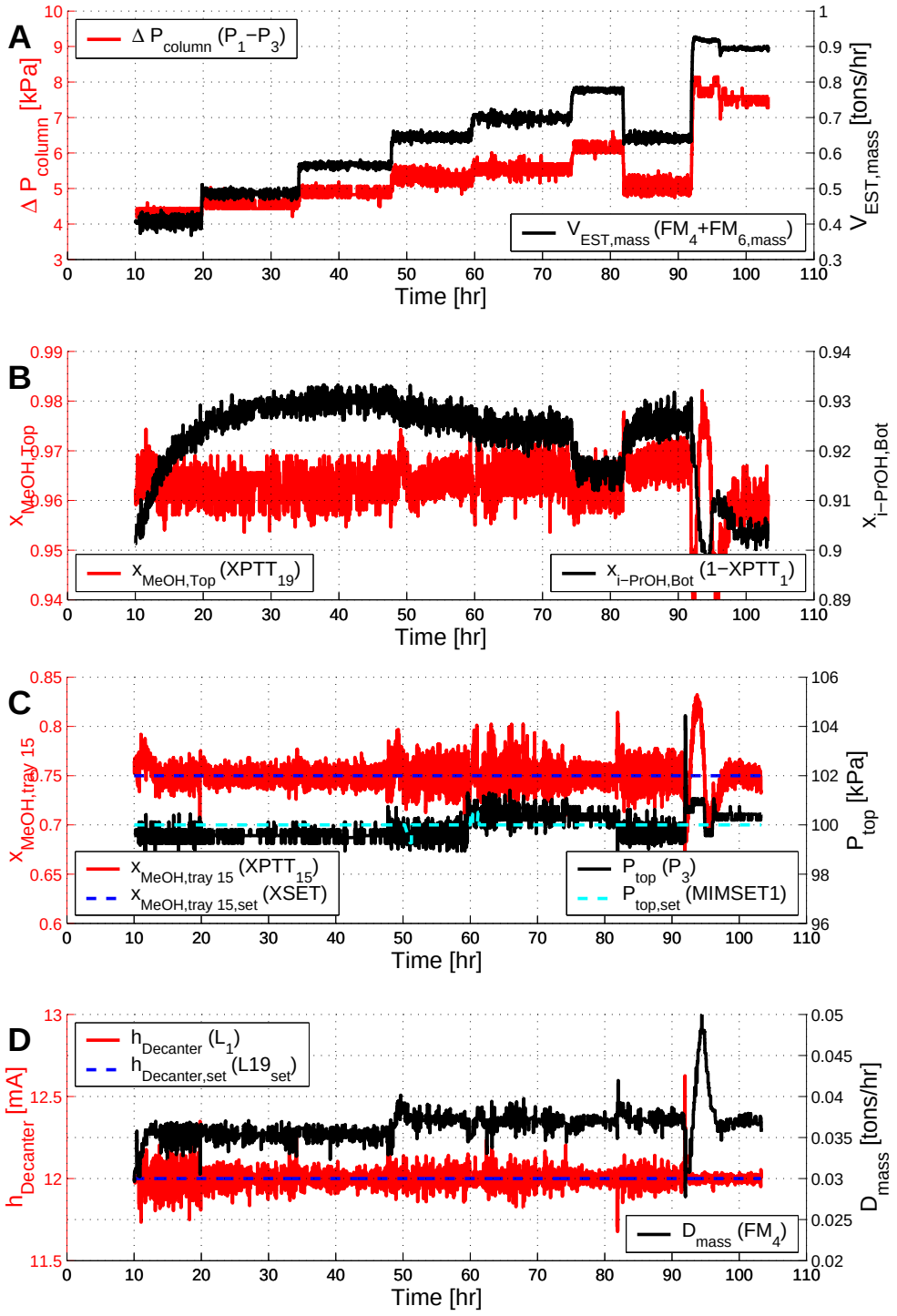

Figure A.3. Dynamic data from input multiplicity experiment, Nov. 14th 2000 - Nov. 19th 2000. Top pressure controlled. **A:** Column pressure drop (ΔP_{column}) and estimated boilup ($V_{EST,mass}$). **B:** Estimated product purities ($x_{MeOH,Top}$ and ($x_{PrOH,Bot}$)). **C:** Estimated composition on tray 15 ($x_{MeOH,tray15}$), setpoint to tray 15 composition controller ($x_{MeOH,tray15,set}$), column top pressure (P_{top}) and setpoint to column top pressure controller ($P_{top,set}$). **D:** Decanter level ($h_{Decanter}$), setpoint to decanter level controller ($h_{Decanter,set}$) and distillate flow rate (D_{mass}).

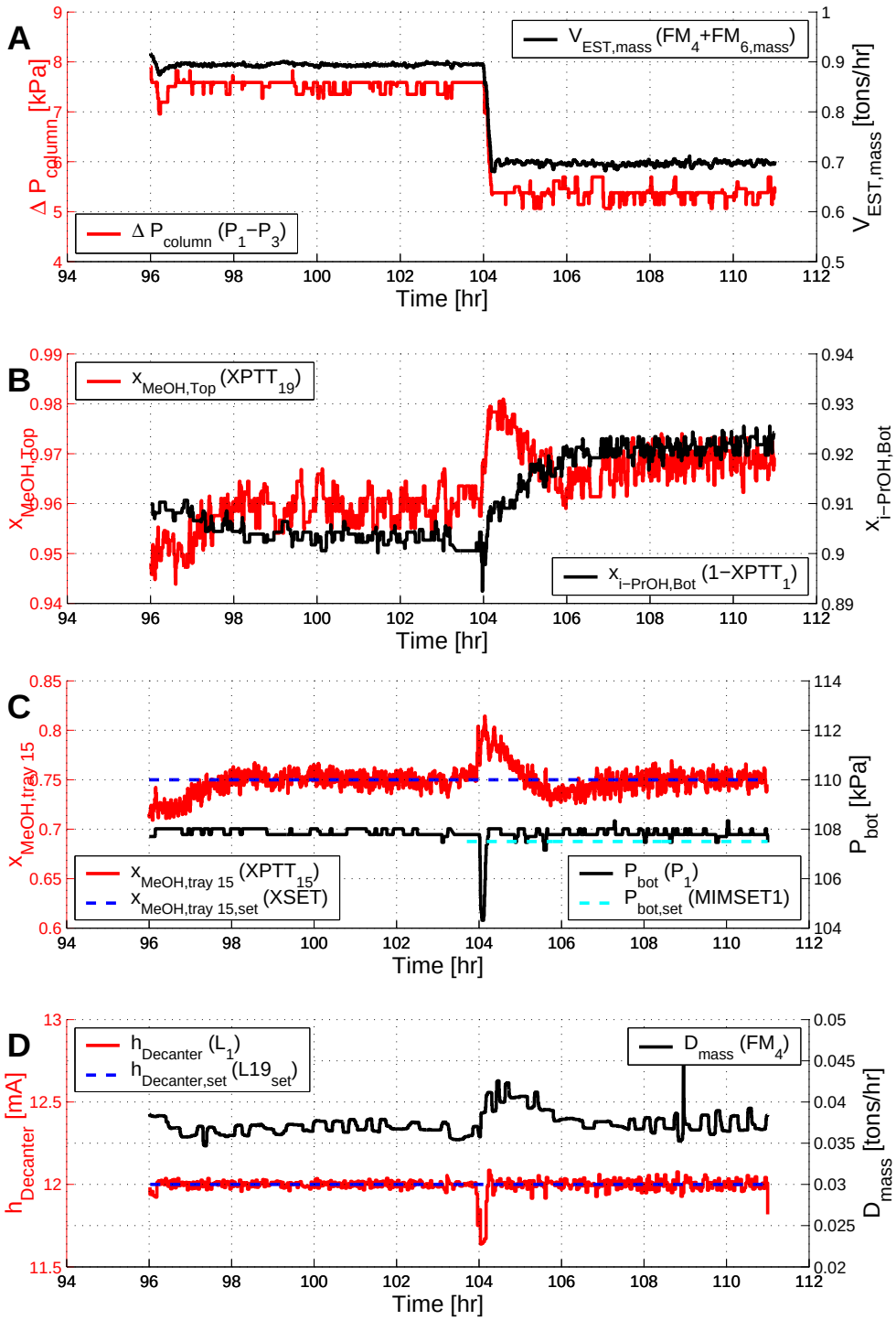

Figure A.4. Dynamic data from input multiplicity experiment, Nov. 14th 2000 - Nov. 19th 2000. Bottom pressure controlled. **A:** Column pressure drop (ΔP_{column}) and estimated boilup ($V_{EST,mass}$). **B:** Estimated product purities ($x_{MeOH,Top}$ and ($x_{PrOH,Bot}$)). **C:** Estimated composition on tray 15 ($x_{MeOH,tray15}$), setpoint to tray 15 composition controller ($x_{MeOH,tray15,set}$), column top pressure (P_{top}) and setpoint to column top pressure controller ($P_{top,set}$). **D:** Decanter level ($h_{Decanter}$), setpoint to decanter level controller ($h_{Decanter,set}$) and distillate flow rate (D_{mass}).

A.3 Steady States and Standard Deviations

A.3.1 Experiment, Feb. 14th 2000 - Feb. 18th 2000

Name	SS1	SS2	SS3	SS4	SS5	SS6	SS7
P_1	108.8	107.7	106.5	106	104.9	103.9	102.8
P_2	104.4	104	103.5	103.3	102.5	101.9	101.3
P_3	100.4	100.3	100.3	100.3	99.58	99.6	99.56
P_8	398.6	424.7	461.9	488.3	506.8	554.2	596.4
P_9	385.5	358.8	325.5	305.5	306.6	274.6	237.6
P_{10}	1226	1210	1198	1189	1179	1160	1123
FM_1	0.0661	0.06619	0.06621	0.06611	0.06615	0.06618	0.06611
FM_3	0.03995	0.04377	0.0443	0.04457	0.04377	0.04416	0.0431
FM_4	0.0205	0.02034	0.02029	0.0206	0.02032	0.02055	0.02045
$FM_6(vol)$[1]	1.378	1.28	1.13	1.029	0.9612	0.7601	0.4627
$FM_6(mass)$	1.089	1.011	0.8927	0.8129	0.7593	0.6005	0.3655
FM_7	5.134	2.811	2.506	2.11	1.665	0.8251	0.162
$V_{EST}(mass)$	1.109	1.032	0.9130	0.8335	0.7797	0.6210	0.3860
DP_1	19.25	19.26	19.14	19.14	19.14	19.17	19.1
DP_2	0.5467	0.4435	0.4163	0.3895	0.3578	0.3374	0.2907
DP_3	0.4431	0.3895	0.3569	0.3285	0.2967	0.2622	0.1946
DP_4	0.6067	0.6248	0.673	0.7031	0.7694	0.8177	0.9141
L_1	12	12	12	12	12	12	12
$XPTT_1$	0.08094	0.07847	0.0691	0.06395	0.06158	0.05876	0.05868
$XPTT_5$	0.1596	0.151	0.1372	0.138	0.1375	0.1367	0.1387
$XPTT_{10}$	0.3519	0.3291	0.3246	0.3246	0.3244	0.3248	0.344
$XPTT_{15}$	0.7496	0.7481	0.7486	0.7509	0.7502	0.7481	0.7511
$XPTT_{19}$	0.9528	0.9569	0.9628	0.9666	0.9677	0.9706	0.9732
PTT_1	82.2	82	81.93	81.92	81.71	81.54	81.27
PTT_5	79.98	79.99	80.09	79.97	79.75	79.59	79.33
PTT_{10}	75.6	75.96	75.92	75.86	75.66	75.52	75
PTT_{15}	68.37	68.34	68.27	68.21	68.02	67.98	67.86
PTT_{19}	64.93	64.86	64.78	64.73	64.52	64.49	64.44
TC_1	62.22	62.4	62.57	62.62	62.43	62.48	62.69
TC_3	60.98	61.12	61.13	61.1	60.92	60.64	59.68
TC_4	50.32	50.65	50.59	50.47	50.66	50.34	49.61
TR_0	82.31	82.11	81.95	81.85	81.65	81.45	80.89
TR_1	85.46	85.53	85.1	84.83	84.42	83.09	81.36
TR_2	83.18	83.1	82.89	82.8	82.55	82.39	82.14
$THCOND$	88.57	87.9	87.48	87.06	86.82	85.94	84.46
$THRECI$	89.3	88.33	87.83	87.52	86.99	86.45	85.25
C_{CYL}	16	16	16	16	16	16	16
C_{POW}	69.55	59.67	56.52	54.25	52.47	48.63	45.64
CV_8	0.3552	0.3382	0.326	0.3349	0.3263	0.3128	0.2654
CV_9	0.7077	0.5135	0.4437	0.4186	0.4061	0.3784	0.3671

Table A.7. Steady State measurement mean data from input multiplicity experiment, February 14th 2000 - February 18th 2000.

[1] Only volumetric measurement of the reflux (FM_6) was available. FM6 was post experiment converted to mass basis ($FM_6(mass)$). $V_{EST}(mass)$ was calculated as FM_4 + FM_6. The calculation is correct from a stationary point of view. It may however be inaccurate in dynamic data, unless the decanter level (L_1) is perfectly controlled.

Name	SS1	SS2	SS3	SS4	SS5	SS6	SS7
P_1	0.143	0.157	0.114	0.148	0.163	0.178	0.248
P_2	0.172	0.256	0.199	0.226	0.215	0.207	0.305
P_3	0.0999	0.151	0.15	0.168	0.195	0.164	0.198
P_8	0.34	1.54	1.55	1.61	2.35	1.45	2.04
P_9	0.349	1.3	1.68	1.9	9.43	3.35	0
P_{10}	1	1.22	1.54	1.8	2.22	2.26	4.1
FM_1	0.000421	0.000591	0.000669	0.000652	0.000625	0.000685	0.00051
FM_3	0.0000291	0.000438	0.000483	0.00025	0.000341	0.000122	0.000262
FM_4	0.00205	0.00201	0.00208	0.00191	0.00189	0.00183	0.00188
FM_6	0.00249	0.00685	0.0052	0.00607	0.00982	0.0101	0.0103
FM_7	0.105	0.0745	0.0342	0.0651	0.0718	0.058	0.0554
V_{EST}	0.0025	0.00589	0.00632	0.0071	0.00978	0.00889	0.0132
DP_1	0	0	0	0	0	0.00589	0.0139
DP_2	0.0036	0.00913	0.00213	0.00281	0.00466	0.00184	0.000712
DP_3	0.00205	0.00384	0.00238	0.0022	0.00297	0.00187	0.00213
DP_4	0	0	0	0	0	0	0
L_1	0.0141	0.0244	0.0229	0.0276	0.0445	0.0428	0.049
$XPTT_1$	0.000944	0.00123	0.00152	0.00151	0.00105	0.000758	0.00124
$XPTT_5$	0.00308	0.00307	0.00284	0.00336	0.00508	0.00233	0.00264
$XPTT_{10}$	0.00405	0.00542	0.00419	0.00533	0.00901	0.00312	0.00638
$XPTT_{15}$	0.00545	0.00631	0.0058	0.00644	0.00943	0.00505	0.00806
$XPTT_{19}$	0.00306	0.00284	0.00252	0.00317	0.00172	0.00235	0.00233
PTT_1	0.0325	0.0451	0.0442	0.0485	0.0484	0.0445	0.0574
PTT_5	0.0661	0.0902	0.0779	0.0843	0.121	0.0684	0.0983
PTT_{10}	0.0804	0.105	0.0994	0.108	0.177	0.0809	0.163
PTT_{15}	0.0825	0.0969	0.0993	0.101	0.136	0.097	0.166
PTT_{19}	0.0439	0.0587	0.0532	0.059	0.056	0.0473	0.0729
TC_1	0.0936	0.144	0.114	0.119	0.112	0.158	0.128
TC_3	0.0865	0.102	0.0933	0.0786	0.0817	0.113	0.0786
TC_4	0.0712	0.0909	0.0767	0.073	0.0966	0.11	0.0719
TR_0	0.0833	0.116	0.098	0.123	0.101	0.134	0.123
TR_1	0.142	0.162	0.195	0.21	0.167	0.218	0.127
TR_2	0.0869	0.122	0.107	0.114	0.123	0.104	0.135
$THCOND$	0.106	0.107	0.102	0.139	0.122	0.126	0.11
$THRECI$	0.107	0.0979	0.106	0.129	0.119	0.164	0.167
C_{CYL}	0	0	0	0	0	0	0
C_{POW}	0.468	0.226	0.228	0.285	0.487	0.385	0.869
CV_8	0.0151	0.0195	0.0227	0.0321	0.0631	0.0441	0.0977
CV_9	0	0.00457	0.00289	0.00281	0.00479	0.00321	0.00423

Table A.8. Standard deviations on Steady State measurement means from input multiplicity experiment, February 14th 2000 - February 18th 2000.

A.3.2 Experiment, Oct. 27th 2000 - Oct. 31st 2000

Name	SS1	SS2	SS3	SS4	SS5	SS6	SS7
P_1	103.9	104.7	106.7	108	103.8	102.8	103.2
P_2	101.5	102	103.2	103.7	101.6	101	101.3
P_3	99.51	99.55	100.4	100.4	99.57	99.56	99.57
P_8	586.2	521.9	440.7	378.6	562	592.8	584.1
P_9	232.6	285.1	327.3	373.1	265.3	250.3	251.9
P_{10}	1113	1154	1188	1208	1135	1101	1113
FM_1	0.06998	0.06981	0.06977	0.0701	0.07004	0.06997	0.06992
FM_3	0.04342	0.04376	0.04438	0.04559	0.04452	0.04479	0.04487
FM_4	0.02415	0.02458	0.02422	0.02327	0.0237	0.02352	0.02359
FM_6	0.3862	0.5807	0.7518	0.8696	0.4831	0.3062	0.3848
FM_7	0.2425	0.8473	1.498	1.545	0.5088	0.008378	0.2176
V_{EST}	0.5191	0.766	0.9825	1.131	0.6409	0.416	0.5152
DP_1	18.01	18	18.01	18	18.01	17.99	18
DP_2	0.3096	0.3856	0.4538	0.5178	0.3513	0.3183	0.3193
DP_3	0.1809	0.2725	0.3526	0.4146	0.2222	0.1805	0.192
DP_4	0.9864	0.863	0.679	0.6067	0.9244	1.011	0.9864
L_1	12	12	12	12	12	12	12
$XPTT_1$	0.06522	0.06233	0.07109	0.08209	0.06358	0.06583	0.06494
$XPTT_5$	0.1349	0.1309	0.1298	0.1511	0.1344	0.1396	0.1358
$XPTT_{10}$	0.3413	0.3298	0.3283	0.3419	0.3332	0.3559	0.3409
$XPTT_{15}$	0.7494	0.7501	0.7496	0.7531	0.7502	0.7507	0.75
$XPTT_{19}$	0.9636	0.963	0.961	0.9589	0.9705	0.9726	0.9746
PTT_1	81.39	81.66	81.94	81.99	81.41	81.1	81.24
PTT_5	79.58	79.82	80.23	79.98	79.58	79.27	79.45
PTT_{10}	75.11	75.43	75.76	75.62	75.27	74.71	75.06
PTT_{15}	67.91	67.96	68.22	68.23	67.91	67.83	67.88
PTT_{19}	64.56	64.58	64.82	64.86	64.48	64.45	64.43
TC_1	62.81	62.58	62.52	62.19	62.66	62.87	62.69
TC_3	60.81	61.21	61.32	61.06	61.02	60.21	60.66
TC_4	52.34	52.69	52.45	51.76	52.44	51.85	52.29
TR_0	81.34	81.69	82.07	82.15	81.39	80.86	81.15
TR_1	82.11	83.53	85.15	85.8	82.58	81.32	82.05
TR_2	82.19	82.47	82.81	82.93	82.2	81.91	82.04
$THCOND$	84.25	85.91	87.16	87.75	85.26	83.85	84.2
$THRECI$	84.97	86.61	88.14	89	85.79	84.67	84.82
C_{CYL}	16	16	16	16	16	16	16
C_{POW}	50.65	67.74	72.41	72.23	66.07	62.4	61.87
CV_8	0.2964	0.3503	0.378	0.406	0.3236	0.2972	0.2757
CV_9	0.3616	0.3985	0.466	0.9664	0.3765	0.3672	0.3647

Table A.9. Steady State measurement mean data from input multiplicity experiment, October 27th 2000 - October 31st 2000.

Name	SS1	SS2	SS3	SS4	SS5	SS6	SS7
P_1	0.195	0.198	0.12	0.103	0.151	0.142	0.31
P_2	0.276	0.272	0.184	0.142	0.227	0.159	0.377
P_3	0.193	0.235	0.143	0.0834	0.132	0.0867	0.279
P_8	1.28	2.16	1.42	0.537	1.66	0.738	2.11
P_9	7.66	11.7	2.19	0.661	1.62	0.688	0.492
P_{10}	2.99	2.57	2.05	1.07	2.38	1.86	3.48
FM_1	0.000934	0.00452	0.00426	0.00357	0.00258	0.00436	0.00401
FM_3	0.00581	0.00221	0.00124	0.000875	0.0000485	0.00163	0.00251
FM_4	0.00132	0.000776	0.000744	0.000651	0.000567	0.000507	0.000772
FM_6	0.0138	0.00589	0.00407	0.00217	0.0055	0.00321	0.0105
FM_7	0.025	0.0354	0.0418	0.0427	0.0357	0.0404	0.028
V_{EST}	0.0138	0.00939	0.00888	0.00407	0.00855	0.00486	0.0147
DP_1	0.0415	0.0225	0	0.00709	0	0.0158	0.0289
DP_2	0.00168	0.00364	0.00328	0.00514	0.00251	0.00259	0.00249
DP_3	0.00305	0.00322	0.00295	0.00339	0.00426	0.00261	0.00278
DP_4	0	0.00215	0	0	0.0077	0	0
L_1	0.095	0.0356	0.041	0.0192	0.0432	0.0251	0.079
$XPTT_1$	0.00126	0.00124	0.00127	0.000987	0.00114	0.000938	0.00141
$XPTT_5$	0.00359	0.00354	0.00359	0.00302	0.00227	0.0031	0.00403
$XPTT_{10}$	0.0076	0.00589	0.00568	0.00573	0.00332	0.00529	0.00573
$XPTT_{15}$	0.01	0.00818	0.00826	0.00661	0.00507	0.00572	0.00706
$XPTT_{19}$	0.00267	0.00231	0.00282	0.00235	0.00304	0.00227	0.00304
PTT_1	0.0573	0.0573	0.0411	0.0282	0.0453	0.0328	0.0745
PTT_5	0.0978	0.102	0.089	0.0658	0.069	0.0779	0.101
PTT_{10}	0.152	0.14	0.126	0.116	0.0812	0.111	0.11
PTT_{15}	0.17	0.144	0.131	0.1	0.0962	0.0983	0.123
PTT_{19}	0.0691	0.0714	0.0504	0.0376	0.0557	0.0431	0.0943
TC_1	0.149	0.171	0.155	0.0908	0.133	0.0877	0.165
TC_3	0.105	0.107	0.0945	0.0821	0.107	0.0857	0.0978
TC_4	0.0908	0.162	0.149	0.108	0.13	0.0953	0.095
TR_0	0.117	0.176	0.104	0.0823	0.138	0.0938	0.117
TR_1	0.164	0.281	0.285	0.201	0.21	0.137	0.159
TR_2	0.118	0.119	0.0948	0.0933	0.121	0.0779	0.138
$THCOND$	0.129	0.11	0.132	0.128	0.122	0.153	0.125
$THRECI$	0.114	0.137	0.146	0.0972	0.149	0.137	0.148
C_{CYL}	0	0	0	0	0	0	0
C_{POW}	0.734	0.936	1.19	1.19	0.936	0.971	0.855
CV_8	0.0575	0.0621	0.0327	0.0195	0.046	0.0483	0.0878
CV_9	0.00355	0.0043	0.0038	0.0446	0.00314	0.00171	0.00432

Table A.10. Standard deviations on Steady State measurement means from input multiplicity experiment, October 27th 2000 - October 31st 2000.

A.3.3 Experiment, Nov. 14th 2000 - Nov. 19th 2000

Name	SS1	SS2	SS3	SS4	SS5	SS6	SS7
P_1	103.9	104.2	104.4	104.8	105.9	106.5	104.7
P_2	101.7	101.8	101.9	102.1	102.9	103.2	102.1
P_3	99.57	99.58	99.6	99.57	100.3	100.3	99.66
P_8	585	571.8	540.2	504.5	479	442.1	502
P_9	247.3	255.5	264	298.2	299	320.8	294.8
P_{10}	1101	1114	1125	1133	1144	1156	1132
FM_1	0.11	0.11	0.1097	0.11	0.1102	0.11	0.11
FM_3	0.07437	0.07108	0.0731	0.07126	0.07098	0.07099	0.07126
FM_4	0.0351	0.03531	0.03534	0.03718	0.03704	0.03695	0.03722
FM_6	0.3726	0.4519	0.5291	0.6072	0.6622	0.7405	0.6041
FM_7	0.2612	0.4455	0.7379	0.9901	1.181	2.674	0.94
V_{EST}	0.5152	0.6159	0.714	0.816	0.8844	0.9841	0.812
DP_1	19.4	19.38	19.38	19.39	19.39	19.4	19.39
DP_2	0.2879	0.3212	0.3478	0.3787	0.3858	0.4244	0.3801
DP_3	0.1899	0.2268	0.2579	0.2924	0.3038	0.3489	0.2943
DP_4	0.9925	0.9442	0.893	0.8328	0.7848	0.7144	0.8207
L_1	12	12	12	12	12	12	12
$XPTT_1$	0.07723	0.07115	0.07026	0.07371	0.07601	0.08488	0.07408
$XPTT_5$	0.1537	0.1462	0.1431	0.1443	0.1443	0.1454	0.1445
$XPTT_{10}$	0.3636	0.3528	0.3463	0.3454	0.3433	0.3434	0.3457
$XPTT_{15}$	0.7505	0.75	0.7505	0.75	0.7496	0.7498	0.7506
$XPTT_{19}$	0.9629	0.9635	0.9647	0.9649	0.9652	0.9632	0.9682
PTT_1	81.12	81.33	81.42	81.43	81.63	81.59	81.4
PTT_5	79.19	79.4	79.52	79.56	79.79	79.87	79.54
PTT_{10}	74.72	74.96	75.11	75.16	75.41	75.48	75.15
PTT_{15}	67.91	67.94	67.95	67.97	68.18	68.21	67.98
PTT_{19}	64.59	64.58	64.57	64.56	64.74	64.78	64.54
TC_1	62.57	62.49	62.38	62.3	62.39	62.26	62.26
TC_3	60.22	60.63	60.78	60.89	61.02	60.97	60.76
TC_4	51.7	52.34	52.31	52.46	52.5	52.26	52.12
TR_0	80.97	81.29	81.4	81.45	81.66	81.65	81.38
TR_1	82.1	82.48	83.67	84.09	84.52	84.3	84.07
TR_2	82	82.21	82.28	82.29	82.51	82.55	82.23
$THCOND$	83.6	84.12	84.49	85	85.34	85.69	84.5
$THRECI$	84.64	84.99	85.35	85.63	86.1	86.64	85.72
C_{CYL}	16	16	16	16	16	16	16
C_{POW}	41.18	42.74	62.2	65.6	65.24	68.02	65.49
CV_8	0.3235	0.2973	0.3197	0.3233	0.3542	0.3691	0.3334
CV_9	0.3597	0.3723	0.3881	0.4068	0.4237	0.4599	0.4063

Table A.11. Steady State measurement mean data from input multiplicity experiment, November 14th 2000 to November 19th 2000, SS1-SS7.

Name	SS8	SS9
P_1	107.9	107.8
P_2	103.6	104.9
P_3	100.4	102.5
P_8	388.1	464
P_9	366.3	324.3
P_{10}	1186	1153
FM_1	0.1101	0.11
FM_3	0.07037	0.07163
FM_4	0.03696	0.03734
FM_6	0.8577	0.6603
FM_7	7.842	1.125
V_{EST}	1.133	0.8829
DP_1	19.41	19.4
DP_2	0.5022	0.386
DP_3	0.4201	0.2993
DP_4	0.6007	0.7694
L_1	12	12
$XPTT_1$	0.09675	0.07833
$XPTT_5$	0.1675	0.1464
$XPTT_{10}$	0.3558	0.3453
$XPTT_{15}$	0.7492	0.7502
$XPTT_{19}$	0.9596	0.9691
PTT_1	81.64	82.04
PTT_5	79.62	80.22
PTT_{10}	75.35	75.87
PTT_{15}	68.28	68.69
PTT_{19}	64.83	65.23
TC_1	61.94	62.98
TC_3	60.72	61.43
TC_4	51.77	52.46
TR_0	81.9	81.99
TR_1	84.51	84.77
TR_2	82.75	82.91
$THCOND$	86.51	85.3
$THRECI$	88	86.67
C_{CYL}	16	14
C_{POW}	69.84	63.95
CV_8	0.3856	0.3402
CV_9	0.6422	0.4325

Table A.12. Steady State measurement mean data from input multiplicity experiment, November 14th 2000 to November 19th 2000, SS8-SS9.

Name	SS1	SS2	SS3	SS4	SS5	SS6	SS7
P_1	0.268	0.187	0.196	0.26	0.182	0.135	0.158
P_2	0.356	0.255	0.231	0.298	0.224	0.219	0.207
P_3	0.288	0.15	0.158	0.296	0.221	0.184	0.199
P_8	2.08	1.81	1.85	3.5	2.24	1.56	3.06
P_9	0.29	0.304	0	9.94	6.14	2.16	8.04
P_{10}	3.53	3.13	2.7	4	2.32	1.79	2.85
FM_1	0.000225	0.00442	0.00493	0.00043	0.00418	0.00255	0.000358
FM_3	0.00446	0.00537	0.00152	0.00178	0.00232	0.00548	0.00153
FM_4	0.00106	0.000833	0.000673	0.000514	0.000738	0.000487	0.000675
FM_6	0.0128	0.00777	0.0054	0.00652	0.00615	0.00369	0.0052
FM_7	0.0325	0.047	0.0404	0.057	0.0608	0.301	0.0463
V_{EST}	0.0181	0.0123	0.00873	0.0132	0.00948	0.00665	0.00983
DP_1	0.03	0.0358	0	0.0151	0.00968	0.0377	0
DP_2	0.0021	0.00266	0.00253	0.00561	0.00506	0.00389	0.0049
DP_3	0.00334	0.0028	0.00217	0.00446	0.0049	0.00334	0.00382
DP_4	0	0	0	0.00807	0.00888	0.00576	0
L_1	0.0967	0.0578	0.0388	0.0581	0.0429	0.0277	0.0433
$XPTT_1$	0.00137	0.00116	0.0012	0.0013	0.00152	0.00173	0.00121
$XPTT_5$	0.00423	0.0027	0.00319	0.00571	0.00394	0.00311	0.00476
$XPTT_{10}$	0.0066	0.00406	0.0044	0.00932	0.00726	0.0049	0.00794
$XPTT_{15}$	0.00853	0.00703	0.00679	0.0126	0.00912	0.00644	0.0104
$XPTT_{19}$	0.00251	0.0036	0.00288	0.00198	0.00275	0.00293	0.00186
PTT_1	0.0683	0.053	0.0549	0.0742	0.0517	0.0494	0.0495
PTT_5	0.0938	0.091	0.0972	0.153	0.1	0.0781	0.122
PTT_{10}	0.118	0.121	0.122	0.209	0.145	0.103	0.17
PTT_{15}	0.139	0.138	0.134	0.202	0.135	0.101	0.158
PTT_{19}	0.0889	0.0629	0.0661	0.0893	0.0573	0.0572	0.0629
TC_1	0.153	0.154	0.144	0.166	0.146	0.147	0.193
TC_3	0.0828	0.118	0.0949	0.0907	0.0936	0.135	0.151
TC_4	0.098	0.132	0.12	0.0804	0.122	0.142	0.166
TR_0	0.11	0.13	0.142	0.102	0.109	0.162	0.149
TR_1	0.222	0.249	0.324	0.275	0.106	0.173	0.245
TR_2	0.12	0.104	0.0986	0.107	0.101	0.099	0.0917
$THCOND$	0.126	0.17	0.131	0.144	0.133	0.15	0.135
$THRECI$	0.159	0.169	0.175	0.14	0.146	0.149	0.17
C_{CYL}	0	0	0	0	0	0	0
C_{POW}	1.13	1.1	1.24	1.25	0.813	1.41	2.16
CV_8	0.0838	0.068	0.0527	0.104	0.0466	0.027	0.07
CV_9	0.00421	0.00387	0.00321	0.00698	0.00449	0.00312	0.00555

Table A.13. Standard deviations on Steady State measurement means from input multiplicity experiment, November 14th 2000 to November 19th 2000, SS1-SS7.

Name	SS8	SS9
P_1	0.12	0.123
P_2	0.19	0.228
P_3	0.108	0.175
P_8	1.02	1.46
P_9	1.33	1.86
P_{10}	1.09	1.39
FM_1	0.00384	0.00365
FM_3	0.00535	0.00582
FM_4	0.000463	0.00146
FM_6	0.0024	0.00457
FM_7	0.0365	0.0321
V_{EST}	0.00389	0.00499
DP_1	0.0389	0.0327
DP_2	0.0137	0.00242
DP_3	0.00256	0.00201
DP_4	0	0
L_1	0.0181	0.0293
$XPTT_1$	0.00109	0.00149
$XPTT_5$	0.00328	0.00327
$XPTT_{10}$	0.00506	0.0051
$XPTT_{15}$	0.00623	0.00652
$XPTT_{19}$	0.00304	0.0023
PTT_1	0.0275	0.0477
PTT_5	0.0681	0.0845
PTT_{10}	0.109	0.109
PTT_{15}	0.092	0.106
PTT_{19}	0.046	0.0538
TC_1	0.122	0.181
TC_3	0.0989	0.111
TC_4	0.0893	0.143
TR_0	0.111	0.133
TR_1	0.114	0.146
TR_2	0.0905	0.0908
$THCOND$	0.118	0.128
$THRECI$	0.136	0.14
C_{CYL}	0	0
C_{POW}	1.34	0.808
CV_8	0.017	0.0273
CV_9	0.00899	0.00282

Table A.14. Standard deviations on Steady State measurement means from input multiplicity experiment, November 14th 2000 to November 19th 2000, SS8-SS9.

A.4 Gas Chromatography Analysis

During the 3 experiments 23 steady state operating points were obtained. For 22 of these the distillate, the bottom product and the feed flow where sampled for later analysis on a gas chromatograph (unfortunately samples were not taken from steady state 8 in the experiment of November 14th-19th 2000). In order to determine the compositions of the samples, calibration standards of known composition are made and analyzed on the gas chromatograph. The results from these analyses are then fitted to a correlation. The GC–results from the 22 samples are thus evaluated on this correlation by which the sample compositions are determined.

A.4.1 Calibration

A total of 27 standards where made for calibration of the Gas Chromatograph, covering 9 standards within the distillate composition region, 9 standards within the feed composition region and 9 standards within the bottom product composition region. Each standard was analyzed 3 times. In order to get good prediction ability, the results from the 81 runs were divided into two groups: 27 runs within the distillate composition region (where no or only traces of water is present) and 27+27 runs within the feed and bottom product compositions region (where water is present). Each group of results were fitted to the same correlation, thus obtaining two different sets of parameters. The following correlations was used for both groups:

$$\hat{x}_i = \frac{\alpha_i A_i^{\beta_i}}{\sum_j \alpha_j A_j^{\beta_j}}, \quad i \in [H2O; MeOH; PrOH] \tag{A.1}$$

where x_i is the weight fraction of component i, A_i is the area on the gas chromatogram of component i. α_i and β_i are coefficients to be fitted for the individual component i.

The coefficients are obtained using NLP (Non Linear Programming in the MINOS5 solver) in GAMS (General Algebraic Modeling System), by minimizing the objective function:

$$\min \sum_k \sum_j \sum_i (\hat{x}_i - x_i)^2, \quad k \in [1; ...; n], \quad i, j \in [H2O; MeOH; PrOH] \tag{A.2}$$

where k is the index of the run number. The obtained coefficients for the weight fraction - area correlation (equation A.1) in each composition region can be seen from tables A.15 and A.16.

Component (i)	α_i	β_i
H2O	10.00	0.981
MeOH	261.1	1.008
PrOH	904.6	0.863

Table A.15. GC coefficients for top product composition region.

Component (i)	α_i	β_i
H2O	10.00	1.147
MeOH	28.15	0.987
PrOH	143.6	0.831

Table A.16. GC coefficients for feed and bottom product composition regions.

A.4.2 GC Analysis Results

The 22 sample sets of distillate, bottom product and feed where each analyzed 3 times on the gas chromatograph. The resulting areas from each chromatogram were evaluated on correlation A.1, with the appropriate set of parameters given in tables A.15 and A.16. The following pages accumulate the results for the obtained compositions as well as standard deviations for each sample.

A.4.2.1 Experiment, Feb. 14th 2000 - Feb. 18th 2000

Name	SS1	SS2	SS3	SS4	SS5	SS6	SS7
x_{F,H_2O}	0.0082	0.0083	0.0088	0.0063	0.0053	0.0103	0.0090
$x_{F,MeOH}$	0.3264	0.3380	0.2977	0.2788	0.2722	0.3041	0.3095
$x_{F,PrOH}$	0.6654	0.6537	0.6935	0.7149	0.7225	0.6856	0.6815
x_{D,H_2O}	0.0001	0.0001	0.0001	0.0000	0.0000	0.0001	0.0000
$x_{D,MeOH}$	0.9505	0.9547	0.9538	0.9460	0.9558	0.9554	0.9550
$x_{D,PrOH}$	0.0494	0.0452	0.0462	0.0540	0.0442	0.0446	0.0449
x_{B,H_2O}	0.0136	0.0137	0.0098	0.0096	0.0094	0.0223	0.0119
$x_{B,MeOH}$	0.0242	0.0217	0.0138	0.0129	0.0088	0.0071	0.0113
$x_{B,PrOH}$	0.9623	0.9646	0.9764	0.9775	0.9818	0.9706	0.9768

Table A.17. GC results: Component mass fractions of external flow samples from experiment, Feb. 14th 2000 - Feb. 18th 2000.

Name	SS1	SS2	SS3	SS4	SS5	SS6	SS7
$\sigma_{x_{F,H_2O}}$	0.00062	0.00032	0.00515	0.00027	0.00094	0.00112	0.00081
$\sigma_{x_{F,MeOH}}$	0.00421	0.01504	0.02251	0.00109	0.00365	0.00397	0.00154
$\sigma_{x_{F,PrOH}}$	0.00474	0.01489	0.02762	0.00083	0.00426	0.00383	0.00133
$\sigma_{x_{D,H_2O}}$	0.00003	0.00001	0.00007	0.00000	0.00000	0.00002	0.00004
$\sigma_{x_{D,MeOH}}$	0.00224	0.00276	0.00370	0.01489	0.00852	0.00168	0.00154
$\sigma_{x_{D,PrOH}}$	0.00226	0.00275	0.00364	0.01489	0.00852	0.00167	0.00156
$\sigma_{x_{B,H_2O}}$	0.00172	0.00085	0.00247	0.00144	0.00135	0.00061	0.00077
$\sigma_{x_{B,MeOH}}$	0.00155	0.00087	0.00136	0.00218	0.00112	0.00079	0.00052
$\sigma_{x_{B,PrOH}}$	0.00310	0.00172	0.00348	0.00362	0.00186	0.00117	0.00117

Table A.18. GC results: Standard deviations of component mass fractions of external flow samples from experiment, Feb. 14th 2000 - Feb. 18th 2000.

Name	SS1	SS2	SS3	SS4	SS5	SS6	SS7
x_{F,H_2O}	0.0210	0.0210	0.0228	0.0167	0.0141	0.0267	0.0232
$x_{F,MeOH}$	0.4692	0.4819	0.4354	0.4154	0.4083	0.4420	0.4493
$x_{F,PrOH}$	0.5098	0.4971	0.5418	0.5679	0.5776	0.5313	0.5274
x_{D,H_2O}	0.0002	0.0001	0.0001	0.0000	0.0000	0.0002	0.0001
$x_{D,MeOH}$	0.9729	0.9753	0.9747	0.9705	0.9759	0.9756	0.9755
$x_{D,PrOH}$	0.0270	0.0246	0.0252	0.0295	0.0241	0.0243	0.0245
x_{B,H_2O}	0.0430	0.0436	0.0315	0.0309	0.0303	0.0704	0.0383
$x_{B,MeOH}$	0.0430	0.0388	0.0249	0.0233	0.0160	0.0126	0.0205
$x_{B,PrOH}$	0.9140	0.9177	0.9435	0.9457	0.9536	0.9170	0.9412

Table A.19. GC results: Component mole fractions of external flow samples from experiment, Feb. 14th 2000 - Feb. 18th 2000.

A.4.2.2 Experiment, Oct. 27th 2000 - Oct. 31st 2000

Name	SS1	SS2	SS3	SS4	SS5	SS6	SS7
x_{F,H_2O}	0.0088	0.0083	0.0138	0.0111	0.0117	0.0097	0.0105
$x_{F,MeOH}$	0.3444	0.3531	0.3464	0.3538	0.3462	0.3372	0.3454
$x_{F,PrOH}$	0.6467	0.6386	0.6398	0.6350	0.6421	0.6532	0.6441
x_{D,H_2O}	0.0000	0.0001	0.0000	0.0000	0.0001	0.0001	0.0001
$x_{D,MeOH}$	0.9594	0.9549	0.9579	0.9555	0.9578	0.9555	0.9567
$x_{D,PrOH}$	0.0406	0.0450	0.0421	0.0444	0.0421	0.0444	0.0432
x_{B,H_2O}	0.0190	0.0138	0.0128	0.0179	0.0156	0.0178	0.0161
$x_{B,MeOH}$	0.0128	0.0120	0.0311	0.0239	0.0126	0.0151	0.0124
$x_{B,PrOH}$	0.9682	0.9742	0.9561	0.9582	0.9718	0.9672	0.9715

Table A.20. GC results: Component mass fractions of external flow samples from experiment, Oct. 27th 2000 - Oct. 31st 2000

Name	SS1	SS2	SS3	SS4	SS5	SS6	SS7
$\sigma_{x_{F,H_2O}}$	0.00026	0.00108	0.00089	0.00016	0.00074	0.00066	0.00095
$\sigma_{x_{F,MeOH}}$	0.00604	0.00152	0.00796	0.01400	0.00399	0.00057	0.00450
$\sigma_{x_{F,PrOH}}$	0.00578	0.00047	0.00885	0.01392	0.00418	0.00109	0.00534
$\sigma_{x_{D,H_2O}}$	0.00000	0.00005	0.00004	0.00004	0.00005	0.00002	0.00002
$\sigma_{x_{D,MeOH}}$	0.00246	0.00403	0.00023	0.00181	0.00183	0.00149	0.00105
$\sigma_{x_{D,PrOH}}$	0.00246	0.00399	0.00019	0.00184	0.00178	0.00150	0.00107
$\sigma_{x_{B,H_2O}}$	0.00102	0.00142	0.00138	0.00122	0.00060	0.00019	0.00024
$\sigma_{x_{B,MeOH}}$	0.00009	0.00026	0.00140	0.00068	0.00030	0.00048	0.00042
$\sigma_{x_{B,PrOH}}$	0.00098	0.00156	0.00164	0.00156	0.00089	0.00065	0.00062

Table A.21. GC results: Standard deviations of component mass fractions of external flow samples from experiment, Oct. 27th 2000 - Oct. 31st 2000

Name	SS1	SS2	SS3	SS4	SS5	SS6	SS7
x_{F,H_2O}	0.0223	0.0208	0.0345	0.0278	0.0294	0.0245	0.0265
$x_{F,MeOH}$	0.4886	0.4985	0.4864	0.4967	0.4880	0.4799	0.4881
$x_{F,PrOH}$	0.4891	0.4806	0.4791	0.4755	0.4826	0.4956	0.4854
x_{D,H_2O}	0.0000	0.0001	0.0001	0.0000	0.0001	0.0001	0.0001
$x_{D,MeOH}$	0.9779	0.9754	0.9771	0.9758	0.9770	0.9757	0.9764
$x_{D,PrOH}$	0.0221	0.0245	0.0229	0.0242	0.0229	0.0242	0.0235
x_{B,H_2O}	0.0599	0.0441	0.0405	0.0561	0.0496	0.0562	0.0512
$x_{B,MeOH}$	0.0228	0.0216	0.0551	0.0422	0.0226	0.0268	0.0222
$x_{B,PrOH}$	0.9173	0.9343	0.9044	0.9017	0.9278	0.9170	0.9265

Table A.22. GC results: Component mole fractions of external flow samples from experiment, Oct. 27th 2000 - Oct. 31st 2000

A.4.2.3 Experiment, Nov. 14th 2000 - Nov. 19th 2000

Name	SS1	SS2	SS3	SS4	SS5	SS6	SS7	SS9
x_{F,H_2O}	0.0163	0.0198	0.0105	0.0243	0.0126	0.0148	0.0228	0.0226
$x_{F,MeOH}$	0.3273	0.3045	0.3332	0.2955	0.3389	0.3465	0.3036	0.3063
$x_{F,PrOH}$	0.6564	0.6757	0.6563	0.6802	0.6485	0.6387	0.6736	0.6711
x_{D,H_2O}	0.0000	0.0000	0.0000	0.0000	0.0001	0.0001	0.0001	0.0001
$x_{D,MeOH}$	0.9547	0.9550	0.9528	0.9527	0.9460	0.9469	0.9463	0.9487
$x_{D,PrOH}$	0.0453	0.0450	0.0472	0.0473	0.0539	0.0530	0.0536	0.0512
x_{B,H_2O}	0.0245	0.0164	0.0182	0.0197	0.0192	0.0195	0.0183	0.0192
$x_{B,MeOH}$	0.0196	0.0187	0.0173	0.0198	0.0176	0.0201	0.0167	0.0261
$x_{B,PrOH}$	0.9559	0.9650	0.9644	0.9605	0.9632	0.9604	0.9650	0.9548

Table A.23. GC results: Component mass fractions of external flow samples from experiment, Nov. 14th 2000 - Nov. 19th 2000.

Name	SS1	SS2	SS3	SS4	SS5	SS6	SS7	SS9
$\sigma_{x_{F,H_2O}}$	0.00437	0.00060	0.00034	0.00140	0.00039	0.00090	0.00103	0.00126
$\sigma_{x_{F,MeOH}}$	0.00343	0.00166	0.00258	0.00029	0.00134	0.00689	0.00757	0.00389
$\sigma_{x_{F,PrOH}}$	0.00762	0.00116	0.00229	0.00112	0.00147	0.00776	0.00855	0.00414
$\sigma_{x_{D,H_2O}}$	0.00000	0.00000	0.00000	0.00000	0.00002	0.00003	0.00000	0.00001
$\sigma_{x_{D,MeOH}}$	0.00155	0.00098	0.00051	0.00172	0.00138	0.00035	0.00113	0.00077
$\sigma_{x_{D,PrOH}}$	0.00155	0.00098	0.00051	0.00172	0.00138	0.00036	0.00113	0.00076
$\sigma_{x_{B,H_2O}}$	0.00080	0.00292	0.00316	0.00286	0.00029	0.00072	0.00124	0.00013
$\sigma_{x_{B,MeOH}}$	0.00038	0.00115	0.00088	0.00058	0.00033	0.00050	0.00061	0.00043
$\sigma_{x_{B,PrOH}}$	0.00048	0.00371	0.00275	0.00229	0.00023	0.00085	0.00181	0.00045

Table A.24. GC results: Standard deviations of component mass fractions of external flow samples from experiment, Nov. 14th 2000 - Nov. 19th 2000.

Name	SS1	SS2	SS3	SS4	SS5	SS6	SS7	SS9
x_{F,H_2O}	0.0410	0.0503	0.0266	0.0616	0.0316	0.0368	0.0577	0.0571
$x_{F,MeOH}$	0.4634	0.4351	0.4748	0.4214	0.4794	0.4857	0.4316	0.4349
$x_{F,PrOH}$	0.4956	0.5146	0.4986	0.5170	0.4890	0.4774	0.5106	0.5080
x_{D,H_2O}	0.0000	0.0000	0.0000	0.0000	0.0001	0.0002	0.0002	0.0002
$x_{D,MeOH}$	0.9753	0.9755	0.9743	0.9742	0.9704	0.9709	0.9705	0.9718
$x_{D,PrOH}$	0.0247	0.0245	0.0257	0.0258	0.0295	0.0290	0.0293	0.0280
x_{B,H_2O}	0.0761	0.0517	0.0575	0.0617	0.0604	0.0612	0.0577	0.0600
$x_{B,MeOH}$	0.0343	0.0332	0.0307	0.0349	0.0311	0.0354	0.0297	0.0458
$x_{B,PrOH}$	0.8896	0.9151	0.9118	0.9034	0.9084	0.9034	0.9126	0.8943

Table A.25. GC results: Component mole fractions of external flow samples from experiment, Nov. 14th 2000 - Nov. 19th 2000.

A.5 Data Reconciliation

In order to obtain consistent sets of data, the results from the GC–analysis and the on–line measurements of external flows from the experiments were reconciled. This is done to ensure that overall mass and component balances are respected from a steady state point of view. Chapter 4 describes the method for performing the data reconciliation in detail.

The objective function used for the data reconciliation is:

$$F = \sum_i \left(w_i(y_i^m - y_i^f)\right)^2$$

here w_i is the weight for measurement i. The measured variables y_i^m are:

$$\begin{aligned} \mathbf{y}^m \quad = \quad & \big[x_{MeOH,F} \quad x_{MeOH,D} \quad x_{MeOH,B} \\ & \ldots \quad x_{PrOH,F} \quad x_{PrOH,D} \quad x_{PrOH,B} \\ & \ldots \quad F \quad D \quad B\big]^T \end{aligned}$$

Minimization of the objective function is performed subject to the overall mass and individual component constraints:

$$\begin{aligned} 0 &= F - D - B \\ 0 &= Fx_{MeOH,F} - Dx_{MeOH,D} - Bx_{MeOH,B} \\ 0 &= Fx_{PrOH,F} - Dx_{PrOH,D} - Bx_{PrOH,B} \\ 0 &\leq x_{k,j} \leq 1 \end{aligned}$$

A.5.1 Experiment, Feb. 14th 2000 - Feb. 18th 2000

Name	SS1	SS2	SS3	SS4	SS5	SS6	SS7
x_{F,H_2O}	0.0231	0.0230	0.0185	0.0178	0.0174	0.0384	0.0214
$x_{F,MeOH}$	0.4684	0.4802	0.4385	0.4160	0.4080	0.4362	0.4505
$x_{F,PrOH}$	0.5085	0.4968	0.5430	0.5662	0.5746	0.5254	0.5282
x_{D,H_2O}	0.0000	0.0000	0.0008	0.0000	0.0000	0.0000	0.0004
$x_{D,MeOH}$	0.9730	0.9754	0.9741	0.9704	0.9758	0.9757	0.9752
$x_{D,PrOH}$	0.0270	0.0246	0.0251	0.0296	0.0242	0.0243	0.0244
x_{B,H_2O}	0.0426	0.0434	0.0322	0.0305	0.0294	0.0685	0.0386
$x_{B,MeOH}$	0.0431	0.0389	0.0248	0.0232	0.0160	0.0129	0.0204
$x_{B,PrOH}$	0.9143	0.9177	0.9430	0.9463	0.9546	0.9186	0.9410
F	0.06353	0.06497	0.06551	0.06577	0.06526	0.06553	0.06494
D	0.02072	0.02194	0.01987	0.01880	0.01820	0.02038	0.02056
B	0.04280	0.04302	0.04563	0.04697	0.04706	0.04515	0.04438

Table A.26. Reconciled results of component mole fractions and mass flow rates [tons/hr] of the external flows from input multiplicity experiment, Feb. 14th 2000 - Feb. 18th 2000.

A.5.2 Experiment, Oct. 27th 2000 - Oct. 31st 2000

Name	SS1	SS2	SS3	SS4	SS5	SS6	SS7
x_{F,H_2O}	0.0303	0.0220	0.0230	0.0288	0.0260	0.0292	0.0263
$x_{F,MeOH}$	0.4845	0.4978	0.4931	0.4956	0.4896	0.4774	0.4879
$x_{F,PrOH}$	0.4852	0.4802	0.4838	0.4755	0.4844	0.4934	0.4857
x_{D,H_2O}	0.0000	0.0000	0.0019	0.0000	0.0007	0.0000	0.0001
$x_{D,MeOH}$	0.9779	0.9755	0.9754	0.9759	0.9765	0.9758	0.9764
$x_{D,PrOH}$	0.0221	0.0245	0.0226	0.0241	0.0228	0.0242	0.0235
x_{B,H_2O}	0.0586	0.0439	0.0422	0.0561	0.0502	0.0555	0.0513
$x_{B,MeOH}$	0.0229	0.0217	0.0547	0.0423	0.0225	0.0269	0.0223
$x_{B,PrOH}$	0.9184	0.9344	0.9031	0.9016	0.9273	0.9176	0.9264
F	0.06894	0.06907	0.06934	0.06928	0.06908	0.06921	0.06911
D	0.02406	0.02496	0.02380	0.02447	0.02441	0.02364	0.02434
B	0.04488	0.04411	0.04554	0.04481	0.04467	0.04557	0.04476

Table A.27. Reconciled results of component mole fractions and mass flow rates [tons/hr] of the external flows from input multiplicity experiment, experiment, Oct. 27th 2000 - Oct. 31st 2000.

A.5.3 Experiment, Nov. 14th 2000 - Nov. 19th 2000

Name	SS1	SS2	SS3	SS4	SS5	SS6	SS7	SS9
x_{F,H_2O}	0.0415	0.0316	0.0305	0.0383	0.0317	0.0325	0.0353	0.0366
$x_{F,MeOH}$	0.4624	0.4468	0.4717	0.4373	0.4790	0.4872	0.4461	0.4488
$x_{F,PrOH}$	0.4960	0.5216	0.4978	0.5244	0.4893	0.4803	0.5186	0.5146
x_{D,H_2O}	0.0000	0.0028	0.0000	0.0035	0.0001	0.0008	0.0037	0.0034
$x_{D,MeOH}$	0.9754	0.9729	0.9744	0.9709	0.9705	0.9704	0.9673	0.9689
$x_{D,PrOH}$	0.0246	0.0242	0.0256	0.0256	0.0294	0.0287	0.0290	0.0278
x_{B,H_2O}	0.0762	0.0543	0.0572	0.0646	0.0605	0.0621	0.0607	0.0625
$x_{B,MeOH}$	0.0344	0.0324	0.0310	0.0337	0.0312	0.0354	0.0287	0.0447
$x_{B,PrOH}$	0.8894	0.9133	0.9119	0.9017	0.9083	0.9025	0.9107	0.8927
F	0.10962	0.10853	0.10892	0.10966	0.10910	0.10879	0.10964	0.10989
D	0.03597	0.03380	0.03657	0.03342	0.03771	0.03830	0.03470	0.03426
B	0.07366	0.07473	0.07235	0.07624	0.07139	0.07049	0.07494	0.07564

Table A.28. Reconciled results of component mole fractions and mass flow rates [tons/hr] of the external flows from input multiplicity experiment, experiment, Nov. 14th 2000 - Nov. 19th 2000.

A.6 Time Constants Estimation

The dynamic composition response for a distillation column may be approximated with a two time constant model. These time constants may be estimated from the relations of Skogestad and Morari (Skogestad and Morari (1987) and Skogestad and Morari (1988)). The following section describes some of the findings in their work, and subsequently the estimated time constants from the three input multiplicity experiments are given.

The largest time constant is associated with changes in external flow rates, whereas the small time constant is associated with changes in internal flow rates. The model can be formulated as:

$$\begin{aligned}\begin{pmatrix} dy_D \\ dx_B \end{pmatrix} &= G(s) \begin{pmatrix} dL \\ dV \end{pmatrix} \\ &= \begin{pmatrix} \frac{g_{11}}{1+\tau_1 s} & (\frac{g_{11}+g_{12}}{1+\tau_2 s} - \frac{g_{11}}{1+\tau_1 s}) \\ \frac{g_{21}}{1+\tau_1 s} & (\frac{g_{21}+g_{22}}{1+\tau_2 s} - \frac{g_{21}}{1+\tau_1 s}) \end{pmatrix} \begin{pmatrix} dL \\ dV \end{pmatrix}\end{aligned}$$

where y_D and x_B are the mole fractions of the light component in the distillate and bottom product respectively. L and V are molar reflux flow rate and molar boilup respectively. g_{ij} represents the steady state gains for the distillation column. τ_1 is the dominant time constant for external flows. τ_2 is the time constant for internal flows.

In the case of binary distillation the two time constant may be estimated from:

$$\tau_{1c} = \frac{M_I}{I_s \ln S} + \frac{M_D y_D (1-y_D)}{I_s} + \frac{M_B x_B (1-x_B)}{I_s} \tag{A.3}$$

$$\tau_{2i} = \frac{(M_I/L_T)N}{2 \ln S} \tag{A.4}$$

Where M_I, M_D and M_B are total holdups of liquid inside the column, in the condenser (reflux drum) and in the reboiler respectively. N is the total number of theoretical trays (including reboiler). I_s and S are the sum of impurities and the separation factor determined by:

$$\begin{aligned} I_s &= D y_D (1-y_D) + B x_B (1-x_B) \\ S &= \frac{y_D (1-y_D)}{(1-y_D) x_B} \end{aligned}$$

Skogestad and Morari recommend estimating τ_2 from τ_1, however for the rough estimate purpose here, the formulations in equations A.3–A.4 are used.

The flow dynamics from the condenser and reboiler may be accounted for, by adding two lags to the model:

$$\begin{pmatrix} dy_D \\ dx_B \end{pmatrix} = \begin{pmatrix} \frac{1}{1+\tau_D s} & 0 \\ 0 & \frac{1}{1+\tau_B s} \end{pmatrix} G(s) \begin{pmatrix} dL \\ dV \end{pmatrix}$$

Here τ_D is the time constant for the condenser, and τ_B is the time constant for the reboiler. These are estimated from:

$$\tau_D = \frac{M_D}{V_T} \tag{A.5}$$

$$\tau_B = \frac{M_B}{L_B} \tag{A.6}$$

Common to the estimations below is that identical parameters have been used for $N_{tray,ideal}$, M_I, M_D and M_B, since these parameters do not differ significantly in the three experiments (reboiler: 300 liters + 19 trays: 150 liters + reflux drum: 50 liters):

$N_{tray,ideal}$	M_I (kmole)	M_D (kmole)	M_B (kmole)
12	2.55	1.22	4.09

Table A.29. Common parameters. $N_{tray,ideal}$: number of theoretical trays (including reboiler). M_I, M_D and M_B: total holdups of liquid inside the column, in the condenser (reflux drum) and in the reboiler respectively.

A.6.1 Experiment, Feb. 14th 2000 - Feb. 18th 2000

Name	F	D	B	V	L	y_D	x_B	τ_{1c}	τ_{2i}	τ_D	τ_B
SS1	1.381	0.632	0.750	33.816	33.184	0.9730	0.0431	12.3	0.07	0.04	0.12
SS2	1.423	0.670	0.752	31.517	30.847	0.9754	0.0389	12.5	0.07	0.04	0.13
SS3	1.393	0.607	0.786	27.892	27.285	0.9741	0.0248	14.0	0.08	0.04	0.15
SS4	1.379	0.572	0.807	25.357	24.785	0.9704	0.0232	13.8	0.09	0.05	0.17
SS5	1.362	0.556	0.806	23.830	23.273	0.9758	0.0160	16.3	0.08	0.05	0.18
SS6	1.417	0.623	0.794	18.979	18.356	0.9757	0.0129	16.0	0.10	0.06	0.22
SS7	1.395	0.628	0.766	11.796	11.168	0.9752	0.0204	14.7	0.18	0.10	0.37

Table A.30. Estimated time constants [hrs] and parameters used in estimation (see description above) from input multiplicity experiment, Feb. 14th 2000 - Feb. 18th 2000.

A.6.2 Experiment, Oct. 27th 2000 - Oct. 31st 2000

Name	F	D	B	V	L	y_D	x_B	τ_{1c}	τ_{2i}	τ_D	τ_B
SS1	1.524	0.737	0.788	12.564	11.828	0.9779	0.0229	13.6	0.17	0.10	0.35
SS2	1.528	0.763	0.765	18.494	17.731	0.9755	0.0217	13.2	0.12	0.07	0.23
SS3	1.531	0.729	0.802	23.770	23.041	0.9754	0.0547	10.7	0.10	0.05	0.18
SS4	1.540	0.748	0.792	27.291	26.543	0.9759	0.0423	11.4	0.08	0.04	0.15
SS5	1.526	0.747	0.779	15.513	14.766	0.9765	0.0225	13.4	0.14	0.08	0.28
SS6	1.522	0.723	0.799	10.077	9.355	0.9758	0.0269	12.8	0.22	0.12	0.44
SS7	1.526	0.745	0.781	12.490	11.746	0.9764	0.0223	13.4	0.17	0.10	0.35

Table A.31. Estimated time constants [hrs] and parameters used in estimation (see description above) from input multiplicity experiment, Oct. 27th 2000 - Oct. 31st 2000.

A.6.3 Experiment, Nov. 14th 2000 - Nov. 19th 2000

Name	F	D	B	V	L	y_D	x_B	τ_{1c}	τ_{2i}	τ_D	τ_B
SS1	2.416	1.099	1.317	12.456	11.358	0.9754	0.0344	7.5	0.19	0.10	0.36
SS2	2.348	1.034	1.313	14.908	13.874	0.9729	0.0324	7.7	0.16	0.08	0.29
SS3	2.389	1.116	1.273	17.230	16.114	0.9744	0.0310	7.8	0.13	0.07	0.25
SS4	2.373	1.022	1.351	19.701	18.679	0.9709	0.0337	7.4	0.12	0.06	0.22
SS5	2.407	1.147	1.259	21.276	20.129	0.9705	0.0312	7.4	0.11	0.06	0.20
SS6	2.414	1.167	1.248	23.678	22.511	0.9704	0.0354	7.2	0.10	0.05	0.18
SS7	2.379	1.058	1.321	19.552	18.494	0.9673	0.0287	7.4	0.12	0.06	0.22
SS9	2.391	1.045	1.346	21.288	20.242	0.9689	0.0447	6.8	0.12	0.06	0.20

Table A.32. Estimated time constants [hrs] and parameters used in estimation (see description above) from input multiplicity experiment, Nov. 14th 2000 - Nov. 19th 2000.

References

Skogestad, S. and Morari, M. (1987). The Dominant Time Constant for Distillation Columns. *Comp. Chem. Engng.*, **11**(6), 607–617.

Skogestad, S. and Morari, M. (1988). Understanding the Dynamic Behavior of Distillation Columns. *Ind. Eng. Chem. Res.*, **27**(10), 1848–1862.

B

Rigorous Model References

B.1 Thermodynamic Models

B.1.1 Modified UNIFAC, 3 parameter model (Lyngby)

As for the original UNIFAC model the molar excess Gibbs energy [J/mol] is calculated as the sum of a "combinatorial" part accounting for molecular size and shape differences, and a "residual" part accounting for molecular interactions:

$$G^E = {G_c}^E + {G_r}^E \tag{B.1}$$

Differentiating G_E yields the following expression for the activity coefficient for component i:

$$\ln \gamma_i = \ln \gamma_i^c + \ln \gamma_i^r \tag{B.2}$$

B.1.1.1 Combinatorial term

The combinatorial term for modified UNIFAC (Larsen *et al.* (1987)) is given by:

$$\ln \gamma_i^c = \ln\left(\frac{\omega_i}{x_i}\right) + 1 - \frac{\omega_i}{x_i} \tag{B.3}$$

where the modified volume fraction of component i in mixture is:

$$\omega_i = \frac{x_i {r_i}^{2/3}}{\sum_j x_j {r_j}^{2/3}} \tag{B.4}$$

Here r_i is the molecular volume parameter for component i:

$$r_i = \sum_k \nu_{ki} R_k \tag{B.5}$$

where R_k is the volume parameter for group k and ν_{ki} is the number of groups k present in molecule i.

B.1.1.2 Residual term

The residual term is for modified UNIFAC given by:

$$\ln \gamma_i^r = \sum_k \nu_{ki} \left(\ln \Gamma_k - \ln \Gamma_k^i \right) \tag{B.6}$$

Here Γ_k is the activity coefficient of group k at mixture composition, and Γ_k^i is the activity coefficient of group k at a group composition corresponding to pure component i. These activity coefficients are given by:

$$\ln \Gamma_k = \frac{z}{2} Q_k \left[1 - \ln \left(\sum_m \theta_m \tau_{mk} \right) - \sum_i \frac{\theta_i \tau_{ki}}{\sum_j \theta_j \tau_{ji}} \right] \tag{B.7}$$

The surface area fraction for component k in mixture is:

$$\theta_k = \frac{n_k \frac{z}{2} Q_k}{\sum_m n_m \frac{z}{2} Q_m} \tag{B.8}$$

where $\frac{z}{2} Q_k$ is the contact number parameter. n_k is the total number of groups in the mixture. Boltzmann factors are obtained from:

$$\tau_{mk} = \exp\left(-a_{mk}/T\right) \tag{B.9}$$

Here the temperature dependent interaction parameter, a_{mk}, is given by:

$$a_{mk} = a_{mk,1} + a_{mk,2}(T - T_0) + a_{mk,3} \left(T \ln \frac{T_0}{T} + T - T_0 \right) \tag{B.10}$$

where T_0 is an arbitrary reference temperature.

B.1.2 Modified NRTL (Darmstadt)

As for the original NRTL model the molar excess Gibbs energy [J/mol] for a multicomponent system is given by:

$$\frac{G^E}{RT} = \sum_i x_i \frac{\sum_j \tau_{ji} G_{ji} x_j}{\sum_k x_k G_{ki}} \tag{B.11}$$

where coefficients G_{ij} are given by

$$G_{ij} = exp(-\alpha_{ij} \tau_{ij}) \tag{B.12}$$

The extended interaction parameters (extended in comparison to the original NRTL model) of equation B.12 are given by the expression (Connemann *et al.* (1990)):

$$\tau_{ij} = \frac{(g_{ij} - g_{jj}) + \sum_{k \neq i,j} x_k \Delta g_{ijk}}{RT} \tag{B.13}$$

B.2 Thermodynamic Data

B.2.1 Ethanol, Water, Cyclohexane

In the following tables of thermodynamic data, ethanol has subscript 1, water has subscript 2 and cyclohexane has subscript 3.

B.2.1.1 Modified UNIFAC (Lyngby)

Main group		Sub group		Structural parameters		Groups present		
No.	Name	No.	Name	R	$(z/2)Q$	ν_{k1}	ν_{k2}	ν_{k3}
1	CH_2	2	CH_2	0.6744	0.540	0	0	6
4	OH	12	OH	1.0000	1.200	1	0	0
6	H_2O	14	H_2O	0.9200	1.400	0	1	0
35	CH_2-alc	59	CH_3-alc	0.9011	0.848	1	0	0
35	CH_2-alc	60	CH_2-alc	0.6744	0.540	1	0	0

Table B.1. Modified UNIFAC: structural parameters for subgroups (Data supplied from CAPEC / Larsen *et al.* (1987))

.

index	k	1	4	6	35
m		CH_2	OH	H_2O	CH_2-alc
1	CH_2	0.0	972.8	1857.0	0.0
		0.0	0.2687	-3.322	0.0
		0.0	8.773	-9.000	0.0
4	OH	637.5	0.0	155.6	637.5
		-5.832	0.0	0.3761	-5.832
		-0.8703	0.0	-9.000	-0.8703
6	H_2O	410.7	-47.15	0.0	1.400
		2.868	-0.4947	0.0	-5.832
		9.000	8.650	0.0	-0.8703
35	CH_2-alc	0.0	972.8	1857.0	0.0
		0.0	0.2687	-3.322	0.0
		0.0	8.7730	-9.000	0.0

Table B.2. Modified UNIFAC: Interaction parameters ($\alpha_{mk,1}$, $\alpha_{mk,2}$ and $\alpha_{mk,3}$) between main groups (Data supplied from CAPEC / Larsen *et al.* (1987))

.

B.2.1.2 Modified NRTL (Darmstadt)

Ethanol(1)/Water(2)		Ethanol(1)/Cyclohexane(3)		Water(2)/Cyclohexane(3)	
$g_{12} - g_{22}$	241.824	$g_{13} - g_{33}$	3663.26	$g_{23} - g_{33}$	36767.0
$g_{21} - g_{11}$	4634.91	$g_{31} - g_{11}$	5966.76	$g_{32} - g_{22}$	14036.3
α_{12}	0.34750	α_{13}	0.46261	α_{23}	0.21159
Ethanol(1)/Water(2)/Cyclohexane(3)					
Δg_{123}	5789.98	Δg_{132}	2573.26	Δg_{231}	17804.3
Δg_{213}	-9645.53	Δg_{312}	-6122.53	Δg_{321}	151.907

Table B.3. NRTL parameters for the system ethanol-water-cyclohexane (Keil *et al.* (1994)). Obtained by regression of $P(x,T)$-data at 333.1 K. Units of g_{ij} and Δg_{ijk} are in J/mol.

References

Connemann, M.; Gaube, J.; Karrer, L.; Pfennig, A. and Reuter, U. (1990). Measurement and representation of ternary vapour-liquid-liquid equilibria. *Fluid Phase Equil.*, **60**, 99–118.

Keil, B.; Paul, H. I.; Pfennig, A. and Gaube, J. (1994). Investigation of the separation of ternary mixtures forming two liquid phases by distillation. *Int. Chem. Eng.*, **34**(3), 315–319.

Larsen, B. L.; Rasmussen, P. and Fredenslund, A. (1987). A Modified UNIFAC Group-Contribution Model for Prediction of Phase Equilibria and Heats of Mixing. *Ind. Eng. Chem. Res.*, **26**, 2274–2286.

C

Example Analyses: ∞/∞ Predictions

C.1 Direct Sequence

Initial Case ($B_1 = 0$) In the initial case, the balance equations are used to position the process variables in the composition simplex. For $B_1 = 0\ moles/hr$ the total balance (Eq. (5.1)) reduces to

$$E \equiv B_2 \tag{C.1}$$

Here, the '$\equiv$' is used, since both rates and compositions must be equal. Furthermore, the column 1 balance (Eq. (5.2)) reduces to

$$D_1 \equiv F \tag{C.2}$$

These equations can be used to determine the initial profiles of the two columns. Since B_2 is situated at E (*inside* a distillation region), the only allowable ∞/∞ profile in column 2 is of type I. As a consequence, the distillate composition, D_2, must be situated at an unstable node, where the only candidate is the ternary azeotrope T as shown in Figure C.1a. The process variables of column 1 can be positioned by considering balance equation 5.3. D_1 must be situated on the straight line between B_2 and D_2, which is inside the simplex. As a consequence B_1 must be at the stable node H (type II profile).

Final Case ($B_1 = E$) In the final case, shown in Figure C.1b, $B_2 = 0$. Hence, the total balance (Eq. (5.1)) reduces to

$$B_1 \equiv E \tag{C.3}$$

Furthermore, the column 2 balance (Eq. (5.3)) reduces to

$$D_1 \equiv D_2 \tag{C.4}$$

Since B_1 is situated inside a distillation region (at E), the condensed vapor of column 1 (V_1) must be situated at the unstable ternary azeotrope (type I profile). This forces D_1 to be situated in S due to the equilibrium reached in the decanter. Since D_2 should be situated at D_1 (and thereby S), which is inside a distillation region, B_2 must be situated in a stable node belonging to that distillation region. Only one candidate exist: The pure component H corner.

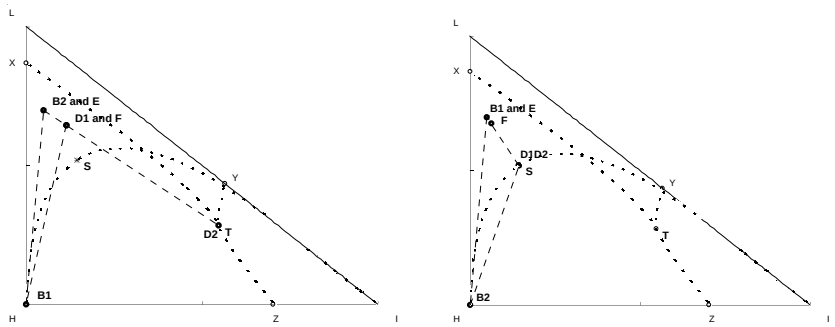

(a) Initial Case (b) Final Case

Figure C.1. Position of the process variables for the direct sequence in the initial a) and final case b). In the initial case, the profile of column 1 is of type II, and the profile of column 2 is of type I. In the final case, the opposite is true. The dashed straight lines are balance equation lines.

First Step Having determined the initial and the final cases, the continuation can commence. This is done by increasing the bifurcation parameter (B_1) from the initial case, under consideration of allowable profile types and balance equations. The profile changes during continuation steps are shown in Table 5.1. The continuation is started by moving B_2 along the total balance line B_1EB_2 in direction away from E. This *increases* the flow rate B_1 (consider the lever rule). Since B_2 is moving inside a distillation region, D_2 stays in the ternary azeotrope (T). As B_2 moves, D_1 moves, since D_1 must stay on the straight line spanned by B_2 and D_2 (column 2 balance, equation 5.3). The movement of D_1 inside a distillation region forces B_1 to stay at H (type II profile of column 1). This move (step) can be terminated in two ways. Either, B_2 reaches the LI edge of the composition simplex demanding a shift in profile type, or D_1 reaches the distillation boundary TX. The latter is the case here, and the implication is the following. If D_1 reaches the TX boundary, the movement can *not* continue since the boundary can not be crossed. This is due to the fact, that the residue curves are restricted to the same distillation region, and B_1 is positioned in the pure component H corner. The movement of the variables during the first step are illustrated in Figure C.2a.

Second Step The termination of the previous step was caused by D_1 reaching the TX distillation boundary. When D_1 moves along the TX boundary in direction T, B_1 must move along the HL edge (type III profile) as sketched in Figure C.2b. Column 2 is not changing profile type, since B_2 still is situated inside a distillation region (uniquely positioned by the balance equations). Therefore D_2 resides in T. This step is terminated when D_1 (or alternatively V_1) reaches the binodal curve, since at this point D_1 and V_1 will split and move in separate directions.

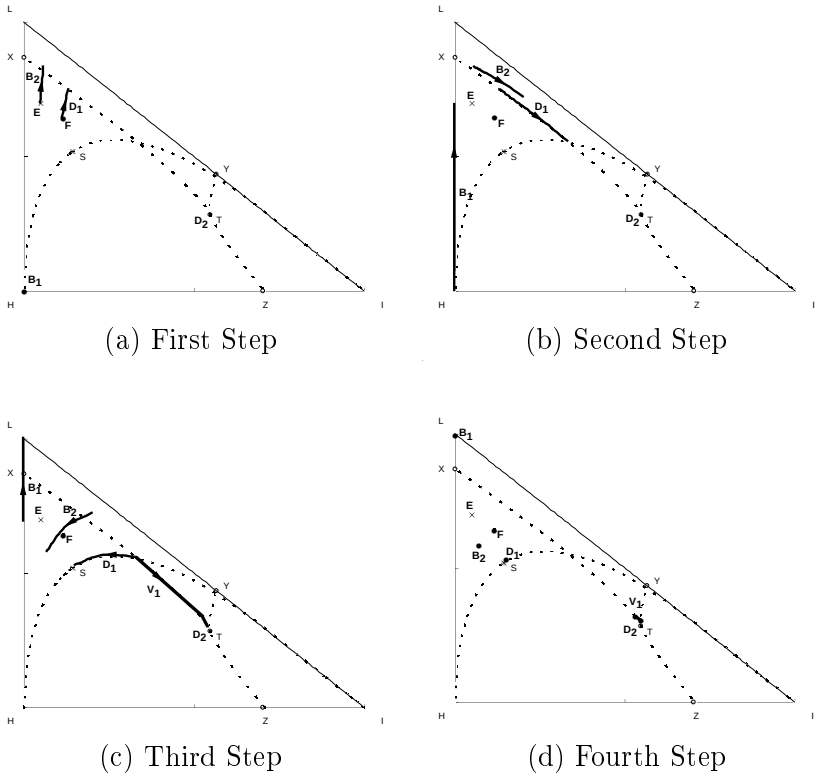

Figure C.2. Continuation path for the process variables B_1, B_2, D_1, and D_2. The first four steps of the bifurcation analysis for the direct sequence.

Third Step The terminating criterion of step 2 implies, that D_1 and V_1 splits and move in separate directions. In previous steps, the overall condensed vapor of column 1 was homogeneous implying homogeneous operation of the decanter. Therefore, V_1 and D_1, till now, were positioned identically. In this step V_1 enter the heterogeneous region of the composition simplex, moving along the TX boundary in the direction of T. D_1 can not enter the heterogeneous region, since the decanter splits the heterogeneous mixture into two liquid phases. Therefore D_1, as sketched in Figure C.2c, moves along the binodal curve on the water-rich side of the plait point (the water-rich phase is fed to distillation column 2). As D_1 moves along the binodal curve, the bifurcation parameter, B_1 *decreases*. The geometric condition for output multiplicity is fulfilled, as the FB_1 lever increases when the D_1F lever decreases. This step is terminated when B_1 reaches the pure component L corner.

Fourth Step Now, B_1 is positioned at the pure component L corner, which is a stable node. V_1 shifts position from the TX boundary towards the TY boundary whereas B_1 is situated at the stable node, and thus yielding a type II profile of column 1 during the shift. Along with this step, the external variables B_1 (fixed in L) and B_2 are not moved implying,

that this shift is occurring for one value of the bifurcation parameter. This constraint on B_1 and B_2 also fixes the positions of D_1 and D_2. As a consequence V_1 moves along *one* tie line from the TX boundary to the TY boundary, fixing D_1 on the binodal curve as shown in Figure C.2d. Thus, for this value of B_1 state multiplicity exists in the azeotropic column, yielding an infinite number of possible profiles.

Fifth Step Once V_1 is situated on the TY boundary, B_1 moves on the LI edge yielding a type III profile (Figure C.3a). The step is terminated when V_1 reaches the ternary azeotrope T and consequently D_1 reaches S.

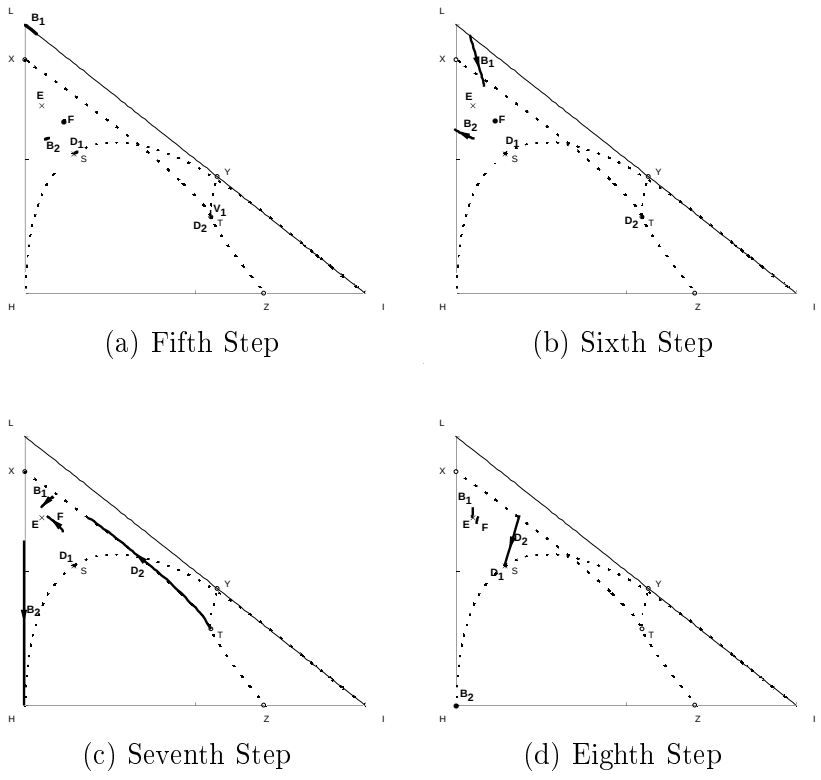

(a) Fifth Step (b) Sixth Step

(c) Seventh Step (d) Eighth Step

Figure C.3. Continuation path for the process variables B_1, B_2, D_1, and D_2. The last four steps of the bifurcation analysis for the direct sequence.

Sixth Step The profile of column 1 is changing to type I since V_1 is now at an unstable node. This implies, that B_1 is entering the simplex, uniquely positioned by the balance equations (see Figure C.3b). Column 2 is still exhibiting a type I profile. D_2 is positioned in the unstable node T. Therefore B_2 is also moving inside the simplex. With D_1 and D_2 fixed at their positions, B_2 moves on the straight line spanned by these towards the HL edge (column 2 balance, equation 5.3). The step is terminated when B_2 reaches the LH edge.

Seventh Step The terminating criterion of step 6 implies, that a profile change in column 2 must occur, since B_2 has reached the HL edge of the composition simplex. It is obvious, that the column profile is now of type III, due to the position of B_2. A further continuation is obtained by moving D_2 away from the ternary azeotrope T along the TX boundary in direction of X as shown in Figure C.3c. Along with this path, B_2 moves in direction of the pure component H corner. The profile of column 1 is not altered through this step. D_1 is positioned in S, and B_1 is moving inside the simplex, subject to the balance equations. The step is terminated when B_2 reaches H.

Eighth Step The previous step was terminated with B_2 at a stable node and V_1 at an unstable node. Therefore, column 1 must have a type I profile and column 2 must have a type II profile. This means, that B_1 is situated inside a distillation region on the total balance line connecting H, E and B_1 (since B_2 is in H). D_2 is leaving the TX distillation boundary, as shown in Figure C.3d, and enters the distillation region moving on a straight line towards S (and D_1). This step is terminated when D_2 is positioned at S (D_1 is positioned at D_2, and thereby at S).

C.2 Indirect Sequence

Initial Case ($B_1 = 0$) As was the case in the initial case for the direct sequence, the balance equations reduce to $E \equiv B_2$ and $D_1 \equiv F$. Since then B_2 is situated at E *inside* the simplex, V_2 must be positioned at the ternary azeotrope T yielding a type I profile. This implies, that D_2 is positioned at S, as shown in Figure C.4a. (Note the difference between this sequence and the direct sequence. The decanter is now connected to the top of column 2, yielding the liquid-liquid phase split there.) Again D_1 (and F) must be positioned on the straight line between D_2 and B_2 (depending of the specified rate of D_1), which is located inside the simplex. Thus, B_1 must be situated at H (type II profile).

Final Case ($B_1 = E$) The balance equations reduce to $B_1 \equiv E$ and $D_1 \equiv D_2$. Since B_1 is positioned in E inside the composition simplex, D_1 must be situated in the ternary azeotrope T (type I profile). However, this profile type is seen to be infeasible. Consider the balance constraint $D_1 \equiv D_2$. This constraint obviously can not be satisfied with D_1 situated in T, since D_2 is positioned on the binodal curve due to the decanter. The final case, thus is infeasible at ∞/∞ conditions.

First Step The continuation commences by moving B_2 along the B_1EB_2 balance line away from E. The flow rate B_1 increases. The movement of B_2 inside the simplex implies moving of D_1 and F due to the balance

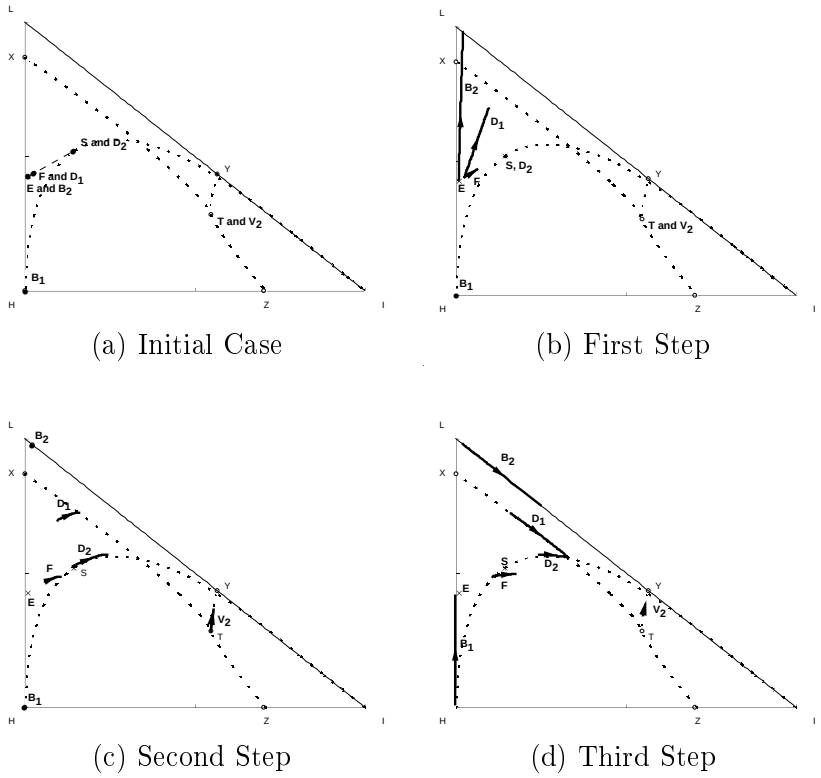

(a) Initial Case (b) First Step

(c) Second Step (d) Third Step

Figure C.4. Path taken by the process variables in the bifurcation analysis of the indirect sequence.

equations. As sketched in Figure C.4b, B_1 stays fixed at H and D_2 at S. This step is terminated when B_2 reaches the LI edge of the composition simplex.

Second Step The termination criterion of step 1 implies, that the profile of column 2 must change to type III, since B_2 is positioned on the LI edge. Then D_2 must move along the binodal curve. D_1 is still positioned inside the simplex, and therefore B_1 is still positioned at H. Thus, the position of B_2 is fixed as well due to the total balance equation (Eq. (5.1)). As a consequence, D_1, D_2, and F move as sketched in Figure C.4c, whereas B_1 and B_2 stay fixed. Thus, the bifurcation parameter is *not* varied. Instead an infinite number of states exist for the same value of the bifurcation parameter, i.e. state multiplicity exists. The step is terminated when D_1 intersects the TX distillation boundary.

Third Step Since D_1 is now situated on the TX distillation boundary, column 1 is changing profile to type III. B_1 moves along the HL edge in direction L, and D_1 on the TX boundary in direction T, as shown in Figure C.4d. D_2 moves on the binodal curve, and B_2 on the LI edge. The step is terminated when the balance constraints refuse movement to continue.

D

Additional calculations

D.1 Feasible Definition Sets for Bifurcation Parameters

This section displays the results from the geometric constructions when obtaining the feasible definition set of the bifurcation parameters B_1 and D_2. Assumptions and description of the method can be read in chapter 5.

D.2 Direct Sequence

$E = 100 moles/hr$
$x_E = [0.05; 0.70; 0.25]$
Decanter operates at 298 K

$B_1 \in [0; 100 moles/hr]$
$D_2 \in [12.2; 51.6 moles/hr]$

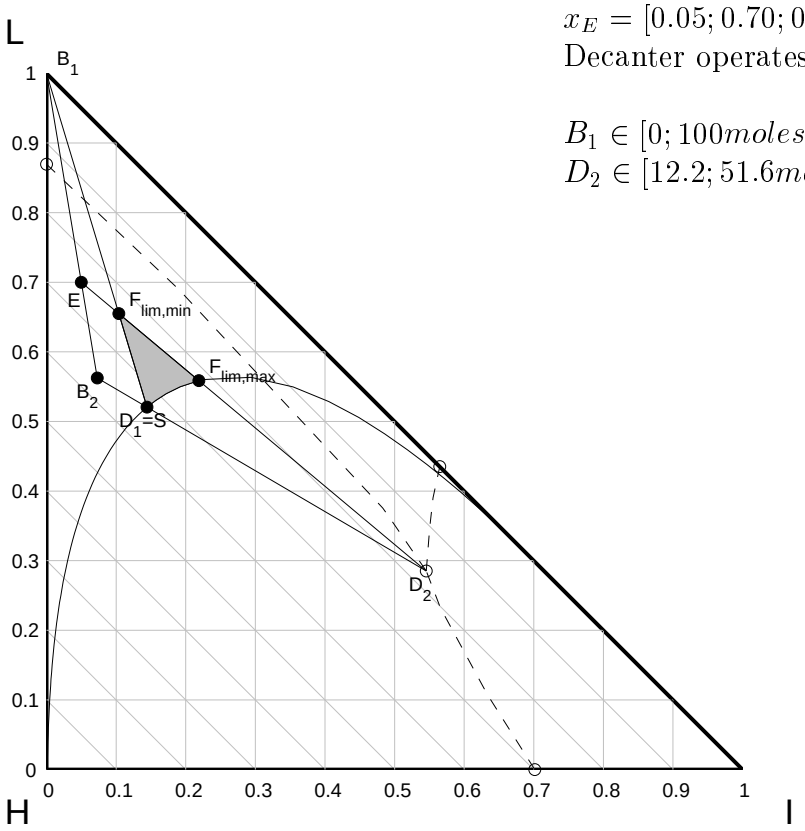

$E = 100 moles/hr$
$x_E = [0.05; 0.70; 0.25]$
Decanter operates at the boiling point

$B_1 \in [0; 100 moles/hr]$
$D_2 \in [13.3; 67.3 moles/hr]$

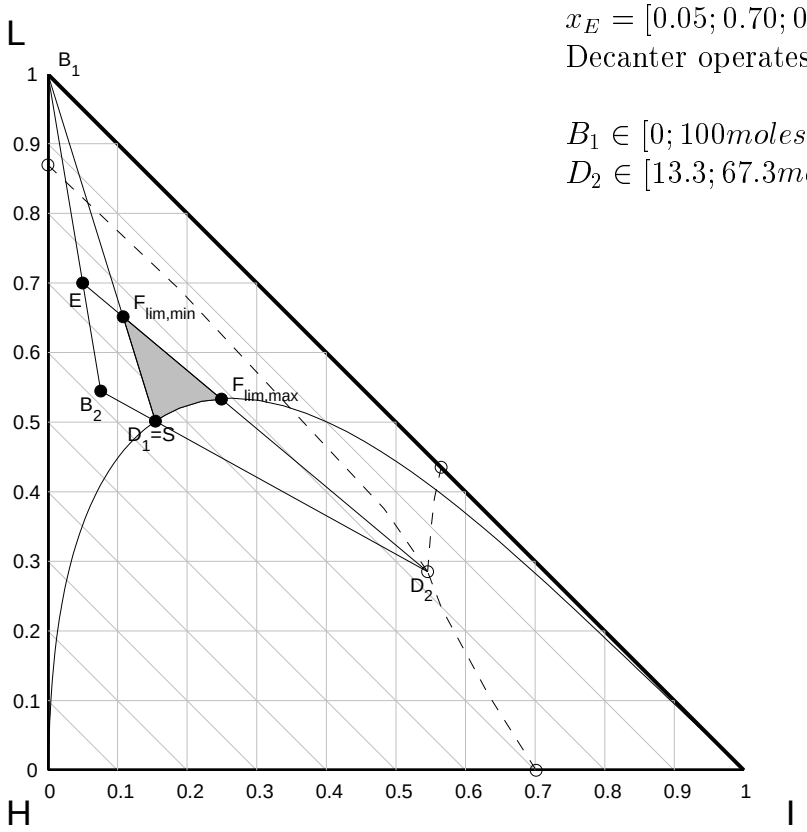

$E = 100 moles/hr$
$x_E = [0.001; 0.870; 0.129]$
Decanter operates at 298 K

$B_1 \in [0; 100 moles/hr]$
$D_2 \in [11.6; 110.5 moles/hr]$

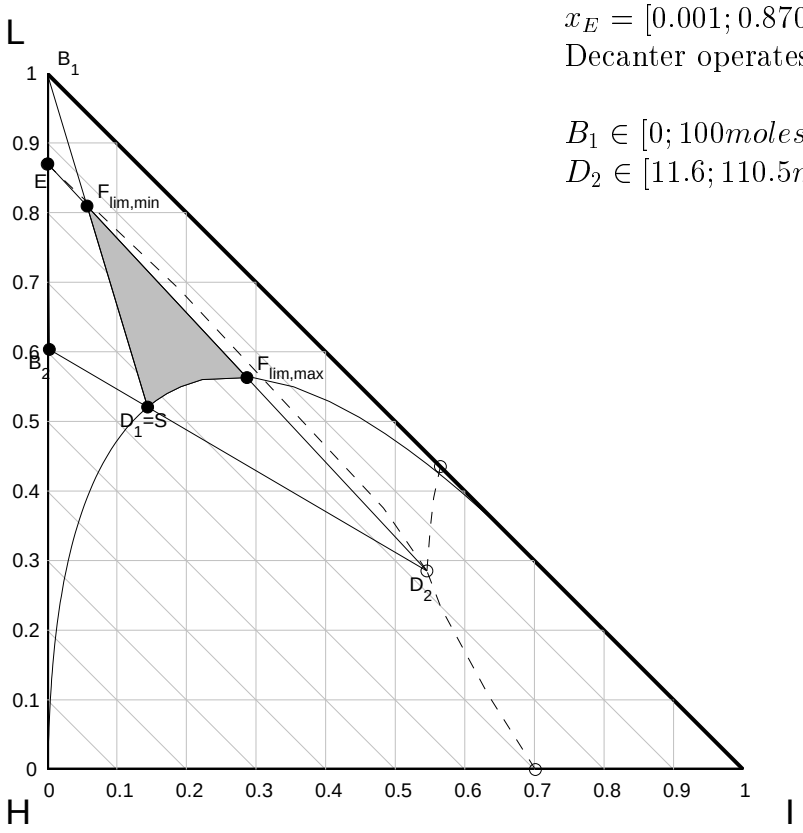

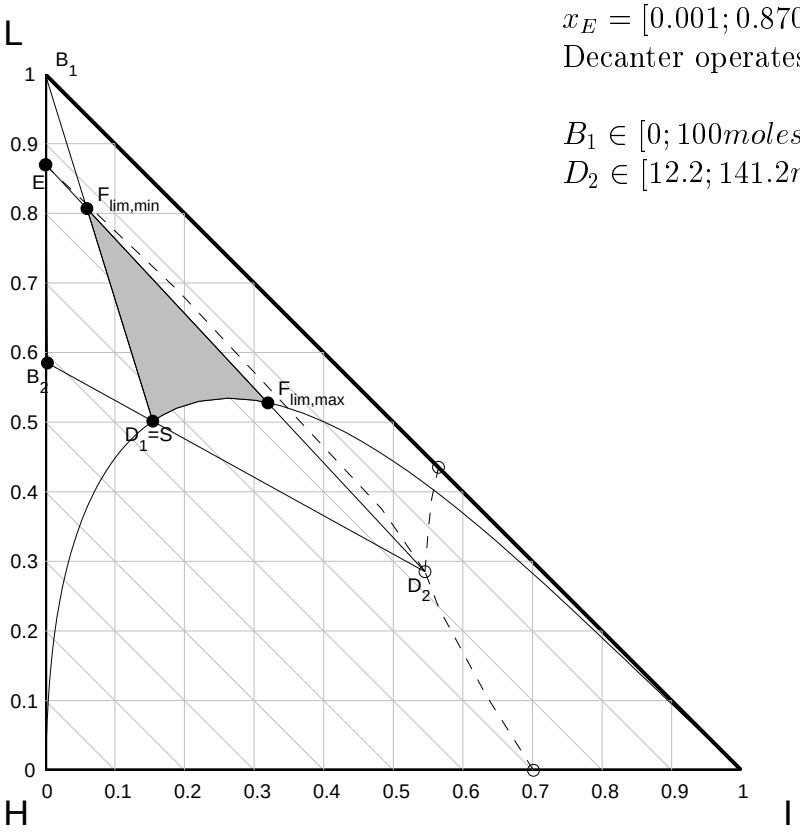

$E = 100 moles/hr$
$x_E = [0.001; 0.870; 0.129]$
Decanter operates at the boiling point

$B_1 \in [0; 100 moles/hr]$
$D_2 \in [12.2; 141.2 moles/hr]$